UNIVERSIDADE FEDERAL DE SÃO CARLOS
CENTRO DE CIÊNCIAS EXATAS E DE TECNOLOGIA
PROGRAMA DE PÓS-GRADUAÇÃO EM CIÊNCIA E ENGENHARIA DE MATERIAIS

REFILL FRICTION STIR SPOT WELDING: INVESTIGATION OF THE SIMILAR AND DISSIMILAR WELDING OF AA5754-H22 AND AA6061-T6 SHEETS.

Antonio Cappelletti Ferreira

SÃO CARLOS - SP
2019

UNIVERSIDADE FEDERAL DE SÃO CARLOS
CENTRO DE CIÊNCIAS EXATAS E DE TECNOLOGIA
PROGRAMA DE PÓS-GRADUAÇÃO EM CIÊNCIA E ENGENHARIA DE MATERIAIS

REFILL FRICTION STIR SPOT WELDING:
INVESTIGATION OF THE SIMILAR AND DISSIMILAR WELDING OF AA5754-H22 AND AA6061-T6 SHEETS.

Antonio Cappelletti Ferreira

Dissertation presented to Programa de Pós-Graduação em Ciência e Engenharia de Materiais (PPGCEM) in partial fulfillment of the requirements for the MASTER OF SCIENCE DEGREE IN MATERIALS SCIENCE AND ENGINEERING.

Supervisor: Dr. Nelson Guedes de Alcântara
Co-supervisor: Dr. Leonardo Conti Campanelli
Grant Agency: CNPq (Process no. 134522/2017-6)

São Carlos-SP
2019

To my beloved family.

RESUME

Bachelor degree in Materials Engineering (2017) from UFSCar

UNIVERSIDADE FEDERAL DE SÃO CARLOS

Centro de Ciências Exatas e de Tecnologia
Programa de Pós-Graduação em Ciência e Engenharia de Materiais

Folha de Aprovação

Assinaturas dos membros da comissão examinadora que avaliou e aprovou a Defesa de Dissertação de Mestrado do candidato Antonio Cappelletti Ferreira, realizada em 03/06/2019:

Prof. Dr. Nelson Guedes de Alcântara
UFSCar

Prof. Dr. Piter Gargarella
UFSCar

Prof. Dr. Celso Roberto Ribeiro
LEMM

ACKNOWLEDGMENTS

In first place, I am thankful to Dr. Leonardo Campanelli, my co-supervisor in Brazil, for the supportive orientation, friendship and trust he has demonstrated throughout the entire path of this work. His mentorship was a decisive factor for the conclusion of this dissertation.

I express my gratitude to Dr. Jorge dos Santos, for the amazing internship opportunity and for guaranteeing all the necessary conditions for my stay in Germany. Dr. dos Santos has also helped several times with publications advises.

My supervisor, Prof. Dr. Nelson Guedes de Alcântara has also played a crucial role in the completion of this work. Alcântara has always been available for consultation and was very generous with opportunities for career growth.

I thank the help and supervision from Dr. Uceu Suhuddin, who was supportive and patience during my internship in Germany. Working with him was very important for my personal growth.

Finally, I am very thankful for the financial support provided by Conselho Nacional de Desenvolvimento Científico e Tecnológico - CNPq (Process no. 134522/2017-6).

This study was financed in part by the Coordenação de Aperfeiçoamento de Pessoal de Nível Superior - Brasil (CAPES) - Finance Code 001

ABSTRACT

The automotive industry is shifting to a new paradigm of material utilization in vehicles. Different parts of the car structural body are increasingly being made of materials selected to have a customized performance according to its position in the car. For that reason, materials are welded in similar and dissimilar combinations beyond the capabilities of traditional welding methods. Refill Friction Stir Spot Welding (RFSSW) is an emerging technology able to weld similar and dissimilar combination of materials in a consistent manner and delivering the quality requirements for car industry. The present research work focused on the RFSSW of similar AA5754-AA5754 and dissimilar AA5754-AA6061, which commonly occur in formed sheets of car door panels. The investigation of internal defects, mechanical properties, metallurgy and material flow were the main objectives of this work. Design of Experiments, Response Surface Methodology and Analysis of Variance were the statistical tools to investigate the window of process parameters where welds were optimized and to find parameter combinations where defects could possibly be present. Mechanical testing was performed with Lap-Shear Strength tests and microhardness measurements. Microstructural analysis was performed with polarized light microscopy. Material flow was analyzed with Stop-Action technique. Statistical analysis revealed a very linear model for the similar combination depending mostly of the individual contribution of parameters, specially Plunge Depth. For dissimilar welding, the model is more dependent on the square and two-way contributions. It was identified internal pores and lack-of-filling defects that explained the poor performance for certain combinations of parameters.

Keywords: Refill Friction Stir Spot Welding; AA5754, AA6061; Response Surface Methodology; Defects; Metallurgy; Mechanical Properties

RESUMO

SOLDAGEM POR FRICÇÃO A PONTO COM PREENCHIMENTO: INVESTIGAÇÃO DA SOLDAGEM SIMILAR E DISSIMILAR DE CHAPAS AA5754-H22 E A6061-T6

A indústria automotiva está mudando para um novo paradigma de utilização de materiais em que partes do chassi são fabricadas em materiais cada vez mais selecionados para terem um desempenho sob medida para sua posição no carro. Assim, materiais são soldados em combinações similares e dissimilares, tornando difícil a utilização de métodos convencionais de soldagem. A soldagem por fricção a ponto com preenchimento (RFSSW) é uma tecnologia emergente de processo capaz de soldar combinações similares e dissimilares de uma maneira consistente e fornecer os requisitos de qualidade para a indústria automobilística. O presente trabalho de pesquisa focou na solda similar AA5754-AA5754 e dissimilar AA5754-AA6061, combinações que comumente ocorrem em chapas conformadas nos painéis das portas do carro. A investigação de defeitos internos, propriedades mecânicas, metalurgia e fluxo de materiais foram os principais objetivos deste trabalho. Planejamento de Experimentos, Metodologia de Superfície de Resposta e Análise de Variância foram as ferramentas estatísticas utilizadas para investigar a janela de parâmetros do processo em que as soldas foram otimizadas e para encontrar combinações de parâmetros onde defeitos pudessem estar presentes. O teste mecânico foi realizado com testes de resistência ao cisalhamento e medidas de microdureza. A análise microestrutural foi realizada com microscopia de luz polarizada. O fluxo de material foi analisado com a técnica *Stop-Action*. A análise estatística revelou um modelo linear para a combinação similar, dependendo principalmente da contribuição individual dos parâmetros, especialmente da profundidade de penetração da ferramenta. Para a soldagem dissimilar, o modelo é mais dependente das contribuições quadráticas e interações bidirecionais. Identificaram-se poros internos e defeitos de falta de enchimento que explicavam o baixo desempenho de certas combinações de parâmetros.

Palavras-Chave: Soldagem por fricção a ponto com preenchimento; AA5754; AA6061; Metodologia de Superfície de Resposta, Defeitos; Metalurgia; Propriedades mecânicas

PUBLICATIONS

Ferreira, A. C., Suhuddin, U. F. H., Campanelli, L. C., Alcântara, N. G. & dos Santos, J. F. “Investigation of internal defects and premature fracture of dissimilar refill friction stir spot welds of AA5754 and AA6061”. The International Journal of Advanced Manufacturing Technology

TABLE OF CONTENTS

APPROVAL SHEET i
ACKNOWLEDGMENTS iii
ABSTRACT.. v
RESUMO vii
PUBLICATIONS ix
TABLE OF CONTENTS.. xi
LIST OF FIGURES xv
LIST OF TABLES xvii
SYMBOLS AND ABREVIATIONS xix
1. MOTIVATION 1
2. OBJECTIVES 5
3. LITERATURE REVIEW 7
 3.1. AA5754-H22 and AA6061-T6...7
 3.2. Microstructure evolution and dynamic recrystallization in aluminum alloys 10
 3.3. Description of RFSSW 11
 3.3.1. Process Parameters 12
 3.3.2. Characterization of the weld zone 14
 3.3.3. Defects in RFSSW 15
 3.4. Design of Experiments 16
4. MATERIALS AND METHODS...19
 4.1. RFSSW Equipment 19
 4.2. Welding of the Samples 20
 4.2.1. Materials description...20

4.3. Specimen preparation 21
4.4. DoE and RSM 21
4.5. Mechanical Characterization – Lap Shear and Microhardness 22
4.5.1. Microhardness testing 22
4.6. Metallurgical characterization 23
4.7. Sample preparation 23
4.8. Stop-action experiments 23
5. RESULTS AND DISCUSSION 25
5.1. Results from similar AA5754-H22 RFSSW 25
5.1.1. DOE and RSM 25
5.1.2. One-Factor-At-a-Time method 29
5.1.3. Weld Characterization and Microstructural Analysis 34
5.1.3.1. Weld Characterization 34
5.1.3.2. Microhardness across weld section. 36
5.1.3.3. Hook characterization 36
5.1.3.4. Fracture behavior 40
5.2. Results from dissimilar AA5754-AA6061 RFSSW 41
5.2.1. Test to evaluate position of alloys during weld 41
5.2.2. Design of Experiments 41
5.2.3. Optimization of parameters using OFAT 44
5.2.4. Hook Characterization 48
5.2.5. Fracture behavior 48
5.2.6. Weld Characterization and Microstructure Analysis 49
5.2.6.1. Stir zone (D) 51
5.2.6.2. Thermomechanical Affected Zones (C) and (F). 52
5.2.6.3. Heat Affected Zone (B) 54

5.2.6.4. BM (A and E) 55

5.2.7. Microhardness in weld section 56

5.2.8. Stop-action experiments 57

5.2.9. Clamping pressure experiments 61

6. CONCLUSIONS 65

7. SUGGESTIONS FOR FUTURE WORK 67

8. REFERENCES 69

ANNEXES 77

LIST OF FIGURES

Figure 3.1 – Lotus Evora® chassis front sub-frame with brakes and suspension’s system assembled [15] 8

Figure 3.2 – Juaguar® XE body mostly built in aluminum [19]. 9

Figure 3.3 – Illustration of RFSSW process using sleeve plunge variant: (1) Clamping and tool rotation; (2) Sleeve plunge and the pin retraction; (3) Parts back to surface level; and (4) Tool removal.[33]. 12

Figure 3.4 – Four typical zones in a RFSSW cross section 14

Figure 3.5 - Macrographs of a typical RFSSW joint cross section showing weld defects [45]. 15

Figure 3.6 – Scheme of the Box–Behnken design for three factors [49]. 16

Figure 4.1 - Flowchart of the experimental activities. 19

Figure 4.2 – RPS 100® tool set. 20

Figure 4.3 – Schematic representation of the friction spot lap weld configuration. 21

Figure 4.4 – Representation of microhardness measurements. 23

Figure 5.1 – Expected versus predicted LSS according to RSM 28

Figure 5.2 – Effect of combined (A) FR and PD; (B) FR and RS; (C) PD and RS on LSS of welded joints 28

Figure 5.3 – Summary of OFAT results 34

Figure 5.4 – Macrograph of the cross section of condition O (1) and a higher magnification (2) showing four different regions of the weld cross section. BM (A), HAZ (B), TMAZ (C), SZ (D). 35

Figure 5.5 – Hardness profile across the weld 36

Figure 5.6 – Hook defect. 37

Figure 5.7 – Lap-shear simulation for similar homogeneous materials joints [57]. 38

Figure 5.8 – Hook and bonding width measurements. 39

Figure 5.9 – Effect of hook and bonding width on mechanical property of the joint 39

Figure 5.10 – Effect of combined (A) FR and PD; (B) FR and RS; (C) PD and RS on LSS of dissimilar welded joints 43
Figure 5.11 – Expected versus predicted LSS according to RSM 44
Figure 5.12 – Box-and-whisker plot of OFAT results means 46
Figure 5.13 – Condition A from OFAT experiments 48
Figure 5.14 - LSS versus h/t showing a negative dependency of LSS on h/t 48
Figure 5.15 – Specimen fracture 49
Figure 5.16 – Cross section of the welded joint (Top picture). Micrographs of AA5754 base material, (A) HAZ (B), TMAZ (C), SZ (D). Micrographs of AA6061 base material (E), TMAZ and SZ (F). Detail of mixture between sheets (G and H). Hook shape (I). 50
Figure 5.17 – OM showing TMAZ and the evolution of grain size 54
Figure 5.18 – OM showing HAZ in AA5754 upper sheet 55
Figure 5.19 – Microhardness profile of weld cross section 57
Figure 5.20 – Cross section of G condition stopped at 1.4 mm depth observed in polarized light. 58
Figure 5.21 – Higher magnification showing the material flow in sleeve periphery 60
Figure 5.22 – Engulfment of AA5754 by AA6061. 61
Figure 5.23 – Macrographies evidencing the influence of clamping pressure on weld characteristics. 63
Figure 5.24 – Area of interest from welds comparing width of HAZ. 63

LIST OF TABLES

Table 4.1 – Chemical composition of the supplied materials..................20
Table 4.2 – Mechanical properties of the supplied materials [50]...........21
Table 4.3 – Welding combination according to Box–Behnken design [52] 22
Table 5.1 – Factors and levels for DOE...25
Table 5.2 – Experimental conditions and results 26
Table 5.3 – ANOVA from the results of similar welds 26
Table 5.4 – Reproducibility tests for optimum result from DOE and evaluation of optimum parameters from RSM 30
Table 5.5 – OFAT results for rotational speed.......................................32
Table 5.6 – OFAT results plunge depth...33
Table 5.7 – OFAT results feeding rate...33
Table 5.8 – Failure modes 40
Table 5.9 – Experiment conditions and results......................................41
Table 5.10 – Experiment factors and levels...42
Table 5.11 – Experiment conditions and results....................................42
Table 5.12 – ANOVA of the Box-Behnken DOE for LSS.......................43
Table 5.13 – OFAT results for RS 45
Table 5.14 – OFAT results for PD 46
Table 5.15 – OFAT results for FR..47

SYMBOLS AND ABREVIATIONS

AA	Aluminum alloy
α	Confidence index
ANOVA	Analysis of variance
ASTM	American Society for Testing and Materials
BBD	Box-behnken design
BM	Base material
CDRX	Continuous dynamic recrystallization
CF	Clamping force
DDRX	Discontinuous dynamic recrystallization
DF	Degree of freedom
DoE	Design of experiments
DRX	Dynamic recrystallization
DT	Dwell time
EBSD	Electron backscatter diffraction
EDS	Energy dispersive spectroscopy
ε	Strain
$\dot{\varepsilon}$	Strain rate
FR	Feeding rate
FSP	Friction-stir Processes
FSpW	Friction spot welding
FSSW	Friction stir spot welding
FSW	Friction stir welding
GDRX	Geometric dynamic recrystallization
HAB	High-angle Boundary
HAZ	Heat affected zone
HVAC	Heating, ventilation and air conditioning
HZG	Helmholtz-zentrum geesthacht
ISO	International Organization for Standardization
LAB	Low-angle Boundary

LSS	Lap-shear strength
OFAT	One-factor-at—a-time
P	Percentage of contribution
PD	Plunge depth
PT	Plunging time
RFSSW	Refill friction stir spot welding
RS	Tool rotational speed
RSM	Response surface methodology
RSW	Resistance spot welding
SFE	Stacking fault energy
SZ	Stir zone
T	Temperature
TMAZ	Thermomechanically affected zone

1. MOTIVATION

The development of new engineering materials is generally guided by the objective of increasing the performance of components. Materials are therefore developed to be lighter, stronger and to be resistant to environmental effects. They are engineered to perform according to the final application for which they are conceived, which means that microstructure, processing and properties are also considered.

Enhancing material quality, in the sense of what is measured in mechanical tests and how rarely defects happen is important for increasing the quality and reliability of components For that reason, quality has to be assured in every processing step of manufacturing a component and much attention must be paid in processes whose the likelihood of defects is high.

Welding in a general sense is one of the most troublesome industrial processes because of the high likelihood of defects that arise from the material physical properties or lack of control of process parameters. The ability of materials to be welded is therefore an important factor that affects the quality and final performance of a given component. In other words, even if a material has the right properties for a given application, it can fall apart if an ineffective joining method is applied between the parts.

Despite the rise of automation and robotics, which solved many of previous industrial issues, welding of high strength aluminum alloys is still troublesome and does not reach the quality standard requirements for high safety industries. As welded junctions are still more susceptible to failure, airspace industry, for instance, avoid structural welds at any cost.

Aluminum alloys (AA) are very cost-effective materials used in a broad range of applications because of their good mechanical properties combined to low density and corrosion resistance, leading to lower energy consumption and a higher performance throughout the component life. Aluminum is especially attractive for automotive, aerospace and marine industries that are always pursuing weight reduction in their products. However, high strength aluminum alloys are quite complex to weld as they tend to lose their properties during the joining process. Besides, the traditional fusion welding of AA is expensive due to energy consumption and decrease of material mechanical properties. Therefore, materials engineers try to solve these problems by either choosing materials with better weldability or improving and creating more effective welding processes [1]. Those are important drivers for the evolution of components.

In the future paradigm of structural component design, advanced materials with specialized properties will only be applied where they are essential [2]. This new standard will require more joints, many of which of dissimilar materials. A small number of traditional welding processes are suitable in those circumstances; new joining processes will be required.

Among the most prospective process able to join dissimilar materials, Refill Friction Stir Spot Welding (RFSSW) arises as a new solid-state welding process. Since its invention in HZG – Germany, it has shown great results in joining dissimilar high strength AA [3]. The process is a promising substitute for mechanical joining and resistance spot welding (RSW) in aerospace and automotive industries, resulting in a significant decrease of weight, energy consumption and costs for companies. RFSSW joints have also been reported to be stronger and more durable than conventional RSW spot welds [4, 5]. In brief, RFSSW has great potential to join a great number of structural components and industries have much to benefit from replacing mechanical joining or fusion welding in their processes. Therefore RFSSW techniques have recently received a great deal of interest from automotive and aircraft industries [6]. However, those industries are waiting this technology to be established as a safe and reliable process.

To meet quality standard from those industries, it is necessary that RFSSW produces sound and strong welds in a consistent manner. For this reason, data on processing parameters must be acquired and a great number of variables that affect the quality of weldments must be controlled. To achieve that, Design of Experiments (DoE) and Response Surface Methodology (RSM) are useful tools to optimize mechanical performance of welded joints, using laboratorial and material resources in an economic and thoughtful manner [7].

Moreover, DoE and RSM are useful tools to open an investigation on weld defects originated from inadequate parameters.

In order to properly apply RFSSW on AA, it is necessary to acquire data concerning three groups of factors: process parameters; microstructure and mechanical properties. With this data in hands, the scientific understanding of each group of factors and the interactive correlation between them are reached using the current knowledge available in bibliographic resources. The scientific information about this topic has grown in the past year and some papers have been published on the subject on different AA in similar and dissimilar joints [4, 8]. Although the interest on the topic has considerably risen, there are many gaps of knowledge to be filled. For instance, no publication has been produced regarding the occurrence of defects in aluminum alloys joined by RFSSW.

In this work, RFSSW of similar AA5754 - AA5754 and dissimilar AA5754 - AA6061 joints are studied in the point of view of materials science, concerning the occurrence of defects and the correlation between process parameters, microstructure and mechanical behavior.

2. OBJECTIVES

This work has two main objectives:

1. Evaluate the occurrence of defects by investigating RFSSW process parameters – tool rotational speed, feeding rate and plunge depth – and lap shear strength of 1.2 mm-thick AA5754-H22 and AA6061-T6 similar and dissimilar welds based on Box-Behnken experimental design (BBD) and RSM aiming to find an optimal welding condition that maximizes lap shear strength and fix the defects.
2. Study the metallurgical phenomena occurring during welding process that affect material properties and grain size, microstructure evolution and texture in welded samples.

3. LITERATURE REVIEW

3.1. AA5754-H22 and AA6061-T6

Aluminum alloys can be processed by many different ways such as rolling; wiring, extrusion, casting and welding making it one the most versatile industrial metals [9]. Due to their high ductility, they are also suitable for friction processing. This work will focus on the solid-state friction welding processing of similar and dissimilar AA5754-H22 and AA6061-T6 alloys.

The designation of four numbers is used by ANSI [10] and in various publications is issued by The Aluminum Association [11] to identify wrought aluminum alloys. The four numbers indicate which is the major alloying element. By this system, AA5754 is majorly alloyed by magnesium and AA6061 is majorly alloyed by magnesium and silicon [10].

The capital letters and numerals system provide significant information about the processing route of a given alloy and consequently its characteristics and properties. Specifically, the capital letter after the hyphen represents the heat or mechanical treatment. In the case of AA5754-H22, the letter “H” stands for products strengthened by strain hardening, with or without additional thermal treatment to produce some reduction in strength. The first numeral after the letter indicates the processing the alloy was subjected. The second digit indicates the level of strain hardening. In the case of AA5754-H22, the first numeral indicates that the alloy has been strain hardened and partially annealed and the second says it was rolled to one quarter of maximum hardness [10].

The 5xxx series are aluminum alloys containing magnesium (Mg) as the main alloying element. A large variety of resistances (80-350 kPa) can be achieved combining Mg and Mn [12]. The alloys from this series present a moderate-to-high-strength and are not heat-treatable. The 5xxx series alloys can be strengthened by solid-solution strengthening mechanism and cold-working. Other alloying elements such as chromium, manganese, and zirconium are added to control grain and subgrain sizes, which also contribute to strengthening [9].

AA5754 alloy is commonly used to manufacture structural sheet components exposed to corrosion environments including automotive and marine but it is also applied in nuclear and chemical industries [13]. In automotive applications, it is worth to cite the front sub-frame of Lotus Evora® chassis. This structure is responsible for holding the suspension, brakes, cooling and steering (Figure 3.1) and is mostly composed by riveted extruded tubes and rolled AA5754 sheets [14].

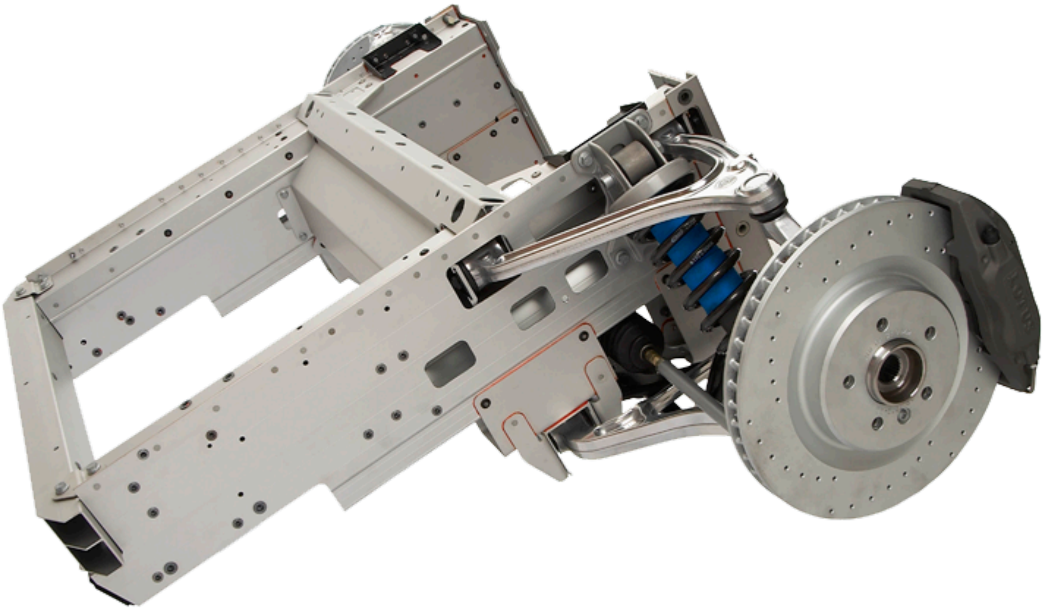

Figure 3.1 – Lotus Evora® chassis front sub-frame with brakes and suspension's system assembled [15]

The rivets in a car structure represent an extra weight to the final product that will produce more fuel consumption and a decrease in performance, which goes against the objectives of the manufacturer [16]. Therefore, an alternative joining method is desired to join the sub-parts of the structure. With that in mind, the RFSSW process is a potential substitute process for the riveting of car structures.

Jaguar® presented a concept car [17] composed by an entire recycled AA5754 structure as shown in Figure 3.2. The alloy is excellent to build inner car structures because of its good formability, which allow pieces to be formed into complex shapes without presenting major defects such as cracks and spring back effect [18].

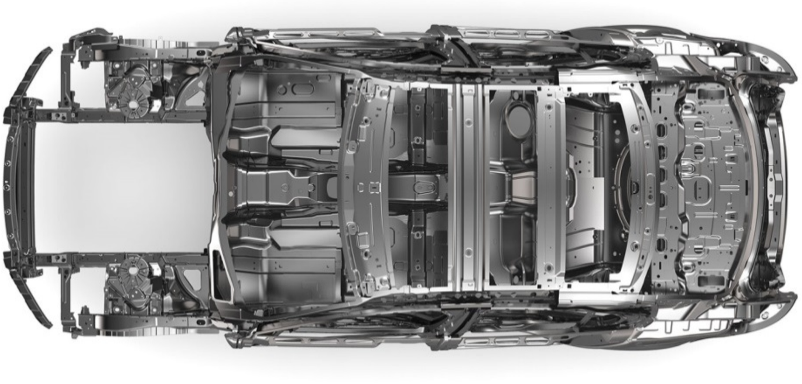

Figure 3.2 – Juaguar® XE body mostly built in aluminum [19].

The alloys from the 6xxx series have additions of Mg and Si as the main alloying constituents. The combination of Si and Mg leads to the occurrence of GP Zones precipitates, making those alloys hardenable by solution followed by precipitation. The fully coherent precipitate, β that occurs in these alloys is the Mg_2Si, whereas the semi-coherent, β" is Mg_5Si_6. Both precipitates have the shape of needles due to the different elastic strain energy in the directions of the matrix crystal lattice [20]. Age-hardenable alloys are severely affected by hot working processes due to the modification of semi-coherent precipitates. A large decrease of hardness can be measured in heat-affected zones of welded samples.

Alloys such as the 6061 present a balanced Mg/Si ratio and a better balance of properties. The Mg/Si ratio considered being balance is 1.73. Alloys whose ratio is less than 1.73 are defined as Si-excess alloys. Gupta et al [21] found out than an excess Si presented reduced time to initiate a strengthening response during aging. However, it leads to a reduction in ductility due to the precipitation of pure Si platelets [21]. Those platelets precipitate in grain boundaries and make the material more susceptible to intergranular fracture and corrosion. An excess of magnesium leads to a better corrosion resistance but lower strength and formability.

3.2. Microstructure evolution and dynamic recrystallization in aluminum alloys

RFSSW is a process that majorly deforms the material at high strain and strain rates. The heat generated during the process can make the material reach more than half of its melting temperature, leading to a change in the microstructure and properties of the welded material [22].

When high temperature and strain are involved, new grains are likely to form due to the reorganization of dislocations in a process referred to dynamic recrystallization (DRX) [23]. There are three different DRX mechanisms in metals: discontinuous dynamic recrystallization (DDRX), continuous dynamic recrystallization (CDRX) and geometric dynamic recrystallization (GDRX). DDRX normally occurs in low to moderate stacking fault energy (SFE) alloys, in which recovery is suppressed [24]. Aluminum alloys have high SFE because of directional bonding of its electronic structure [25], which makes the probability of undergoing DDRX very low. It has been suggested that solute atoms present in AA5754 and other Al-Mg alloys would decrease SFE and hinder metal ability to dynamically recover thus increasing the likelihood of DDRX [26]. However, there are no works in literature suggesting the occurrence of the phenomena in this alloy. Likewise, DDRX is not expected to occur to AA6061.

At elevated temperature, strain and strain rate, high SFE alloys undergo CDRX and GDRX as reported in literature [27–29]. Both mechanisms are driven by similar boundary conditions and result in a very fine equiaxed grain microstructure emerged from the subdivision of grains of larger initial diameter. A careful investigation carried out by Electron Backscatter Diffraction (EBSD) is usually necessary to determine which mechanism develops in the material. CDRX starts with the accumulation and entanglement of dislocations into low-angle grain boundaries (LAB) to form subgrains walls. As dislocation density intensifies, LABs progressively develop into high-angle boundaries (HAB) when the misorientation angle reaches a critical value, $\theta \approx 15^{\circ}$. The resulting microstructure is characterized by a collection of crystallites bound by low to high angle boundaries.

The other mechanism for dynamic recrystallization in aluminum alloys is GDRX. In GDRX, severe plastic causes the width of original grains to approach the dimension of sub-boundaries [30]. With further strain, HABs become perpendicular to the shearing plane and acquire a serrated shape. Kassner and McMahon [31] observed that the serration consists of two HABs (the serrated boundary) and one LAB. As deformation proceeds, the separation between the serrated boundaries at the opposite sides of the grain decreases making the total area of HAB to increase. The critical deformation is reached when the average width of the grain thins to approximately twice the sub-boundary width. At this point, the HABs begin contact each other at the serrations, causing grains portions (or subgrains) to “pinch-off”. When it occurs, one part of HABs is annihilated and the other remains stable with increasing strain. Roughly one-third of LAB that were within the grain becomes HAB when the grain boundaries “pinch-off” [30]. When a steady state is reached, the final recrystallized grain should be in a range of 1 to 6 μm depending on the strain rate.

In friction-stir processes (FSP), geometric and continuous DRX are important metallurgical phenomena that determine the microstructure of the final processed piece and therefore its properties. RFSSW can not only join dissimilar materials together but also make the processed zone stronger than the base material. Because of that, understanding CDRX and GDRX is critical to better develop strong welds.

3.3. Description of RFSSW

RFSSW, a cutting-edge technology invented in Helmholtz Zentrum Geesthacht [32] radically innovated spot welding. With a specially designed tool, the resulting surface of the weld is completely flat, as the weld cavity is completely refilled during the process. Three parts, being them the pin, the sleeve and the clamping ring, form the tool. The welding process can be programmed in many ways by controlling position, rotation and time for each movement step of the pin and the sleeve. In order to produce a weld between two overlapping sheets, it is necessary that the material be plunged by either the pin or the sleeve. Therefore, two main variants of the process arise based on the part that plunges the material:

The sleeve-plunge variant and pin-plunge variant. Previous works compared the performance between the two variants [3]. Although the pin plunge-variant consumes less energy and requires less power from the welding machine, sleeve-plunge produces wider and stronger welds [3].

In the sleeve-plunge variant of the process, the sheets are pressed against the clamping ring by a pneumatically driven actuator. Then, the rotating sleeve penetrates the sheets at specified time, plunge depth and rotational speed while the pin retracts, leaving space for the material to flow upwards. In this first stage, the high rotational speeds cause the material to heat and soften without reaching the melting point. In a second state, the tool returns to zero position as the rotating sleeve retracts whereas the pin pushes the material back to the weld cavity. Finally, the pressure against the clamping ring is relieved and the welding of sheets is finished. A better illustration of RFSSW process is shown in Figure 3.3.

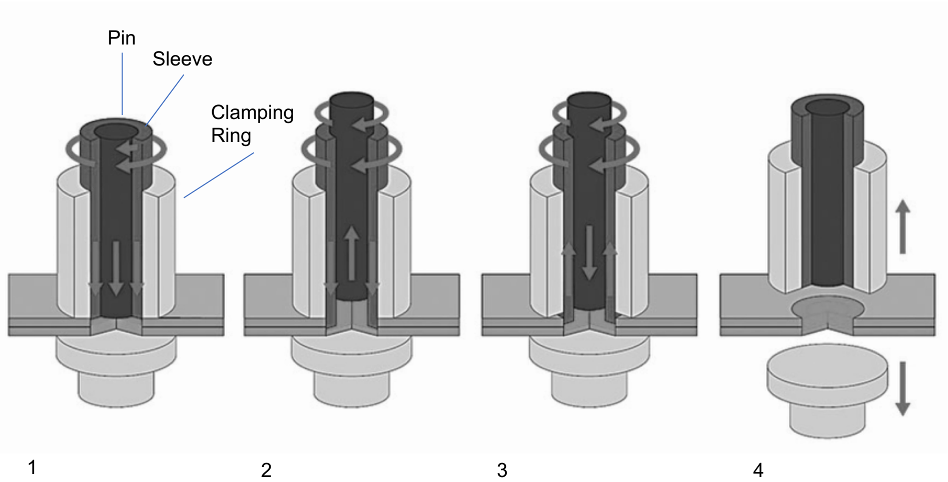

Figure 3.3 – Illustration of RFSSW process using sleeve plunge variant: (1) Clamping and tool rotation; (2) Sleeve plunge and the pin retraction; (3) Parts back to surface level; and (4) Tool removal.[33].

3.3.1. Process Parameters

Although different parameters can be used, Rotational speed (RS), plunge depth (PD) and feeding rate (FR) are the main parameters utilized in this work. Occasionally, clamping force (CF) can be varied to understand its individual effect. Different combination of these parameters can result in inadequate material flow and heat input, which can lead to defects and premature failure in welded samples [34]. A detailed description of each parameter is given below:

RS – angular velocity of the spin and sleeve during welding process rotations per minute (RPM). RS is directly related to material intermixing and heat input, which affect the microstructure in the stir zone (SZ) and thermomechanical affected zone (TMAZ) [34].

PD – Maximum depth the sleeve reaches during the welding process. It can surpass the thickness of one sheet and is directly related to weld strength and failure mode [35].

FR – Linear velocity of the tool during welding process. In former studies[44, 45], dwell time (DT), time during which the plunging tool is held at the desired PD, was commonly used as welding parameter. In this work, the process is made in a continuous manner, *i.e* the tool penetrates the workpiece and, as soon as it reaches the plunge depth, it immediately retracts. Lower FR is undesirable in a perspective of production efficiency and it is generally avoided. On the other hand, FR should be sufficiently low to allow the proper material intermixing and heat input.

CF- Force necessary to generate friction between tool and workpiece. It holds the sample against the backing plate during the welding process. It is also a source of decomposable hydrostatic stress state during the process, enabling the material to be subjected to high strains without cracking [38].

Previous studies reported that RFSSW is dependent on macrostructure features originated by process parameters. Tier et al [39] reported higher lap-shear strengths for lower values of RS due to larger bonded regions in the stir zone. However, other works found that low rotational speeds fail to deliver proper heat input to the process, thus leading to macroscopic defect and worse mechanical properties [48, 49]. PD is a parameter directly related to the amount of energy transferred from the machine to the workpiece and to the total volume of sheared material. FR is related to the total welding time. Longer times have a tendency to activate recrystallization and modify material microstructure, which in many cases are detrimental. Usually, shorter times are preferred in a production efficiency perspective .

3.3.2. Characterization of the weld zone

RFSSW introduces severe plastic deformation and high temperatures to the base material, which affects the character of grain boundaries, precipitates and texture within and around the stirred zone [22].

The welded sample observed in an optical microscope, after proper polishing and etching, can be divided into four distinct key zones: stir zone (SZ), thermomechanical-affected zone (TMAZ), heat-affected zone (HAZ) and base material (BM), the latter displaying no modification coming from the process. SZ comprises the material directly mixed by the spinning of the tool and is subjected to the highest degrees of strain (ε), strain rates ($\dot{\varepsilon}$) and temperature (T), which causes the manifestation of dynamic recrystallization phenomena. TMAZ is a circumferential layer of material that involves the sleeve periphery and is also subjected to high degrees of ε, $\dot{\varepsilon}$ and T but rapidly decrease as we move in the direction of BM. HAZ is not always easy to detect by observing under the microscope, but hardness measurements can often reveal it. Finally, BM here is defined as the portion of the sample not affected by the welding process and therefore is identical to the as-received material condition. The four zones can be distinguished in Figure 3.4.

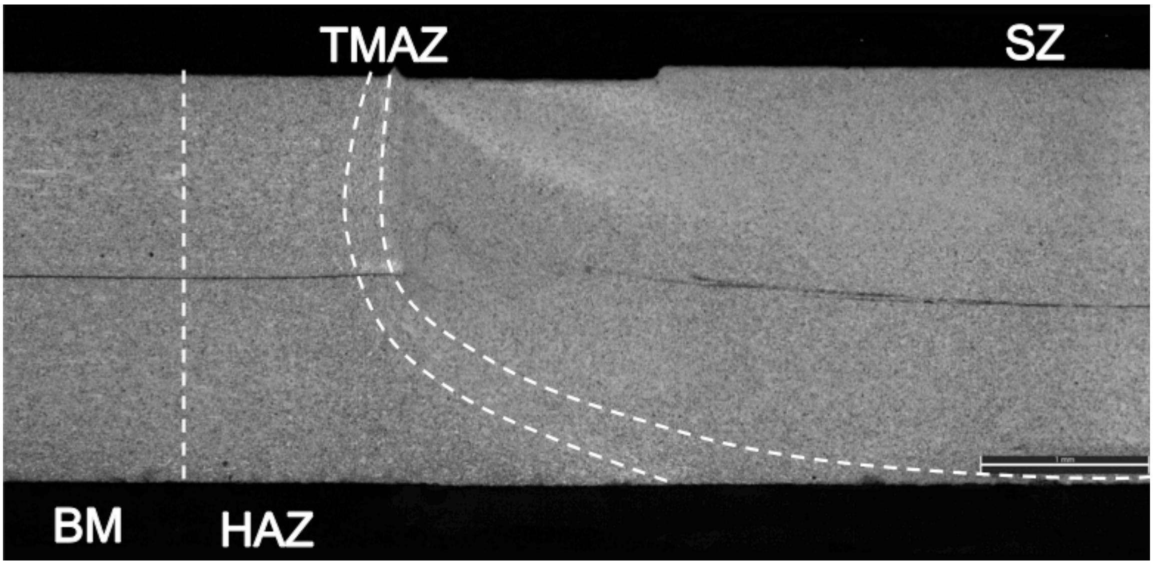

Figure 3.4 – Four typical zones in a RFSSW cross section.

3.3.3. Defects in RFSSW

Many typical defects are usually found in samples welded by RFSSW. Some, like the “hook” are inherent to the process and very difficult to eliminate, even though they can be studied and minimized. Many works correlate geometric aspects of the hook and mechanical properties [44, 51–53]. Nevertheless, depending upon the materials, the presence of pores, cracks and refilling defects in the weld represents, due to its size, a much more critical stress concentrator than the hook itself. Figure 3.5 shows typical defects visible when analyzing a etched cross section of a RFSSWed sample [45]. Although those defects may not be visible on the surface of the weld, they can cause premature failure, and therefore it is very important to study the underlying phenomena that produce them.

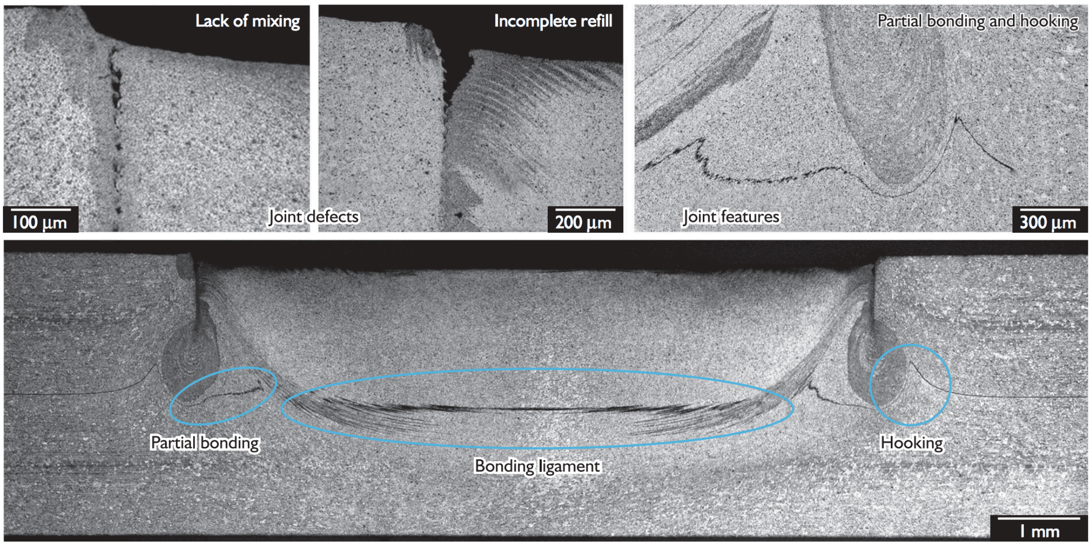
Lack of mixing
Incomplete refill
Partial bonding and hooking
100 µm
Joint defects
200 µm
Joint features
300 µm
Partial bonding
Bonding ligament
Hooking
1 mm

Figure 3.5 - Macrographs of a typical RFSSW joint cross section showing weld defects [45].

The existence of large defects is usually linked with inadequate process parameters and material flow inside the weld cavity. Previous works [42, 55] attributed the occurrence of voids to different circumstances that dictate material flow in the TMAZ/SZ. Xu et al. [47] also reported incomplete refilling and void defects in RFSSW of 2 mm 5083-O aluminum sheets. They attributed those defects to an insufficient flow of the SZ material at the refilling stage. Once the material does not reach a sufficiently high temperature due to lower friction-al heat, its flowability is reduced resulting in not being able to fill the corners of the welding cavity. Another cause of insufficient refilling proposed by Song et al. [18] and hold by Xu et al. [47] is the weak metallurgical bonding effect and heat residual stress after welding. The different temperature cycles between TMAZ and SZ materials lead to residual stresses in TMAZ/SZ interface, which may cause the defects. Song et al. [34] suggested that the interface could be torn apart if the residual stresses exceed the bonding strength. Material loss during welding procedure is also pointed as a factor that contributes with insufficient refilling [34].

3.4. Design of Experiments

In order to carry out an investigation on process parameters and mechanical performance, it can be used mathematical tools to build regression models. RSM is a powerful regression modeling technique that enables the development, improvement and optimization of the process by offering the evaluation of the synergistic effects of a set of experimental factors on a response output. The methodology involves the input of data from an experimental design such as full-factorial, Taguchi or Box-Behnken [48].

In the current work, a DoE and BBD were utilized, given the requirement of analyzing quadratic relationships and the lowest possible number of necessary experiments. This design additionally shows no combination of extreme parameter settings due to a non-observance of the design space edges, which might cause an unstable welding process (Figure 3.6) [49].

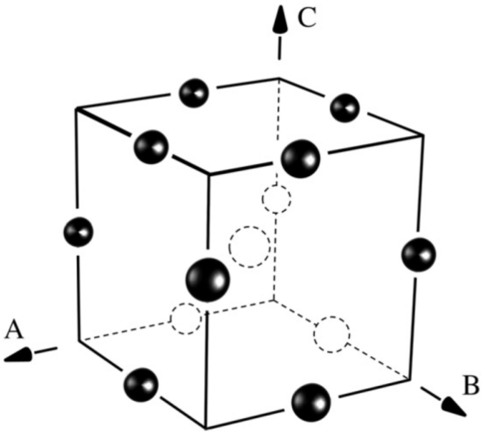

Figure 3.6 – Scheme of the Box–Behnken design for three factors [49].

In RSM, a least-square algorithm built is used to find the coefficients that maximize the correlation between experimental data and the fitting curve. A quadratic model according to Equation 1 is used [48].

$$y = \beta_0 + \sum_{i=1}^{k} \beta_i x_i + \sum_{i=1}^{k} \beta_{ii} x_i^2 + \sum_{i=1}^{k-1} \sum_{j=2}^{k} \beta_{ij} x_{ii} x_j + \epsilon \tag{1}$$

where y is the process response or output (dependent variable), k is the number of patterns, i and j are the index numbers for pattern, β_0 is the free or offset term called intercept term. $x_1 . x_2 . \cdots . x_k$ are the independent variables, β_i are the coefficients of the first-order (linear) main effect, β_{ii} are the coefficients of the quadratic (squared) effect, β_{ij} are the coefficients of the interaction effect, and ε is the random error or allows for discrepancies or uncertainties between predicted and measured values [48].

After the curve is fitted, it is possible to plot three-dimensional surfaces fixing one factor at the middle level. Parallel to this, an Analysis of Variance (ANOVA) is run to evaluate the fitting of the model, extracting information such as correlation, F-test statistics and p-value. Significance levels (α) are set at 5% level using the p-value test. ANOVA provides quantitative information about the fitting whereas the surface enables us to see the contribution of factors by observing the declivity and twisting of the curve [7].

4. MATERIALS AND METHODS

The experimental procedure of the present work is presented in this chapter. Figure 4.1 shows a flowchart with those experimental activities. The work started with defining parameter windows for the similar and dissimilar welds of AA5754-H22 and AA6061-T6 sheets with the dimensions of 120 × 30 × 1.2 mm produced by Refill Friction Stir Spot Welding. Next, DoE in the form of BBD is designed and executed and samples are tested for LSS. The results are optimized and analyzed with RSM and ANOVA. Further optimization is carried out with OFAT, from which samples and test specimens were welded and prepared for mechanical and metallurgical characterization in order to optimize weld strength, investigate the occurrence of defects and analyze the behavior of material flow. Metallurgical visualization was performed via microscopic analyses with polarized light

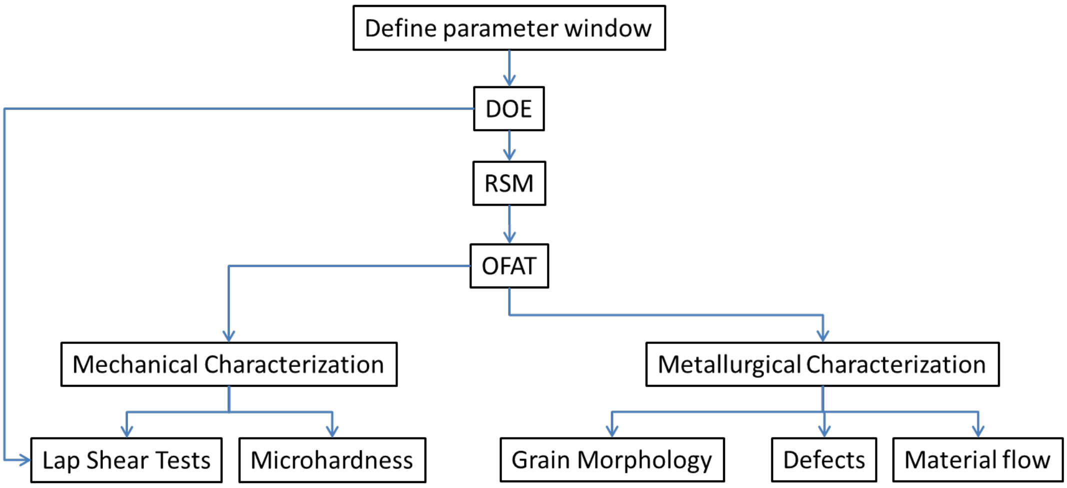
Define parameter window
DOE
RSM
OFAT
Mechanical Characterization
Metallurgical Characterization
Lap Shear Tests
Microhardness
Grain Morphology
Defects
Material flow

Figure 4.1 - Flowchart of the experimental activities.

4.1. RFSSW Equipment

All the friction spot welds were executed using a Harms Wende RPS100® machine owned by and located in HZG. The interface software of this equipment allows the programming of the rotational speed of both pin and sleeve, as well as the plunging depth of the tool and the time interval of each stage. This machine has a maximum clamping force of 20 kN, a maximum rotational speed of 3300 rpm and a maximum torque of 14.5 N.m. The tool used to perform the RFSSW welds has three components: the pin with 6 mm of diameter; the sleeve, with 9 mm of outer diameter and outer grooves for better material mixing; and the clamping ring with 18 mm of outer diameter. The tool set is shown in Figure 4.2.

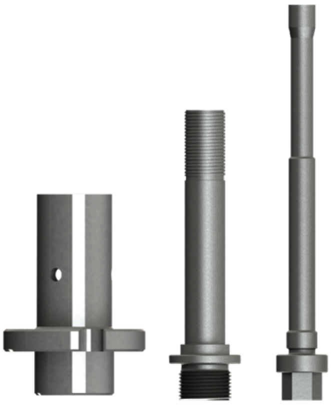

Figure 4.2 – RPS 100® tool set.

4.2. Welding of the Samples

4.2.1. Materials description

AA 5754-H22 and AA 6061-T6 alloys have been provided by TWI in the shape of (110 × 30 × 1.2) mm sheets. Chemical composition was determined in a Spectromaxx® optical emission spectrometer, the results are displayed in Table 4.1

Table 4.1 – Chemical composition of the supplied materials

	Al	Si	Fe	Cu	Mn	Mg	Cr	Zn
AA5754	bal	0.193	0.423	0.026	0.245	2.810	0.018	0.005
AA6061	bal	0.570	0.485	0.218	0.131	0.870	0.182	0.048

Mechanical properties as found in literature are displayed in Table 4.2.

Table 4.2 – Mechanical properties of the supplied materials [50].

	Ultimate Tensile Strength (MPa)	**Brinell Hardness**	**Young Modulus (GPa)**	**Elongation at Break (%)**
AA5754	240	63	68	8.4
AA6061	310	93	69	10

4.3. Specimen preparation

The specimens were produced at HZG by RFSSW process in a lap-shear configuration with 30 mm overlap, as shown in Figure 4.3.

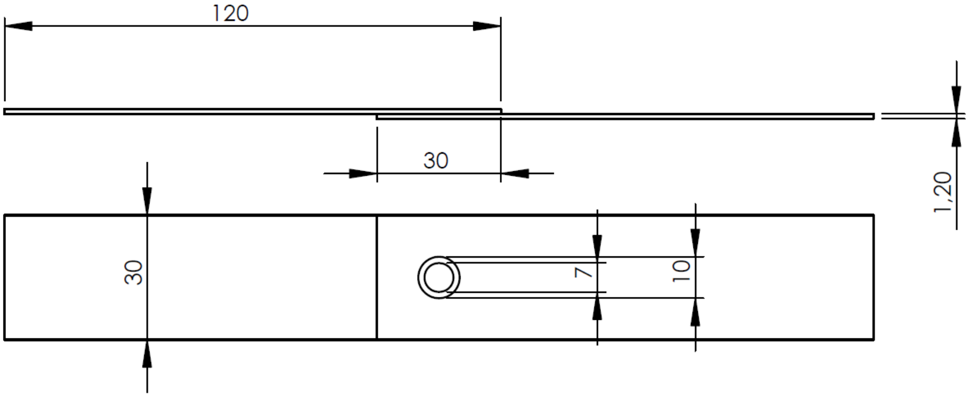

Figure 4.3 – Schematic representation of the friction spot lap weld configuration.

The lap-shear sample is designed to evaluate both tensile and shear joint strength, as the joint rotates during loading due to the low stiffness of the metal sheet [51].

4.4. DoE and RSM

The process parameters, RS, PD and FR were varied on three different levels (-1, 0, 1) according to BBD methodology. Through this, 13 combinations with widely varying lap-shear strength were produced. In order to estimate the variance of the experiment within each treatment (sample), a triplicate of the central point was required. This leads to 15 welds, organized and randomized by Minitab® according to Table 4.2. The specimens were welded according to the parameters and tested for maximum Lap Shear Strength (LSS) in a screw-driven Zwick/Roell® testing machine.

After finding the surface region for which the LSS is the highest, a one-factor-at-a-time (OFAT) approach was performed to extend the investigation. In this method, two parameters are fixed and one in varied form a central point, which is chosen as the parameters that provide the best LSS results .

Table 4.3 – Welding combination according to Box–Behnken design [52]

Combination	Rotational speed (rpm)	Plunge depth (mm)	Feeding rate (mm.s^{-1})
1	-1	0	0
2	-1	1	0
3	0	0	0
4	0	1	-1
5	1	-1	0
6	-1	0	1
7	1	0	1
8	1	0	-1
9	1	1	0
10	0	0	0
11	0	1	1
12	0	-1	1
13	0	0	0
14	0	-1	-1
15	-1	-1	0

4.5. Mechanical Characterization – Lap Shear and Microhardness

Welds were tested for LSS. The clamping area of the specimen covers a 30 mm × 30 mm square as required in ISO14273 [53], a test standard for resistance spot and embossed projection welds, as there is no specific standard for lap-shear testing of friction spot-welds. This Microhardness measurements were performed in weld cross sections to evaluate the change of properties in different weld zones.

4.5.1. Microhardness testing

Microhardness was measured along the weld section as shown in Figure 4.4.

In this work, a Zwick/Roell-ZHV® machine was used. A conventional indenter with 0.2 Kg and load time holding for 10 seconds was applied. The microhardness was used to measure the hardness profile along the weld region and its surroundings in order to characterize the BM, HAZ, TMAZ and SZ. A major advantage of this test is the possibility of reusing the sample for other analysis; due to the minimal dimension of indentation (roughly 100 μm), the sample can be repolished and tested again. Another advantage of using microhardness is that it allows to map the hardness of an entire analyzed area, or direction, giving to the experimenter a broader comparative vision of the internal stresses of the material.

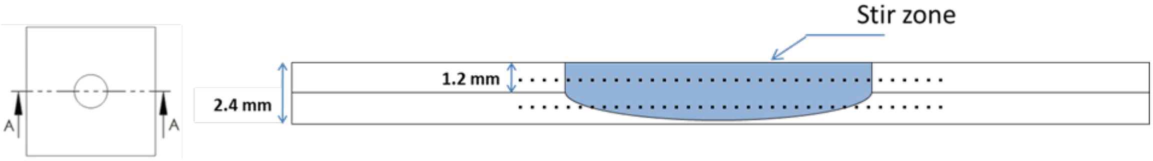

Figure 4.4 – Representation of microhardness measurements.

4.6. Metallurgical characterization

4.7. Sample preparation

The preparation of samples for metallurgical characterization was performed in four main steps: samples welding; cutting; embedding; grinding/polishing and etching.

4.8. Stop-action experiments

Stop-action experiments were performed at HZG. Samples were cut, embedded and polished for metallurgical evaluation. The stop-action experiments are a method of observing events taking place in the transition intervals between RFSSW process steps. The idea of this technique is to interrupt the welding process at determined plunge depths in order to produce samples of the transitory state of the weld. The following method was used:

- Picking the best set of welding parameters from lap-shear results to produce welding samples;

- Choose plunge depths at which the process will be interrupted;
- Re-program welding steps in RPS100® to insert a short dwell time after the desired plunge depth;
- Monitor sleeve path in RPS100® software and press emergency button right after the tool dwelling starts;
- Quenching sample in cold water and remove from tool;

5. RESULTS AND DISCUSSION

5.1. Results from similar AA5754-H22 RFSSW

5.1.1. DOE and RSM

BBD was used to design RFSSW experiments. Three factors, RS, PD and FR were used in three levels as shown in Table 5.1.

Table 5.1 – Factors and levels for DOE

Factor	Level 1	Level 3	Level 3
RS	1800	2400	3000
PD	1.1	1.3	1.5
FR	3	3.5	4

It was performed one replicate per parameter set, except for the central set, for which three replicates were made. The fifteen combinations of factors were organized and randomized by Minitab® software, according to Table 5.2. The specimens were welded according to the parameters and tested for maximum Lap Shear Strength (LSS), which was the response variable in DOE. The results from Lap Shear Testing (Table 5.2) were inserted back into the software in order to generate ANOVA. To compare the LSS results, a three-way ANOVA F-test was used. Significance levels, α were set at the 5% level using the p-value test. The ANOVA results are shown below in Table 5.3.

Table 5.2 – Experimental conditions and results

Exp. No	RS (RPM)	FR (mm/s)	PD (mm)	LSS (N)
1	1800	3.00	1.3	5053.09
2	1800	3.50	1.5	5335.41
3	2400	3.50	1.3	4625.39
4	2400	3.00	1.5	5307.67
5	3000	3.50	1.1	3732.93
6	1800	4.00	1.3	4674.24
7	3000	4.00	1.3	4018.44
8	3000	3.00	1.3	4501.47
9	3000	3.50	1.5	4749.48
10	2400	3.50	1.3	4673.93
11	2400	4.00	1.5	4889. 14
12	2400	4.00	1.1	4149.01
13	2400	3.50	1.3	4785. 16
14	2400	3.00	1.1	3887.81
15	1800	3.50	1.1	4110.01

Table 5.3 – ANOVA from the results of similar welds

Source	DF	Adj SS	Adj MS	Contribution [%]	P-Value
Model	9	3348302	372034	97.559	0.002
Linear	3	3140831	1046944	91.514	0.000
RS	1	588847	588847	17.157	0.002
PD	1	2422135	2422135	70.574	0.000
FR	1	129849	129849	3.783	0.039
Square	3	78344	26115	2.283	0.309
RS.RS	1	40503	40503	1.18	0.181
PD.PD	1	43176	43176	1.258	0.169
FR.FR	1	2953	2953	0.086	0.692
2-Way Interaction	3	129127	43042	3.762	0.167
RS.PD	1	10905	10905	0.318	0.456
RS.FR	1	2714	27 14	0.079	0.704
PD.FR	1	115509	115509	3.366	0.047
Error	5	83772	16754	2.441	.
Lack of Fit	3	70353	2345 1	2.05	0.230
Pure Error	2	13419	6709	0.391	
Total	14	3432074			

It is apparent from this table is that the four lowest results are linked to the plunge depth of 1.1, indicating a significant detrimental effect to the LSS. Indeed, ANOVA shows a p-value for PD of 0.000, which is a strong evidence that PD has a high influence on LSS.

Furthermore, it can also be verified by ANOVA that p-values for all the three factors, independently, were lower than 0.05, meaning that there is a very small likelihood of mistakenly assuming that all linear factors have direct influence on LSS. It is then assumed the hypothesis that all factors independently contribute on LSS. On the other hand, p-values for square interactions are all above the significance of 0.05, which is the criterium for not rejecting the hypothesis that there is no square dependence of factors on LSS (null hypothesis, μ_{Sq})

The null hypothesis for the two-way interaction is also not rejected except for the one between PD and FR, as it presented a p-value less than α .

It is possible to conclude so far that all the factors, if taken independently, are very likely to affect the resistance of the weld. The same level of certainty is not possible to be assumed when considering a square or 2-way interaction.

A regression model was calculated by the software from the experimental data. The model is given by Equation 2 below:

$$\begin{aligned} LSS(RS, PD, FR) & \\ &= -4765 - 0.4522 \times RS + 8699 \times PD + 1954 \times FR \\ &- 1699 \times PD \times FR \end{aligned} \tag{2}$$

In order to evaluate the fitting of the model into experimental data, the experimental and predicted values for LSS were plotted in Figure 5.1. Predicted values fit the experimental data indicating a good fitting of the model ($R^2 = 0.976$).

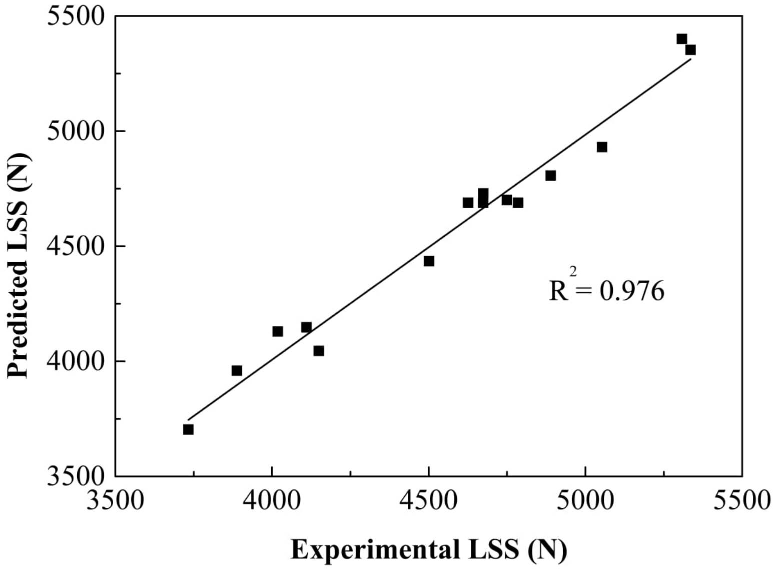

Figure 5.1 – Expected versus predicted LSS according to RSM

By keeping one factor fixed at a time, it is possible to graphically visualize the effect of two combined factors on LSS in a contour plot and give a practical meaning for the analyzed statistics. Figure 5.2 shows the response surface generated by Equation 2.

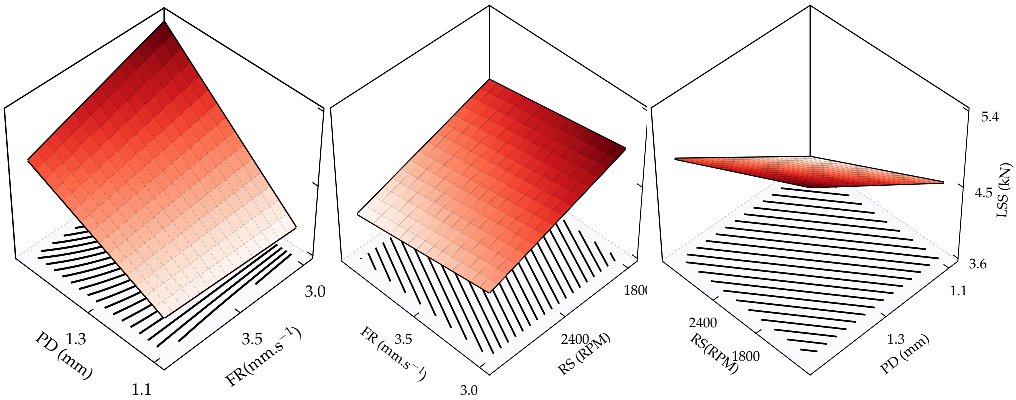

Figure 5.2 – Effect of combined (A) FR and PD; (B) FR and RS; (C) PD and RS on LSS of welded joints

Figure 5.2 shows clearly that LSS reaches its maximum for the following set of parameters: [RS = 1800; D = 1.5; FR = 3.0]. That is, LSS is maximized when rotational speed and feeding rate are minimized and plunge depth is maximized. Furthermore, it can be observed on the direction of the color gradient that plunge depth plays a major role on LSS. Indeed, the ANOVA shows the substantial contribution of PD on LSS (70.57%). However, the other factors, RS and FR do not influence the weld strength in a substantial manner, as there is a low variation of color gradients in RS and FR axis direction.

It is also possible to observe that the hyper-surfaces are presented as flat surfaces (planes) instead of curved surfaces such as parabolic and hyperbolic surfaces, indicating the much stronger influence of the linear part of the model compared to the interactional and square parts. Indeed, ANOVA confirms this overwhelming contribution of the linear part, 91.514% compared to 2.283% and 3.762% respectively to the square and two-way interaction parts.

In a previous work, Suhuddin et al [54] worked on a series of experiments designed with Taguchi DoE method using similar welds of AA5754 produced with RFSSW on 2 mm rolled sheets. The factors considered were RS, PD and DT (time for which the tool remains rotating in the plunging position). DT is a factor analogous to FR, as both, together with PD, describe the total welding time of a sample, which in turn, will directly affect the weld microstructure. The strength of the weld was also measured by Lap-Shear Tests. ANOVA indicated that Plunge Depth was not a significant factor in LSS being the least contributing factor with only 5.35% of contribution to LSS. Furthermore, other factors as RD and DT, showed to be the most contributing factors. Those results go in an opposite direction to the one found in the present work as PD was shown to have the greatest influence on LSS, whereas RS and FR showed to be the least contributing factors.

Further studies should be done in order to investigate the source of those differences. Apparently, the thickness of the sample might be an important factor to contribute to weld strength. There is also the possibility that PD is not a significant factor when worked together with DT instead of FR.

5.1.2. One-Factor-At-a-Time method

The following subsection moves on to describe in greater detail the optimization by OFAT approach. This method consists on changing one single parameter at a time while keeping the others in a predetermined central position. The central position is usually chosen as the combination of parameters that produce the best LSS results in DOE. In this work, the best LSS result was observed for the following set of parameters:

$$S_1 = [RS = 1800; PD = 1.5; FR = 3.5]$$

which showed an LSS of 5335 N, however, according to RSM, the weld strength should reach its maximum at:

$$S_2 = [RS = 1800; PD = 1.5; FR = 3.0]$$

which had not been tested in the initial DoE. To distinguish between these two possibilities, it was necessary to test the hypothesis of S_2 being the best set of parameters. At the same time, S_1 had its reproducibility tested. Therefore, three replicates were tested for S_2 and two more replicates were produced and tested for S_1 condition. The results for LSS, including average and standard deviation are shown in Table 5.4below.

Table 5.4 – Reproducibility tests for optimum result from DOE and evaluation of optimum parameters from RSM

	S. Number	**RS [RPM]**	**PD [mm]**	**FR [mm/s]**	**LSS [N]**	**Average [N]**	**STDV [%]**
S_1	16				5077		
	17	1800	1.5	3.5	5180	5197	2.5
	2				5335		
S_2	18				5172		
	19	1800	1.5	3	5167	5143	0.9
	20				5088		

S_2 showed good reproducibility and high values for LSS, which is in accordance with RSM prediction. The average of LSS for S_2 is slightly lower than S_1 even though its standard deviation is lower, meaning a better accuracy.

S_1 was chosen as the favorite to be the central point for OFAT because of its higher feeding rate compared to S_2. The higher feeding rate means a shorter welding time and thus a better productivity in an industrial process. Sample S_1 will be referred from now on as O, for Optimum.

After having chosen the central point (O), it was determined two new levels of variation for each parameter in a way that one level would be outside the RSM domain and the other step inside. By this approach, it is possible to measure how accurate the RSM can be for predicting LSS values outside its parameters domain and how reliable it is for calculating the expected results for a certain combination of parameters. By choosing OFAT it is also possible to find out if the vicinity of the chosen central point presents a better performance than the central point itself. It also makes the comparison between weld microstructure more feasible as it makes possible to compare the effect of changing each factor individually on the weld microstructure while keeping the other factors fixed.

Six conditions of parameters A; B; C; D; E; F with three replicates each were prepared and tested for LSS. Table 5.5 displays the combination of parameters in which RS was changed by ±600 RPM (A and B and the comparison with the optimum parameter, O). The results show that O has remained as the best combination of parameters, however the B condition also showed good results. This was expected as the B condition is inside the domain of the RSM. The A condition showed, however, a large deviation (8.6%) thus indicating that the obtained result is discrepant from the one predicted on the model. The A condition had a lower performance than predicted RSM (4902 N against the predicted 5365 N). A preliminary analysis of this result shows that, out of the original DOE window, a low value of RS may have a detrimental effect on weld strength. The OFAT method for the RS confirms the fidelity of the model for values comprised with the DoE parameter window, but discrepancies are found for RS values out of it.

Table 5.5 – OFAT results for rotational speed

Condition	Sample No	RS [RPM]	PD [mm]	FR [mm/s]	LSS [N]	Average [N]	STDV [%]	RSM Value [N]	Dev [%]
A	18 19 20	1200	1.5	3.5	4993 4908 4805	4902	1.9	5365	8.6
O	16 17 2	1800	1.5	3.5	5077 5180 5335	5197	2.5	5353	2.9
B	21 22 23	2400	1.5	3.5	5170 5089 5231	5163	1.4	5132	0.6

Table 5.6 compares the effect of the individual change of PD on LSS. Once again, the model shows good accuracy to predict LSS values for combinations of parameters inside the original DoE parameter window. C condition shows a low but fortunately positive deviation (4.2%) from the LSS result predicted on the model. Condition D, among all the other conditions, presented the lowest LSS and the greatest negative deviation from the model (15.6%) which indicated that plunge depth is also detrimental when values are too high. This result is especially useful for further investigation to find an optimization point, comprised in a PD range between 1.5 and 1.7. Another observation that can be made from the D condition is that the standard deviation for this result was also high compared to the other combinations, meaning a higher level of uncertainty of the mechanical behavior of the weld. Certain that the used equipment for producing and testing the welds have a good accuracy, the higher uncertainty of this condition is likely to be linked to its microstructure, or more precisely, to its microstructural defects such as the ”hook” and voids that occur due to lack of material filling. In order to discover the reasons for this unexpected result, a more profound investigation has been executed to find microstructural defects that can explain the low performance of the D condition. The results of the mentioned investigation are presented in Section 5.1.3.

Table 5.6 – OFAT results plunge depth

Condition	**Sample No**	**RS [RPM]**	**PD [mm]**	**FR [mm/s]**	**LSS [N]**	**Average [N]**	**STDV [%]**	**RSM Value [N]**	**Dev [%]**
C	24 25 26	1800	1.3	3.5	5203 4996 4986	5062	2.4	4853	4.2
O	16 17 2	1800	1.5	3.5	5077 5180 5335	5197	2.5	5353	2.9
D	27 28 29	1800	1.7	3.5	4994 4560 4706	4753	4.6	5632	15.6

Table 5.7 presents the results for the OFAT method on the single variation of FR and its effects on weld performance. In this case, the combination of parameters comprised within the RSM domain (E) challenges the reliability of the model to predict LSS. The E combination, comprised in RSM domain, showed a high deviation from the model (8.1%). On the other hand, the F condition, whose combination of parameters steps outside RSM domain, presented a low deviation (0.3%). This shows that FR might be the parameter that influences weld strength the least.

Table 5.7 – OFAT results feeding rate

Condition	**Sample No**	**RS [RPM]**	**PD [mm]**	**FR [mm/s]**	**LSS [N]**	**Average [N]**	**STDV [%]**	**RSM Value [N]**	**Dev [%]**
E	30 31 32	1800	1.5	3.0	5167 5167 5088	5141	0.9	5596	8.1
O	16 17 2	1800	1.5	3.5	5077 5180 5335	5197	2.5	5353	2.9
F	33 34 35	1800	1.5	4.0	5120 5224 4871	5072	3.6	5055	0.3

In order to better illustrate the effect of the individual change of each parameter, Figure 5.3 summarizes the results from OFAT experiments. Once again, it is possible to see that FR has no much effect on LSS, whereas RS and PD graphs present severe slopes showing big influence on LSS.

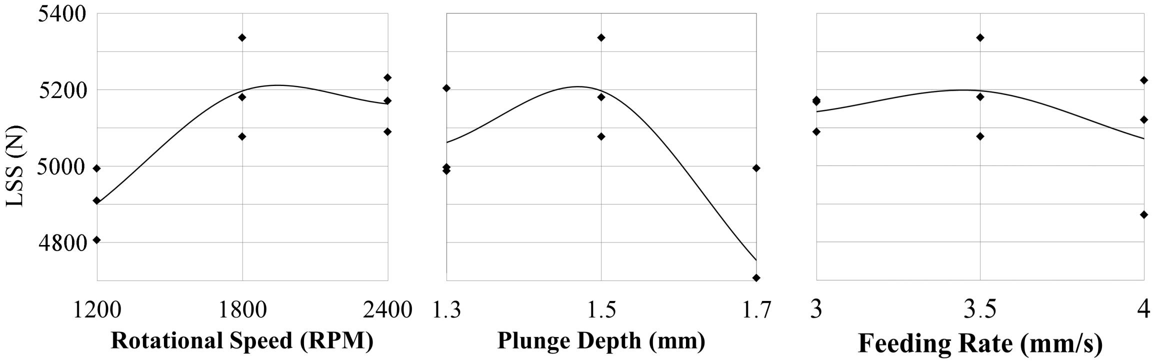

Figure 5.3 – Summary of OFAT results

5.1.3. Weld Characterization and Microstructural Analysis

The conditions A to F and the optimum condition, O were welded for microstructural analysis. Each condition was replicated in order to guarantee the consistency of the hook shape. The macrographs of all the welded conditions are displayed in Annex. This section will first cover the following results:

- the characterization of the weld, including base material; heat affected zone and stir zone;
- the observations regarding the occurrence of volumetric defects with special attention to the hook's shape including measurements of the hook height and bonded width.

5.1.3.1. Weld Characterization

In Figure 5.4, the etched polished cross section of an O - condition sample is shown. The four distinct zones are readily identified: SZ (D); TMAZ (C); HAZ (B) and BM (A). BM is distinguished for its elongated grains, which were originated during the rolling process, reminding that the AA5754 material had been rolled up to a quarter of maximum hardness.

HAZ (B) stands out by the equiaxed grains that could have been formed from recrystallization because welding thermal cycle that this region undergoes. As those grains are subjected to static stress from the clamping ring while a considerable amount of heat from the processes is flowing, dynamic recovery and dynamic recrystallization processes are possible mechanisms for changing grain shape. However, RFSSW is a process occurring in very short times (1-2 s), which is a counterargument for the hypothesis of static recrystallization (SRX).

TMAZ (C) is characterized by finely recrystallized grains which are formed due to a moderate frictional heat and strain rate [55]. The boundary of TMAZ and SZ is clearly distinguished for the variation in grain size in the surroundings of the sleeve-plunge region. The periphery of SZ is subjected to high frictional heat and plastic deformation during the welding cycle causing an increase of the recrystallization rate and thus the formation of new grain boundaries.

SZ (D) is characterized by fine equiaxed grains distributed in an axisymmetric pattern generated by material flow during RFSSW.

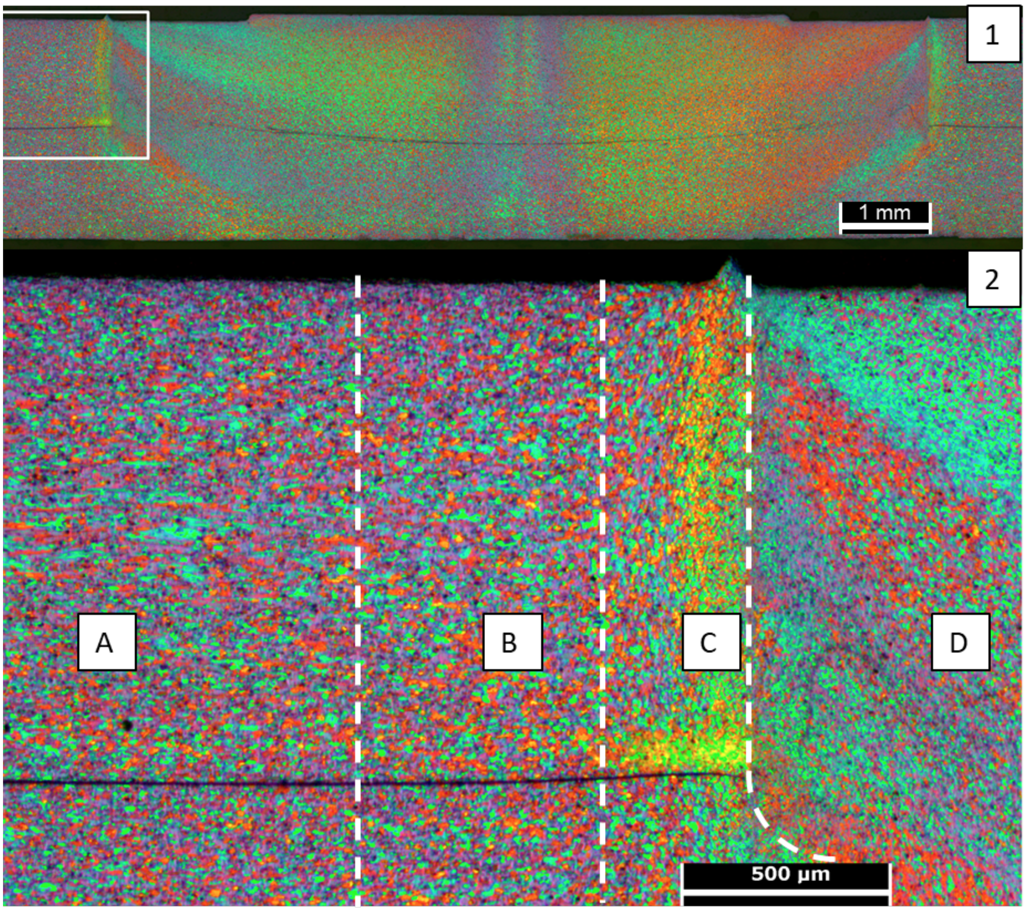

Figure 5.4 – Macrograph of the cross section of condition O (1) and a higher magnification (2) showing four different regions of the weld cross section. BM (A), HAZ (B), TMAZ (C), SZ (D).

5.1.3.2. Microhardness across weld section.

Figure 5.5 shows the microhardness profile measured along the cross section of condition O revealing three distinct zones SZ, HAZ and BM. The weld has lower Vickers microhardness in the SZ and HAZ than the base material. The SZ (distance from weld center of -4.5 – 4.5 mm) has an average microhardness of 67 HV0.2. HAZ is distinguished for an increasing hardness gradient towards SZ. The material in HAZ has experienced a thermal cycle and the mechanical properties have been modified due to the decline of dislocation density. The thermal cycle could also make grain boundaries in HAZ to rearrange themselves forming new equiaxed grains as shown in Figure 5.4. The SZ hardness recovery is due to recrystallization of very fine grain structure, during RFSSW, which eliminates some or all the cold work effects of the as rolled BM microstructure meaning that dislocation density is considerably dropped in those regions.

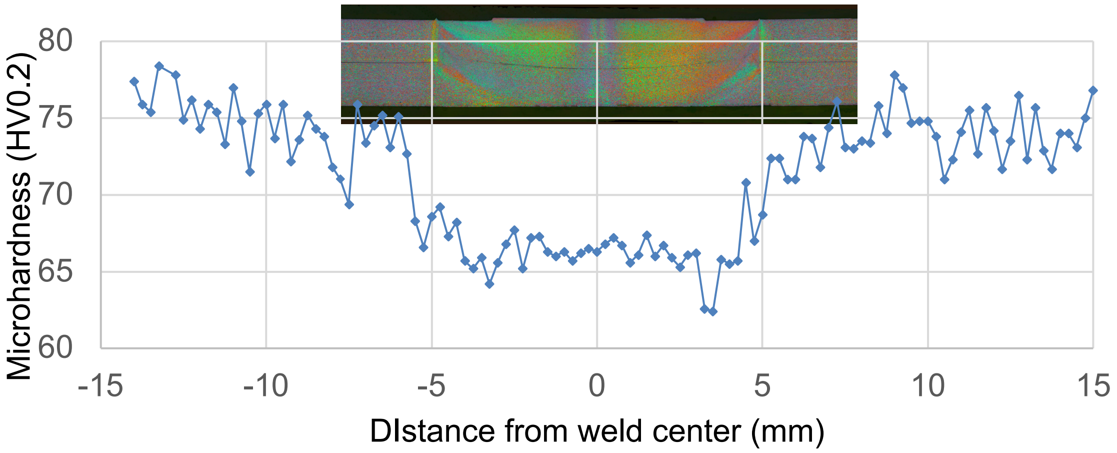

Figure 5.5 – Hardness profile across the weld

5.1.3.3. Hook characterization

The Hook is a common geometric feature appearing in the interface of overlapping RFSSW welds [35]. This kind of defect is usually formed in the region where the sleeve had been plunged and below the gap between the clamping ring and the sleeve. The hook is formed due to the upward bending of the overlap interface caused by the tool penetration into the bottom sheet. As the tool penetrates and cause the material to flow, the interface comprised of an oxide layer bends and, in some cases, breaks, separating the interface. In Figure 5.6 , the hook in condition O is shown and it is possible to see the bonding ligament and a part of the hook that is bonded downwards.

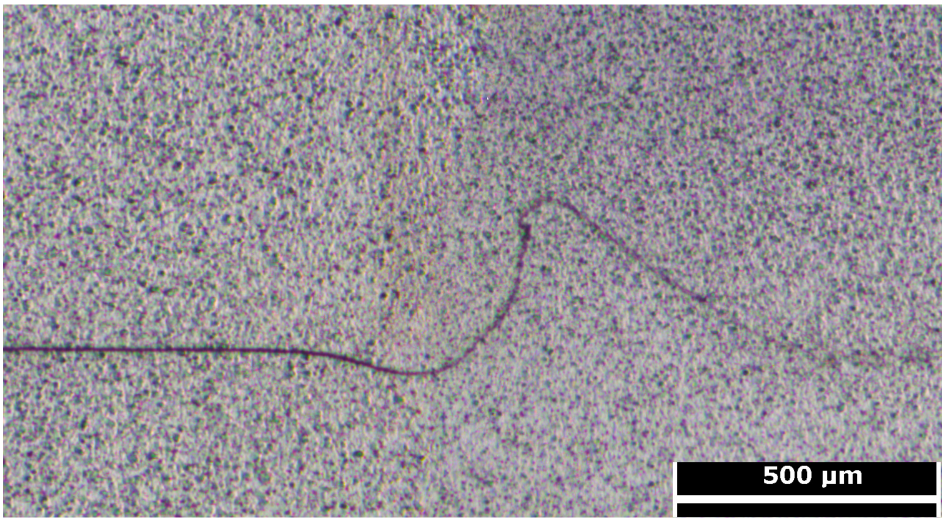

Figure 5.6 – Hook defect.

There is a large volume of published studies describing the Hook as the starting site for crack initiation and propagation [56]. Depending on the direction that the hook points at, different fracture behaviour can happen. Campanelli et al. [57] studied the fracture behavior in similar material overlap joints. In his work using FEM, similar material joints were simulated for the lap-shear test. The simulation has shown that the loaded specimen presents a positive tension field just above the separation line between the sheets. Furthermore, the fixed sheet presents, in a symmetrical manner, the same positive tension field just below the separation between the sheets. In Figure 5.7, it is shown what have been explained above.

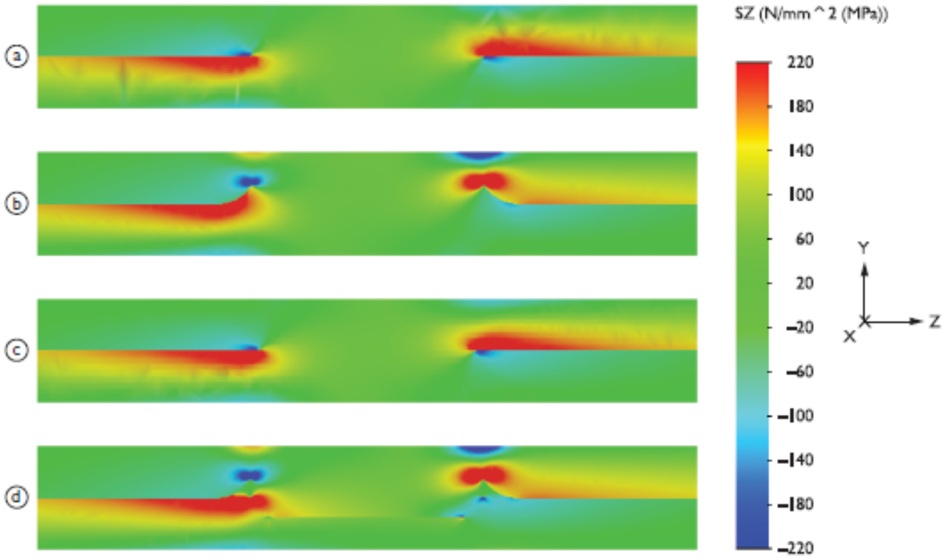

Figure 5.7 – Lap-shear simulation for similar homogeneous materials joints [57].

It can be seen from Figure 5.7 that a small Hook make the situation to approach to the *a* and *c* scenarios, in which no hook exists. The presence of a hook has the consequence of intensifying the tension fields around the SZ. The tip of the Hook acts as a stress concentrator, requiring less energy to open the crack. In the right side of the welding, in the upper sheet, a tractive (positive) tension field surrounds the tip of the Hook making the crack to open. In contrast tip of the Hook at the left side is surrounded by a compression field, which constricts the tip of the crack.

The height of the hook and the width of the SZ are also factors reportedly detrimental for mechanical properties [46, 67]. The bonding width of the weld and the hook height were measured according to Figure 5.8. In Figure 5.9, the plots of LSS results against hook height (left) and bonding width (right) are shown. There is a tendency from LSS to decrease in so far as hook height increase. In this work, it has been concluded that hook height is a factor that directly affects the weld strength in the similar welds. No significant positive or negative effect in LSS was found when comparing the bonding width. In can be seen that the data seems to be dispersed within the graph and no tendency was observed.

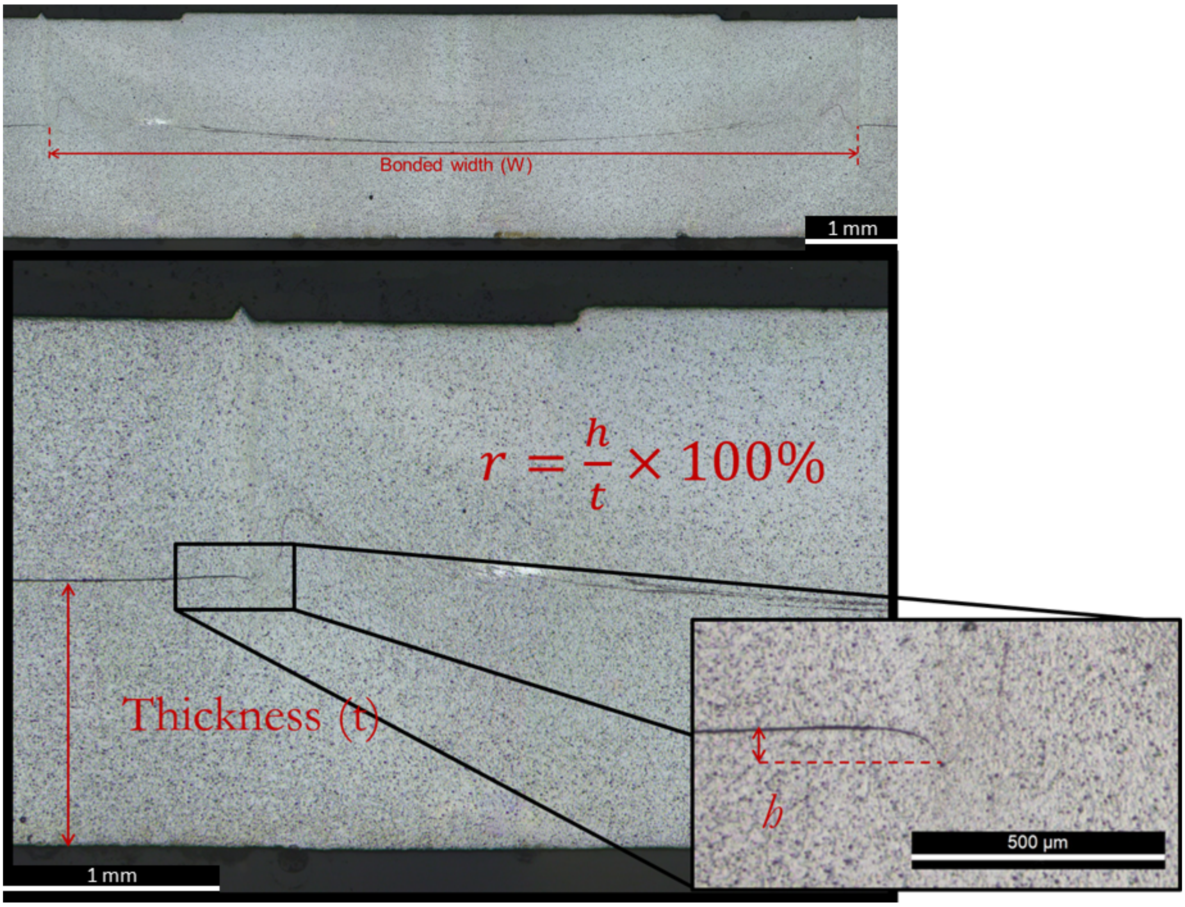
Bonded width (W)
1 mm
$r = \frac{h}{t} \times 100\%$
Thickness (t)
h
500 µm
1 mm

Figure 5.8 – Hook and bonding width measurements.

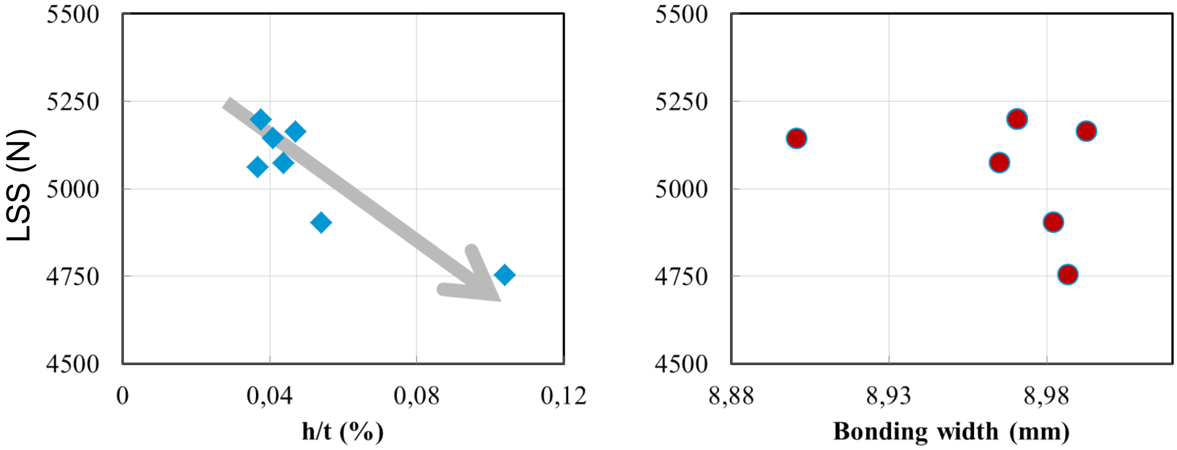

Figure 5.9 – Effect of hook and bonding width on mechanical property of the joint

5.1.3.4. Fracture behavior

In Figure 5.7, the stress concentration effect arising from the size and pointing direction of the hook is shown. By analyzing this work, another outcome is that welds that approaches the *b* or *d* situation are more likely to display Plug Shear Fracture (PSF) as shown in Table 5.8. The explanation for what has been observed is that the crack at the right side (loaded side) of the weld reaches the sheet surface prior to the left side. One reason for that is the compression zone around the Hook that makes the crack to propagate more slowly.

The cases *a* and *c* are more closely related to the type of fracture known as Plug Type Fracture (PTF). In this case, with a small or inexistent Hook, the crack is supposed to propagate in a symmetrical manner for both sides. Indeed, the weld nugget is torn around the SZ making a bridge between the two sheets during the lap-shear test.

In this work, the strongest welds are related to PT fracture, which, as mentioned above, present a short hook height. On the other hand, PS fractures presented a lower strength and higher hook height. Those results can be seen in Annex.

Table 5.8 – Failure modes

Failure Mode	**Lower Sheet Plug Out**	**Upper Sheet Plug Out**
Plug Type Fracture	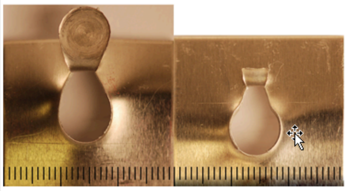	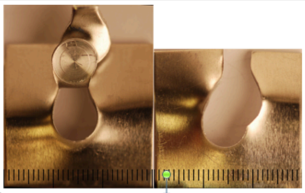
Plug Shear Fracture	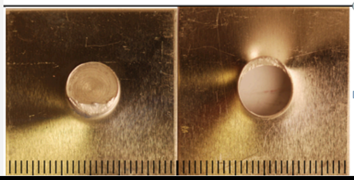	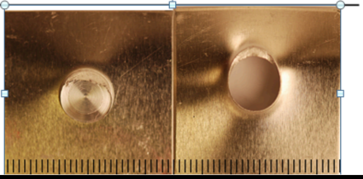

5.2. Results from dissimilar AA5754-AA6061 RFSSW

5.2.1. Test to evaluate position of alloys during weld

Before performing DOE with dissimilar AA5754-AA6061 joints, it was necessary to know the position of sheets to produce the best LSS. There were two possibilities: (i) placing AA5754 sheet on top, directly in contact to the welding tool or (ii) placing AA5754 on bottom - and AA6061 on top - in contact with the tool.

Therefore, two sets of parameters were welded in duplicates, considering the two possibilities of alloy placement. Thus, making a total of eight specimens, which were thereafter tested for LSS in a tensile test machine.

The conditions of experiments and results are shown in Table 5.9.

The two sets of parameters were chosen from results of similar AA5754 and AA6061 from previous HZG works [59].

AA5754 on top leads to a better performance of the weld. Therefore, this placement of alloys was chosen for the upcoming experiments. AA5754 was preferably chosen as top sheet also because of its lower yield strength, which facilitates the tool’s stirring.

Table 5.9 – Experiment conditions and results

RS	PD	FR	Upper Sheet	Average LSS	STD DEV.
1800	1.5	3.50	AA5754	5382.11	47.50
1800	1.5	3.50	AA6061	5373.76	33.58
1300	1.4	4.00	AA5754	5524.37	77.80
1300	1.4	4.00	AA606 I	5029.23	0.00

5.2.2. Design of Experiments

RFSSW was performed to produce dissimilar AA5754-AA6061 welds. It was used BBD design to produce thirteen combinations of parameters. The central point was performed in triplicates. The factors and conditions were in three levels as shown in Table 5.10.

Table 5.10 – Experiment factors and levels

Factor	Level 1	Level 2	Level 3
RS	1000	1500	2000
PD	1.2	1.4	1.6
FR	3	3.5	4

Table 5.11 shows the combinations following BBD approach and the results for LSS.

An ANOVA was made on the results and the results are shown in Table 5.12.

Although RS and FR are factors that are not statistically relevant for the linear model, they were included because of the square and 2-way interaction, in which they show relevancy.

A minimum-square method is applied on experimental results to generate the following 4-dimension hyper-surface equation:

$$LSS = 9433 - 1.33 \cdot RS + 1297 \cdot PD - 2640 \cdot FR - 0.0017 \cdot RS^2 + 1.750 \cdot RS \cdot FR \tag{3}$$

Table 5.11 – Experiment conditions and results

Exp. No	RS (RPM)	FR (mm/s)	PD (mm)	LSS (N)
1	1000	3.0	1.4	5500
2	1000	3.5	1.6	5659
3	1500	3.5	1.4	5480
4	1500	3.0	1.6	5588
5	2000	3.5	1.2	4654
6	1000	4.0	1.4	4561
7	2000	4.0	1.4	5111
8	2000	3.0	1.4	4302
9	2000	3.5	1.6	5381
10	1500	3.5	1.4	5305
11	1500	4.0	1.6	5487
12	1500	4.0	1.2	5401
13	1500	3.5	1.4	5383
14	1500	3.0	1.2	5231
15	1000	3.5	1.2	4753

Table 5.12 – ANOVA of the Box-Behnken DOE for LSS

Source	DF	Adj. SS	Adj. MS	Contribution	P-Value
Model	5	2095840	419168	0.856	0.001
Linear	3	670430	223477	0.274	0.018
RS	1	131336	131336	0.054	0.101
PD	1	538623	538623	0.220	0.005
FR	1	471	471	0.000	0.915
Square	1	660126	660126	0.270	0.003
RS.RS	1	660126	660126	0.270	0.003
2-WayInteraction	1	765284	765284	0.312	0.002
RS.FR	1	765284	765284	0.312	0.002
Error	9	353552	39284	0.144	-
Lack-of-Fit	7	338242	48320	0.138	0.144
Pure Error	2	15310	7655	0.006	
Total	14	2449392		1.000	

The model is then plotted as three surfaces using the intermediate levels of factors as hyper-planes sections. The surfaces sections are shown in Figure 5.10.

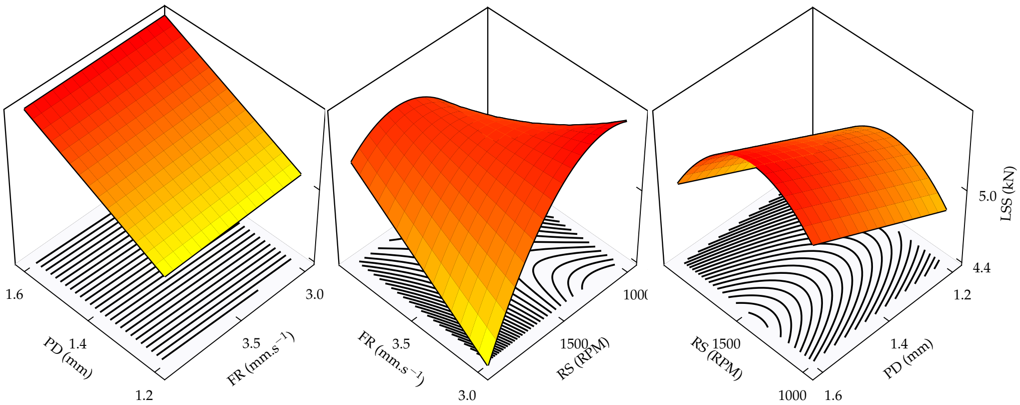

Figure 5.10 – Effect of combined (A) FR and PD; (B) FR and RS; (C) PD and RS on LSS of dissimilar welded joints

As it can be seen, PD is the factor that most influences weld mechanical performance for dissimilar AA5754-AA6061 joints showing a P-Value of 0.005 and the largest gradients on the surface. The square component RS·RS and the 2-Way interaction component RS·FR are also relevant for the model.

Figure 5.11 shows how accurately the model fits to experimental data. A R^2 of 0.86 means a reasonable fitting of the model but not excellent. This result can be attributed to the large chosen parameter window.

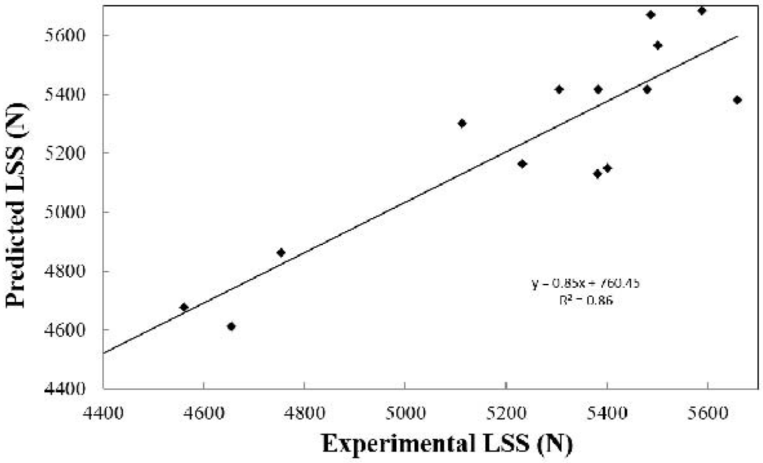

Figure 5.11 – Expected versus predicted LSS according to RSM

5.2.3. Optimization of parameters using OFAT

The model illustrated in Figure 5.10 indicates that the best set of parameters is located around in the red region of RSM, from which the following parameters were chosen as central point for optimization.

Central = [RS = 1150; PD = 1.6; FR = 3.0]

OFAT approach was used to investigate the surroundings of central point in RSM. Table 5.13 show the parameters welded and tested for investigation.

Table 5.13 – OFAT results for RS

Condition	**Replicate**	**RS [RPM]**	**PD [mm]**	**FR [mm/s]**	**LSS [N]**	**Average [N]**	**STDV [%]**	**RSM value [N]**	**Dev [%]**
A	1 2 3	800	1.6	3	4092 4505 4521	4373	5.6	5648	22.6
B	1 2 3	1000	1.6	3	5517 5788 5658	5655	2.4	5826	2.9
Central	1 2 3	1150	1.6	3	5621 5739 5751	5704	1.3	5872	2.9
C	1 2 3	1500	1.6	3	5725 5699 5739	5721	0.3	5684	0.7

Figure 5.12 shows a box-and-whisker plot of OFAT results means. This kind of chart is useful for describing data behavior in the middle as well as in the ends of a distribution of values.

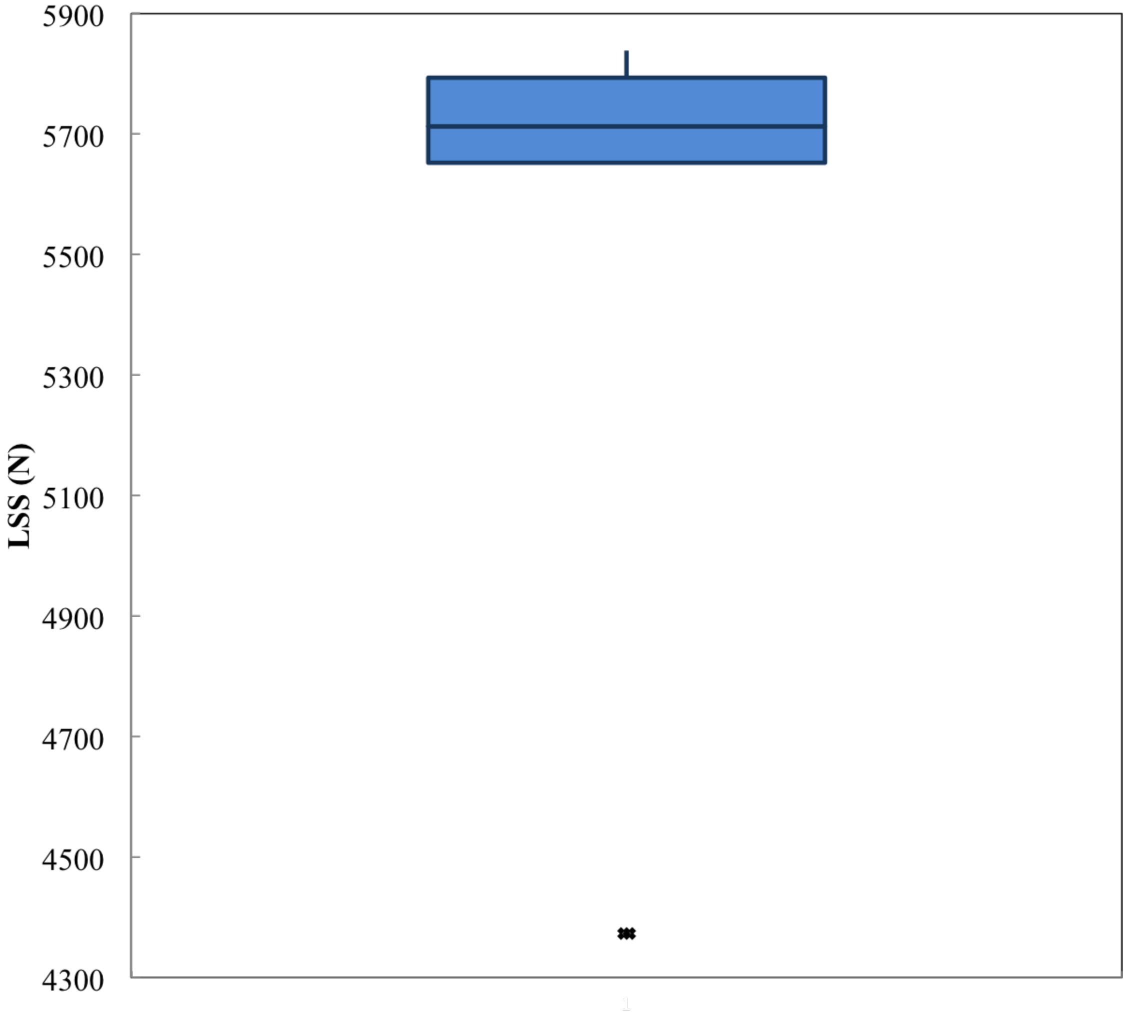

Figure 5.12 – Box-and-whisker plot of OFAT results means

Table 5.14 – OFAT results for PD

Condition	**Replicate**	**RS [RPM]**	**PD [mm]**	**FR [mm/s]**	**LSS [N]**	**Average [N]**	**STDV [%]**	**RSM value [N]**	**Dev [%]**
	1				4092				
D	1	1150	1.4	3	5664	5643	1.2	5612	0.6
	2				5701				
	3				5565				
Central	1	1150	1.6	3	5621	5704	1.3	5872	2.9
	2				5739				
	1				5751				
E	2	1150	1.8	3	5794	5790	0.1	6131	5.6
	3				5781				

Table 5.15 – OFAT results for FR

Condition	**Replicate**	**RS [RPM]**	**PD [mm]**	**FR [mm/s]**	**LSS [N]**	**Average [N]**	**STDV [%]**	**RSM value [N]**	**Dev [%]**
F	1	1150	1.6	2.5	5824	5803	0.6	6186	6.2
	1				5823				
	2				5761				
Central	3	1150	1.6	3	5621	5704	1.3	5872	2.9
	1				5739				
	2				5751				
G	1	1150	1.6	3.5	5778	5839	0.9	5558	5.1
	2				5863				
	3				5875				

Values are narrowly distributed in an interval within the range of 5650 and 5800 N. This chart also shows that there is one outlier among the other results. An outlier is an observation that lies an abnormal distance from other values in a random sample from a population.

This outlier was identified as being the set of parameters:

A = [RS = 800; PD = 1.6; FR = 3.0]

The low rotational speed was responsible for the poor mechanical performance of this set. RS is directly correlated with frictional heat generated in the process, which in turn is responsible for material's ductility during severe plastic deformation. An insufficient frictional heat can lead to internal cracks in weld cavity as well as lack of filling defects, which are extremely detrimental do mechanical performance.

In Figure 5.13, it is shown the cross section of A-condition (Table 5.13) as seen under the microscope.

Internal defects such as cracks in the bonding ligament and lack of filling defects near the hook and on weld surface are observable. An early rupture during lap-shear testing due to the stress-concentration effect around the defects is a probable cause of the lower mechanical performance.

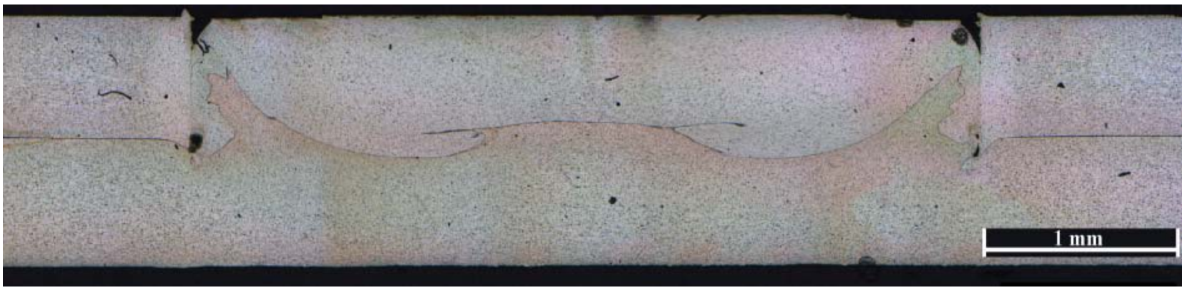

Figure 5.13 – Condition A from OFAT experiments

5.2.4. Hook Characterization

Hook height – thickness ratio (h/t) was measured in all samples of OFAT experiment with the aid of ImageJ® software. Figure 5.14 shows the correspondence between LSS and h/t in a scatter plot. It shows that LSS decreases with larger h/t confirming the results obtaining in literature [36].

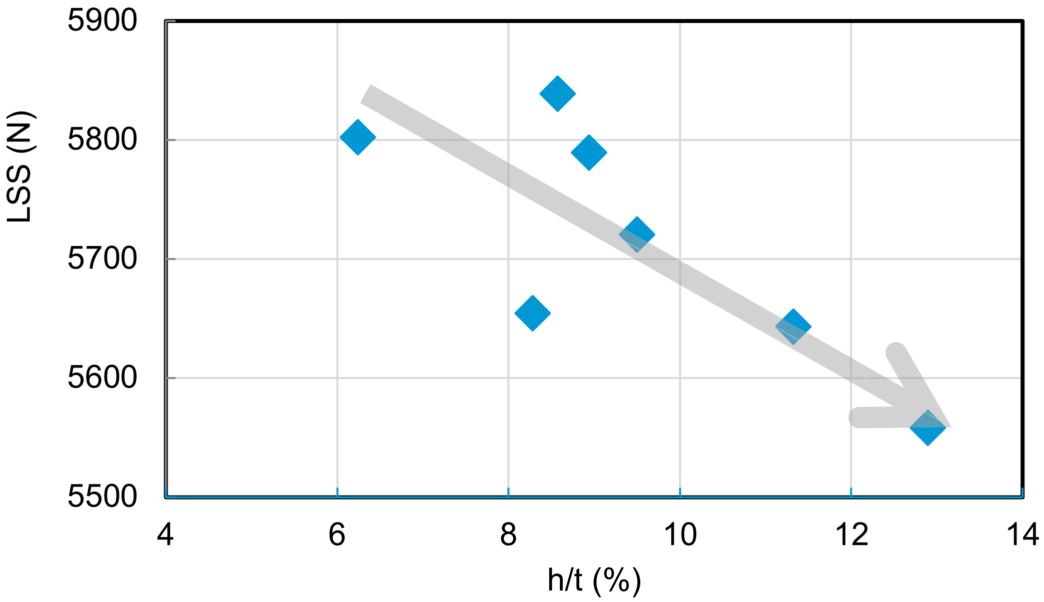

Figure 5.14 - LSS versus h/t showing a negative dependency of LSS on h/t.

5.2.5. Fracture behavior

Figure 5.15 - A shows the fracture behavior of condition F in an LSS test. Fracture propagated through BM, which does not often occur in this type of weld. According to Campanelli et al [57] compression and traction fields surround the

hook as shown in Figure 5.15 B. Cracks are more prone to propagate in traction fields as indicated by the red circles. At the same time, AA5754 is less tough than AA6061and cracks propagate more easily through it. For this reason, fracture occurs as shown in Figure 5.15 C and D: At the left (C), the crack opens more slowly in the traction field than at the right (D) during LSS test.

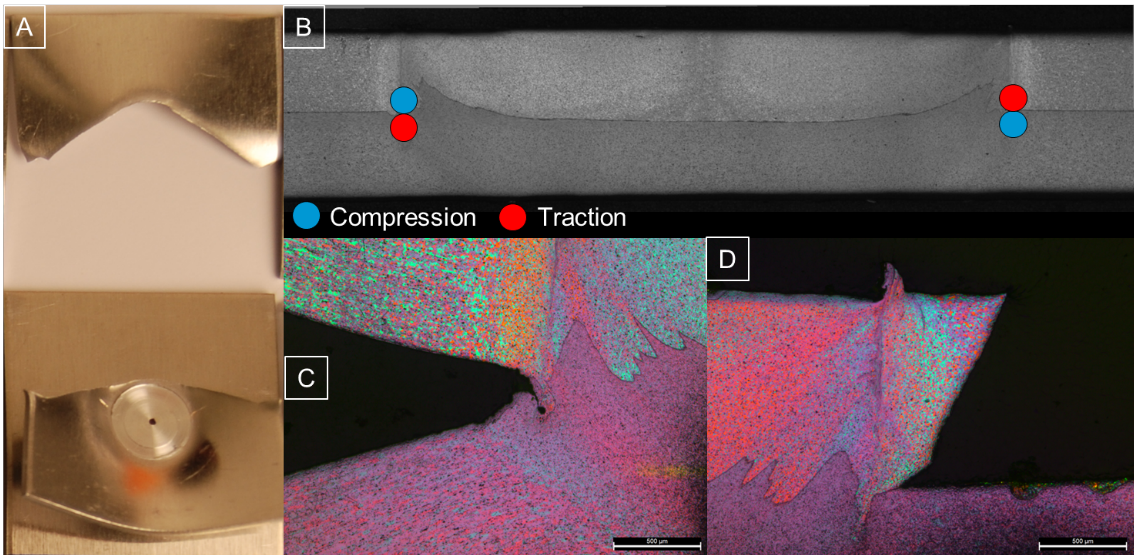

Figure 5.15 – Specimen fracture

5.2.6. Weld Characterization and Microstructure Analysis

In Figure 5.16, it is shown a macrograph picture of an etched RFSSW weld cross section observed under polarized light through an optical microscope. Different zones in that picture are detached to show the microstructure in different locations of the weld cross section. In all detached zones, the microstructure is comprised of α-Al grains with 2 µm Al6(Fe, Mn) intermetallic dispersoids, typical of AA 5XXX series alloys [60]. In AA6061, fine precipitates typically present in peak-aged AA6061-T6 are expected; they are however only able to be seen by transmission electron microscopy (TEM), which was not explored in this work. In the following subsections, each analyzed region from the weld is better characterized regarding the position of each region relative to the weld center.

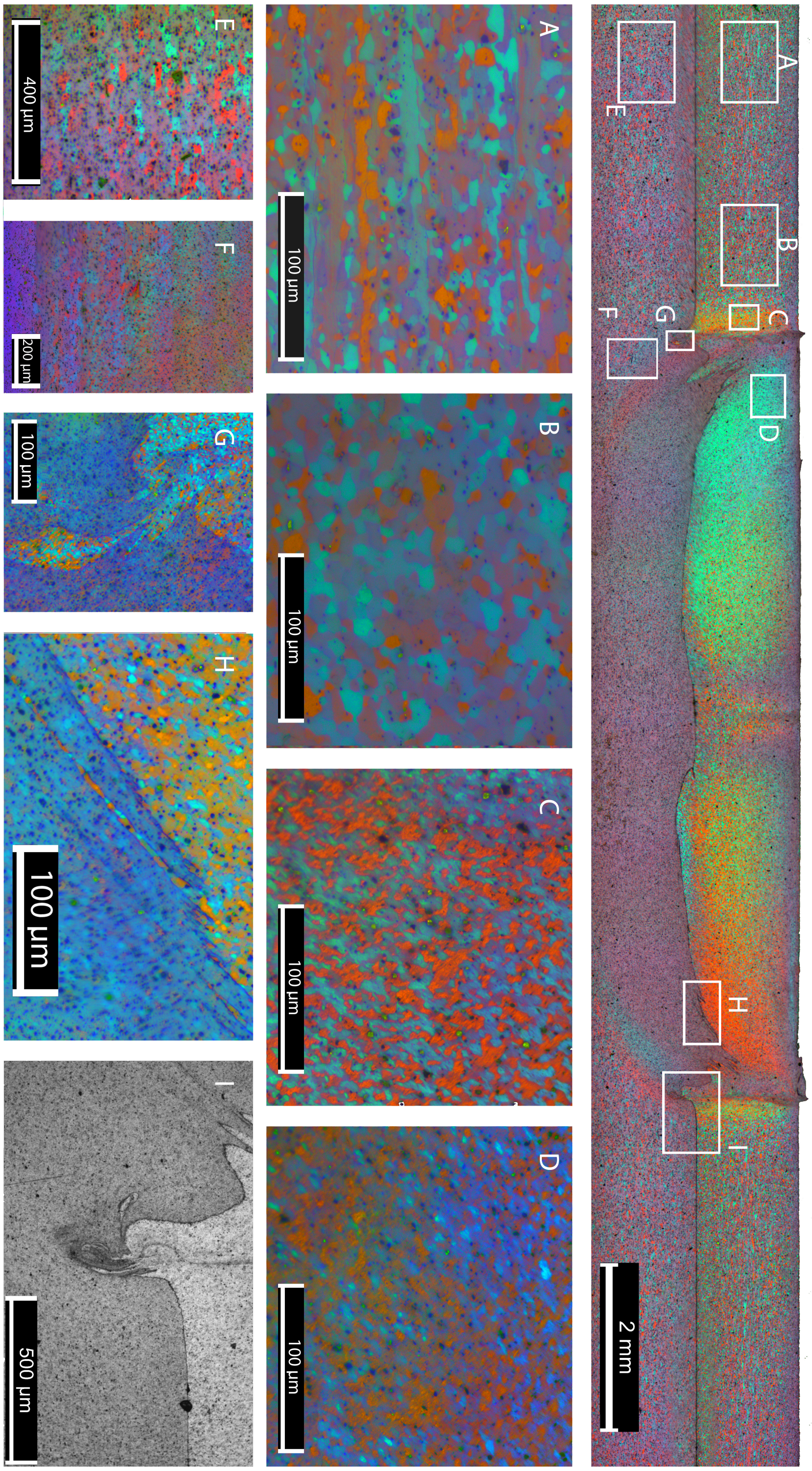
A
B
C
D
E
F
G
H
I
2 mm
100 µm
100 µm
100 µm
100 µm
400 µm
200 µm
100 µm
100 µm
500 µm

Figure 5.16 – Cross section of the welded joint (Top picture). Micrographs of AA5754 base material, (A) HAZ (B), TMAZ (C), SZ (D). Micrographs of AA6061 base material (E), TMAZ and SZ (F). Detail of mixture between sheets (G and H). Hook shape (I).

5.2.6.1. Stir zone (D)

The SZ (D) has a microstructure of fine equiaxed grains disposed in a radial flow pattern due to the rotation of the sleeve and plunging of the pin, which is believed to cause the material to flow outwards in its plunging due to pressure gradients.

By comparing region (D) and region (A) in regard to grain shape and size, it is clear that the microstructure underwent transformation as it changed from 24 - 100 µm elongated to equiaxed 5 - 18 µm grains. The mechanism of this transformation is discussed in this subsection.

The general hypothesis is that the grains in SZ went through dynamic recrystallization DRX. However, aluminum alloys are not likely to undergo DRX due to their high SFE unless high magnitudes of ε and $\dot{\varepsilon}$ are applied. This transformation mechanism is observed in aluminum alloys subjected to large ε and $\dot{\varepsilon}$ in conjunction with high temperature (> 0.5 Tm) such as in the outer layer of extruded billets. It is known that the RFSSW process submits the SZ to large ε and $\dot{\varepsilon}$ and temperature coming from the sleeve friction. In this work, no attempt to determine the $\dot{\varepsilon}$ of the process was made. However, previous works [61] investigated and calculated ε and $\dot{\varepsilon}$ values for friction stir process in AA2524 from a three-dimensional coupled viscoplastic flow and heat transfer model. ε and $\dot{\varepsilon}$ were in the ranges −10 to 5 and −9 to 9 s^{-1} respectively.

Mukherjee e Ghosh [62] calculated strain rates of 87 s^{-1} for AA5083 0.29 mm plates. Other authors [63] calculated strain rate in FSSW using the Zener-Hollomon relation and found values in the range of 20 s^{-1} to 650 s^{-1} for AA7075. The work that provided the most useful information about $\dot{\varepsilon}$ is from Gerlich et al. [60] who found a relationship between the rotational speed of the tool and $\dot{\varepsilon}$ in FSSW of AA5754 and AA6061 in 5 mm sheets. The author found a value of approximately 200 s^{-1} for $\dot{\varepsilon}$ in FSSW of AA5754 and AA6061 for a rotational speed of 1200 RPM.

From this bibliography, it is noticeable that ε and $\dot{\varepsilon}$ values for friction-based processes are not readily available from measurements, but instead they can only be estimated by simulation and calculations, being sometimes the range of values in between more than one degree of magnitude. The range of $\dot{\varepsilon}$ found is nevertheless enough for dynamic recrystallization to occur. This assertion is found in the work of Geertruyden et al. [64]. By performing hot-torsion experiments, the authors found the critical value of $\dot{\varepsilon}$ of 2.5 s^{-1} for DRX to occur.

It is believed that $\dot{\varepsilon}$ during RFSSW in this work reached values above the critical value and therefore DRX could occur. In the case of aluminum alloys, the nucleation and growth of new grains can be induced by hard second phase particles dispersed in the Al matrix [30].

There are however three different mechanisms of DRX in metals: DDRX, CDRX and GDRX. Aluminum alloys, in a general way, due to their high SFE, do not undergo DDRX [24]. Therefore, the probable mechanism for grain refinement in SZ is CDRX and/or GDRX. CDRX and GDRX are very similar in nature and the final grain structure provided by both mechanisms is the same, *i.e* very fine equiaxed grains. In order to evaluate the kind of mechanism (CDRX or GDRX) is happening during the welding process, it is necessary to gather evidences by means of experiments. Optical microscopy (OM) already provides cues of the occurrence of GDRX. As it can be seen in Figure 5.16-D, some grains show serrations in their grain boundaries, which can be a hint that GDRX was undergoing until the moment that shear ceased. Other equiaxed grains would be the final form of a fully GDRX-recrystallized grain.

5.2.6.2. Thermomechanical Affected Zones (C) and (F).

RFSSW process joins overlap sheets by means of the stirring of top and bottom sheets. The low-pressure zone created by the retraction of the pin is what allows the softened material to make a complex flow path that will further create the stir zone. Thermomechanical-affected zone (TMAZ), regarding the material and heat flow, is nevertheless a less complicated zone to be analyzed. This zone comprises a shell of deformed grains with some degree of recrystallization that surrounds the SZ. Apparently, the grain and subgrain size are smaller in the proximity of SZ and evolves to a bigger size in direction to HAZ. In Figure 5.17, the evolution of recrystallized grains in the TMAZ of upper sheet AA5754 can be seen. Five sub-zones comprised by fine equiaxed and serrated grains are observable. The zone shows deformed grains with serrated grain boundaries just like in SZ, resembling GDRX. In a layer of grains very close to the sleeve (1), with an estimate thickness of 150 µm, measured in ImageJ® image analyzer software, GDRX seems to be the dominant recrystallization mechanism, showing a noticeable amount of equiaxed grains ranging in size from 3 to 6 µm. By going further in the thickness of the shear layer (2-4), the grain size increases, and the occurrence of equiaxed grains diminishes, whereas larger serrated grains become dominant. In (4), equiaxed grains smaller in comparison to HAZ are still observed. After (5), the grains are still deformed and serrated, but they start to acquire an equiaxed shape by going further than that point.

The Zener-Hollomon parameter (Z), also known as the temperature compensated strain rate [65], correlates the strain rate with temperature according to the following equation:

$$Z = \dot{\varepsilon} \exp\left(\frac{Q}{RT}\right) \tag{4}$$

where Q is the activation energy, R is the gas constant and T is temperature. This parameter plays an important role when dynamic recrystallization phenomena are studied.

Many studies [66], [67] investigated the relationship between Z and the final dynamically-recrystallized subgrain diameter (d). For many aluminum alloys the following equation could be verified:

$$d^{-1} = a + b\log(Z) \tag{5}$$

where *a* and *b* are empirically derived constants. Therefore, the higher the value of Z, the smaller the dynamically recrystallized subgrain size and vice-versa. In that sense, from calculated values of a and b obtained in literature and by measuring the recrystallized grain size, it is possible to obtain Z and, thus, obtain the strain rate as a function of the shear layer thickness.

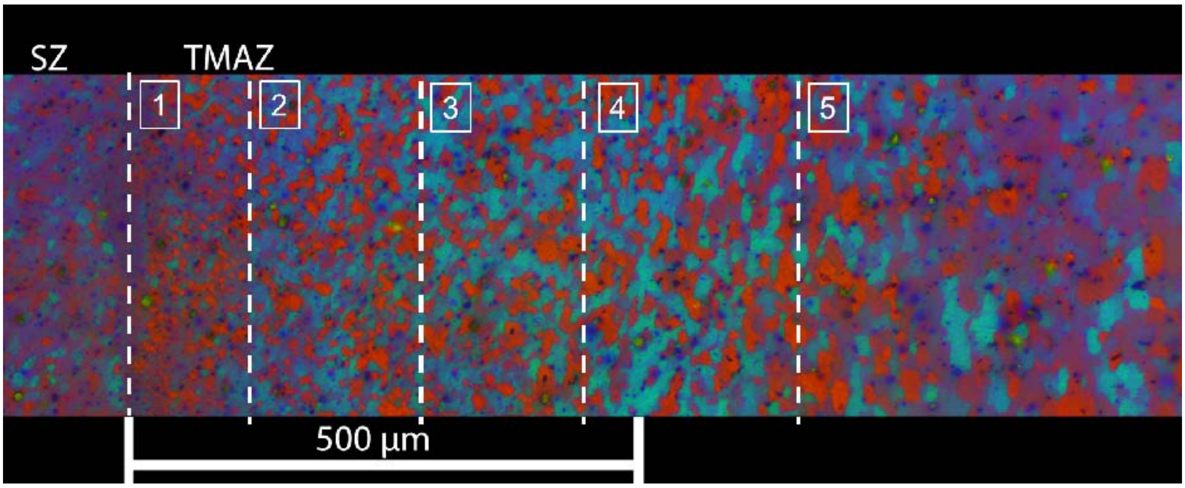

Figure 5.17 – OM showing TMAZ and the evolution of grain size

5.2.6.3. Heat Affected Zone (B)

HAZ in AA5754 is shown in Figure 5.18. It can be readily seen that this zone presents a grain shape that differs from the base material. Whereas in base material the grain shape is clearly elongated due to rolling process, grain shape in HAZ is fairly equiaxed. Little or no strain rate is expected at this point of the weld and OM shows no deformed grains perpendicular to weld axis. Therefore, temperature and stress from the clamping pressure are the agents able to transform the microstructure of this zone. The possible thermal-activated mechanisms able to rearrange grain morphology are SRX and DRX [23]. It is arguable that SRX can occur in the studied process, as welding time is close to 1 s in average. The kinetics of SRX usually requires the material to be exposed to high temperatures during long annealing times, which enables the material to recover, new nuclei to form and grow. Moreover, aluminum alloys, in a general way, do not simply undergo SRX due to its high SFE [23]. On the other hand, AA5754 is an alloy with high Mg and other solution-strengthening elements purposely added to lower Al SFE and make this alloy more work hardenable [67]. As a consequence, this alloy tends to present a higher dislocation density within its grains and a better ability to recrystallize. Indeed, the equiaxed shape found in AA5754 HAZ is very rare to be found in other alloys submitted to the same process. For instance, AA6061 has shown no modification in grain shape and size in the threshold between BM and TMAZ.

Etter et al [68] examined the recrystallization mechanisms in cold-rolled and annealed AA5251, an alloy that is like AA5754 in Mg content. Using EBSD techniques, the authors found that a partial SRX took place in the cold-rolled sample.

Another fact that supports SRX in AA5754 is that the material was partially annealed after it was rolled. The annealing might have allowed the material to partially recover thus speeding up the recrystallization process.

Another possible theory for the change of morphology in the observed grains is that DRX might have occurred. As the recrystallized material was under stress from the clamping pressure, this stress might have been superior to the critical stress needed for triggering DRX in AA5754. Further discussion and investigation on this transformation phenomenon will be continued in Section 5.2.9.

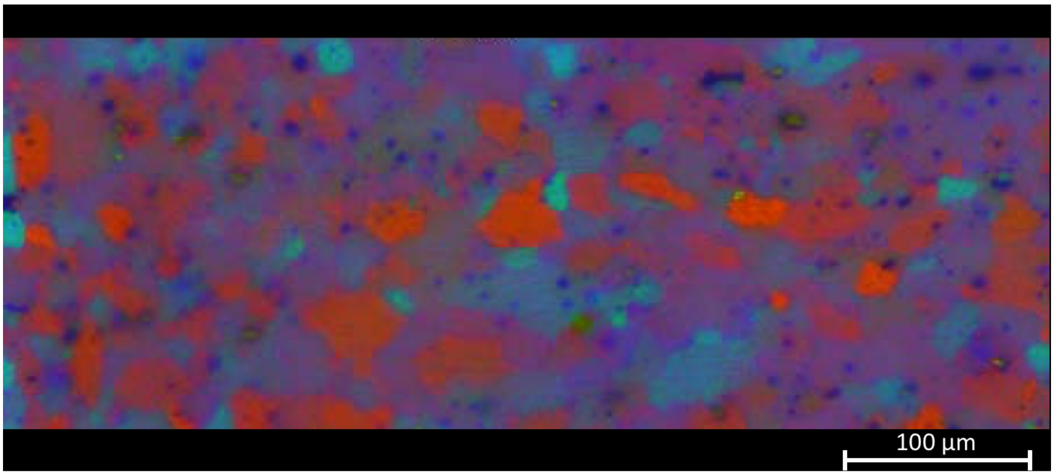

Figure 5.18 – OM showing HAZ in AA5754 upper sheet

5.2.6.4. BM (A and E)

The upper sheet material, AA5754 was rolled up to a quarter of maximum hardness and partially annealed (H22 treatment). The elongated grains originated from the rolling process can clearly be seen in Figure 5.16 - A. Nevertheless, close to the surface of the sheet, the shape of grains seems to become equiaxed. Those equiaxed grains were probably originated from the annealing step subsequent to cold rolling. The presence of those equiaxed grains are a hint for the occurrence of a partial SRX process. Indeed, microhardness measurements throughout upper sheet thickness show a slight softening in the outer layers of the material (Figure 5.19). According to the recrystallization theory proposed by Cahn [69], recrystallized grain nucleation takes place in pre-existing sub-grains and cells formed during recovery step. The sites where the likelihood for a nucleus to appear, where surface tension is higher, is in the triple junction formed by two HAB and one LAB. Scanning electron microscopy and EBSD are useful techniques to observe the occurrence of such nuclei in elongated grains triple joints.

In lower sheet material, AA6061, no deformed grains have been observed in its base material. Due to the T6 treatment by which the material had been submitted, it is believed that any rolling textured was completely undone. From Figure 5.5 (E), it can be seen that grain size is much larger than in AA5754 and grains have an equiaxed shape.

5.2.7. Microhardness in weld section

Microhardness has been carried out throughout the weld section. Figure 5.19 shows the point-to-point hardness of the whole section. Lower sheet indentations are represented in the chart by blue diamond markers. AA6061 hardness drops from 110-120 HV0.2 to 70-80 HV0.2 in the region surrounded by the HAZ. As AA6061 is an age-hardenable alloy, this large drop is attributed to the dissolution and coarsening of β' (semi-coherent Mg_5Si_6) and β" (coherent Mg_2Si) precipitates. Aval et al [70] observed the shape and size of those precipitates in a transmission electron microscope (TEM) for a friction stir welded sample. The visual characterization allowed them to see that the base material contains needle-shaped semi-coherent β' precipitates, responsible for a peak hardness. In HAZ, the β" precipitates are coarsened to incoherent precipitates, causing hardness to decrease.

From Figure 5.19, it can be seen that the decrease in hardness from BM to HAZ does not happen abruptly, suggesting that the occurrence of β" dissolution and coarsening intensify as it runs from TMAZ to SZ. Therefore, it can be concluded that the dissolution and coarsening of semi-coherent precipitates is higher in the direction of higher temperature gradients. The TMAZ and SZ contain large plate-shaped incoherent precipitates, which give lower mechanical properties [70] to the material. The author's conclusions are consistent to the hardness results presented in this work.

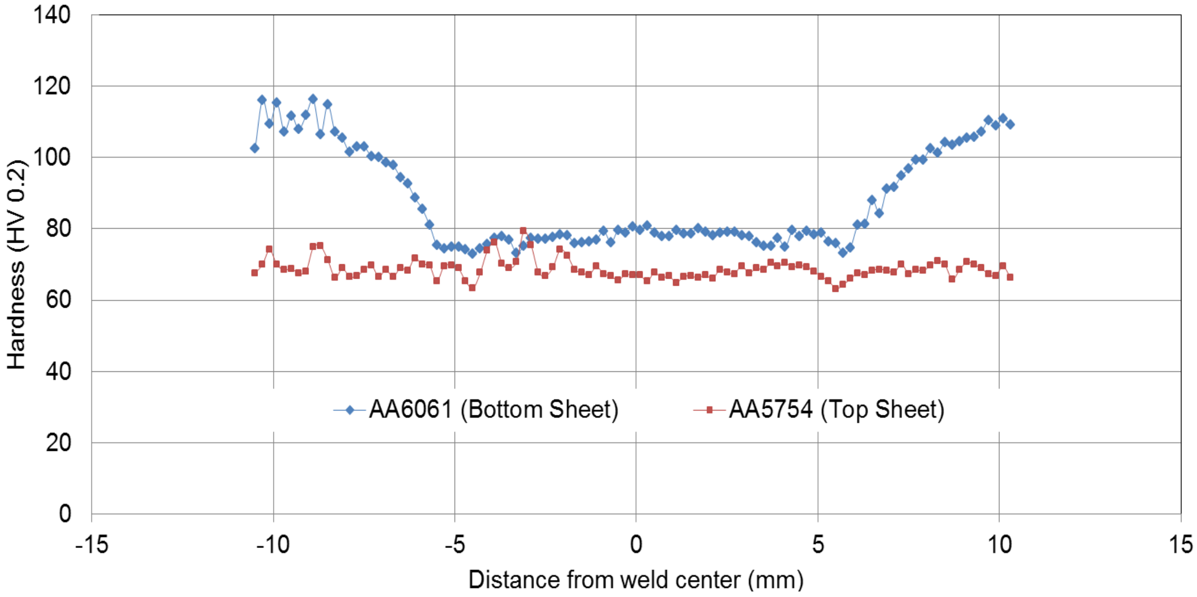

Figure 5.19 – Microhardness profile of weld cross section

5.2.8. Stop-action experiments

RFSSW is a complex process regarding material flow inside weld cavity. Although the welded material is at solid state, during the welding process it behaves in a way that resembles non-Newtonian fluid. This behavior is attributed to severe plastic deformation (SPD) of solid-state metal making it a fully coupled thermo-mechanical process. In order to SPD happens, a high hydrostatic pressure, together with adequate strain rate and temperature are needed [71]. The material flow is complex; however, it is possible to make observations using "stop-action" technique. Stop-action consists on interrupting the weld at any stage between the start and end of the process, by turning off the RPS100® equipment. Condition G (Table 5.15) was investigated by observing microscopy samples produced with this technique. The weld process was interrupted at plunge depths of 1, 1.2, 1.4 and 1.6 mm. Observations regarding microstructure and flow were made.

Figure 5.20 shows a metallography from the G condition stopped at 1.4 mm depth. Microstructure at that stage varies according to the position within the weld. In number 1, microstructure is comprised by equiaxed grains with no sign of deformation, meaning that some recrystallization phenomena took place, changing the material from elongated directionally rolled grains to equiaxed. In number 2, grains seem to become smaller and with some degree of deformation. The shape and size of grains continues to change as we observe pictures 3 and 4 until it reaches the condition shown in picture number 5 where grains are the smallest and most serrated, indicating the occurrence of higher shear rates and temperature. Dynamic recrystallization is believed to have occurred in that condition. GDRX or CDRX are probable mechanisms.

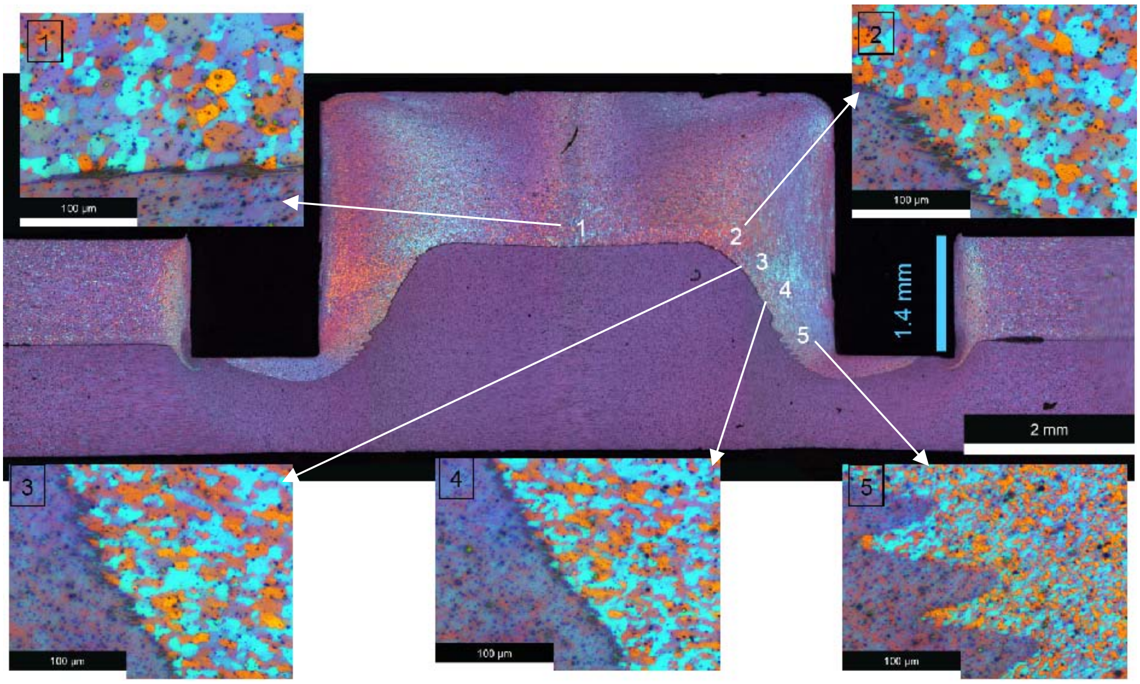

Figure 5.20 – Cross section of G condition stopped at 1.4 mm depth observed in polarized light.

Stop-action experiments were also useful for investigating the material flow during the sleeve-plunge step of RFSSW. Figure 5.21 shows a higher magnification of the area named "sleeve periphery" where material was in close contact to sleeve. Yellow and light blue dashed arrows indicate the probable flow path of 5754 and 6061 alloys. The light blue arrow indicates that the upper sheet material moves downwards aided by the motion of tool thread whereas the yellow arrow shows that lower sheet material moves upwards and outwards in a helical motion. The latter can be a consequence of conservative motion as upper sheet material moves downwards pushing lower sheet material to a low-pressure zone.

This motion behavior may explain a common feature observed in dissimilar welds characterized by an engulfment of upper sheet material by the lower sheet material. Figure 5.21 pictures the described phenomena. Pin plunge step may be responsible for creating an outward motion of materials causing this feature to happen.

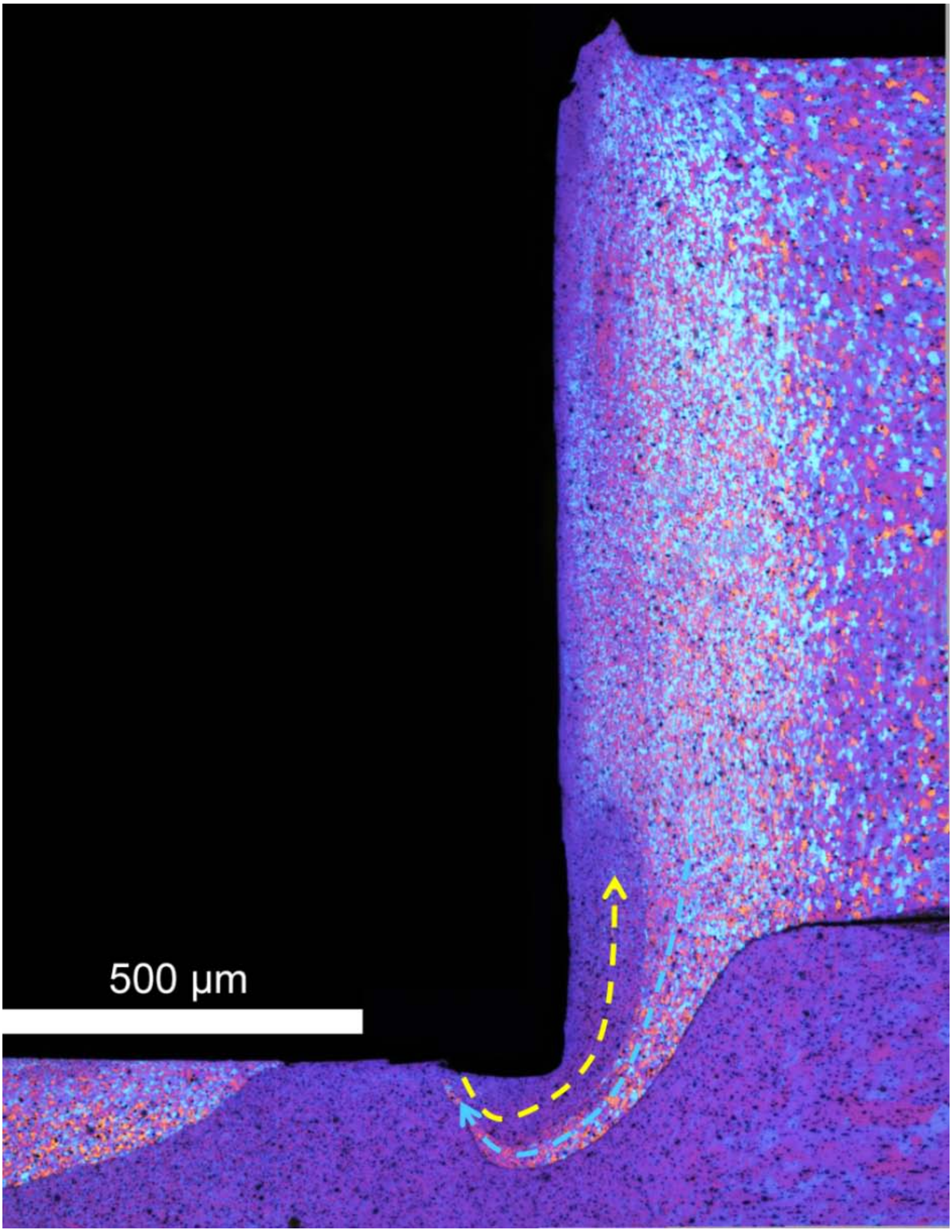

Figure 5.21 – Higher magnification showing the material flow in sleeve periphery

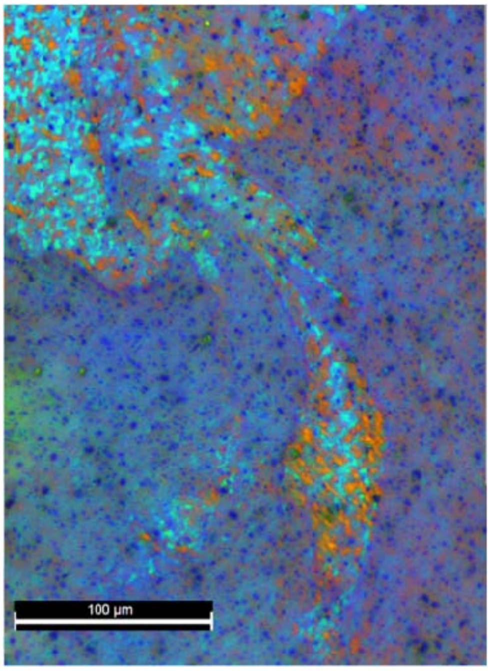

Figure 5.22 – Engulfment of AA5754 by AA6061.

5.2.9. Clamping pressure experiments

In Subsection 5.2.6.3, it was discussed the occurrence of microstructural modification in a volume of material comprised between BM and TMAZ. This volume, sectioned and observed under optical microscope, was referred as HAZ. HAZ presented an equiaxed grain structure that much differs from that of TMAZ and BM. One hypothesis was that temperature was responsible for recovery and recrystallization in the material. However only recrystallization could have effectively changed grain shape and it would not simply occur by temperature elevation solely as welding time is too short for this phenomenon to occur. A second hypothesis consider the clamping pressure as a factor that influences the thickness of HAZ.

In order to investigate this effect, an experiment was designed. In such experiment, the material was welded under different clamping pressures. Three samples were produced, at 2, 4 and 8 bars of clamping force. Each weld was sectioned at its diameter and prepared for microscopy. The whole weld HAZ was measured with the aid of ImageJ® graphic software.

Figure 5.24 shows the macrographies and the area of interest of HAZ. HAZ area increases with clamping pressure. Therefore, strain provided by the clamp may interfere in the modification of microstructure. The mechanism by which this change occurs is however not yet fully understood. At first, it was thought that SRX would be right mechanism for this transformation, as no strain rate is involved to trigger DRX [23].

RFSSW subjects the material to a unique set of conditions rarely seen in any other metallurgical process: temperature increase at very high rates, severe plastic deformation and area subjected to a high static load. Some works on the influence of static loads on recrystallization have been produced [82, 83]. In a previous work, comparison of the kinetics of recrystallization of heavily cold-rolled polycrystalline copper (99.999 % purity) at atmospheric pressure and at a hydrostatic pressure of 42 kilobars has shown that high pressure retards both the initiation and the rate of recrystallization [72]. A similar effect of recrystallization retardation was observed during annealing at 300 ^{o}C of an Al-2%Mg alloy under an applied stress of 10 MPa [73]. In this work, the calculated stresses applied by the clamping ring were 42, 84 and 168 MPa respectively for each pressure. In the present work, the applied pressure seems to accelerate the pace of recrystallization.

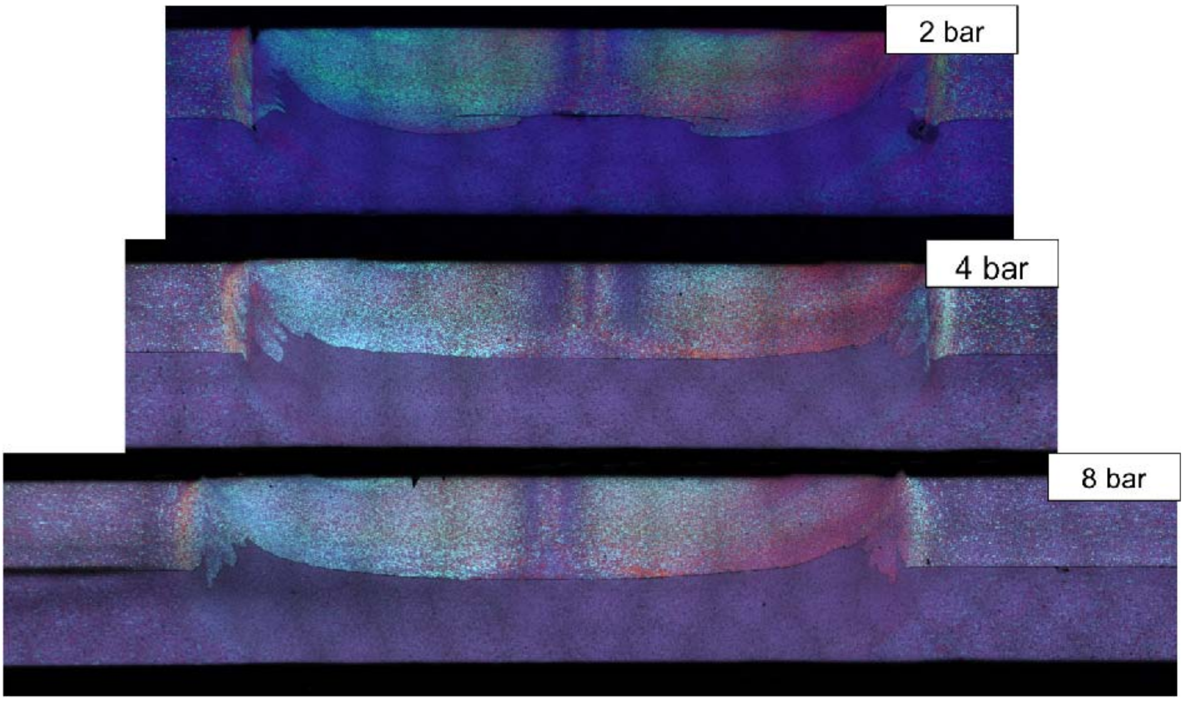
2 bar
4 bar
8 bar

Figure 5.23 – Macrographies evidencing the influence of clamping pressure on weld characteristics.

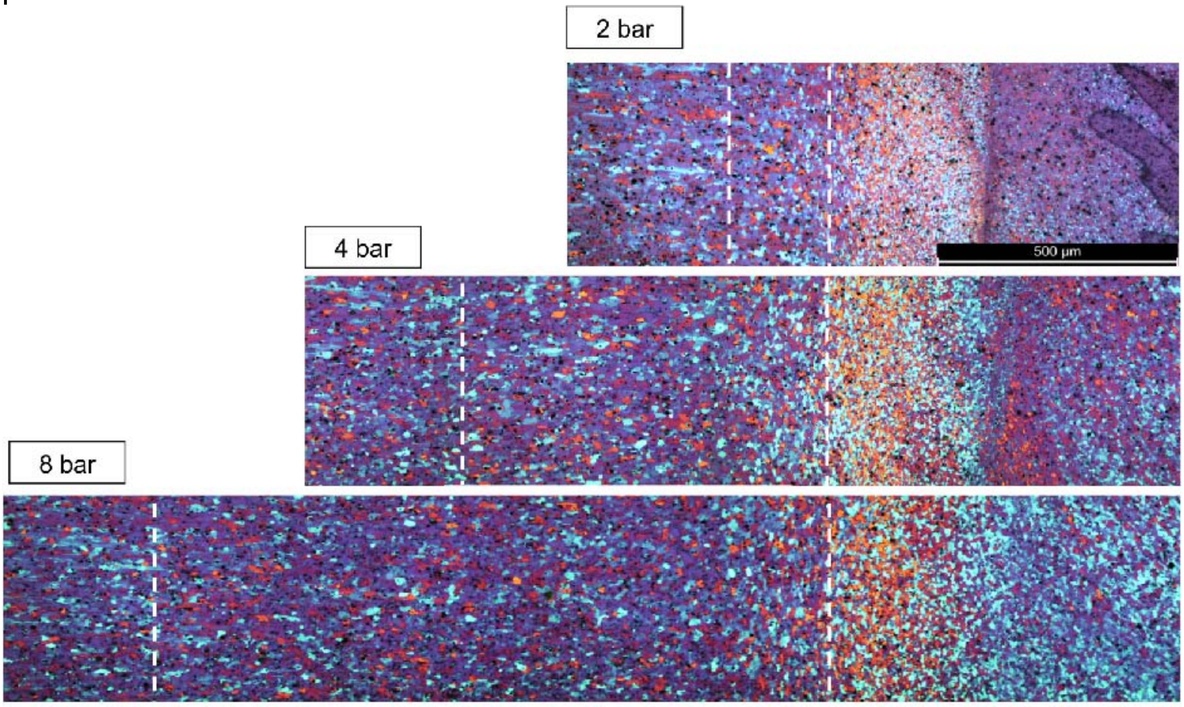
2 bar
500 µm
4 bar
8 bar

Figure 5.24 – Area of interest from welds comparing width of HAZ.

6. CONCLUSIONS

This work disserted about the optimization of parameters, incurring defects, metallurgical phenomena and mechanical properties of similar and dissimilar RFSSW of AA5754 and AA6061. Based on the performed tests and results obtained throughout this work, the following conclusions can be drawn:

(1) The combination of statistical tools comprised of DoE, Box-Behnken approach and OFAT, RSM and ANOVA were found to be an efficient systematic method for optimizing welding process parameters and revealing possible defects present in RFSSW welds. For the similar combination, RSM and ANOVA showed that weld lap-shear strength mainly depends on the linear combination of parameters, which translates to planar surfaces in RSM visualization. The optimization revealed that a rotational speed of 1800 rpm, plunge depth of 1.5 mm and a feeding rate of 3.5 mm/s results in the strongest weld. The same approach for the dissimilar combination of alloys showed hypersurface sections of parabolic shape showing a big dependency of LSS on square and two-way components of the model. OFAT also helped to reveal the occurrence of defects inside the weld, which resulted in a much lower LSS compared to the other combinations inside the parameter window.

(2) Microhardness measurement in the similar combination revealed that hardness is slightly lower in the SZ, but apparently it is not affected in the HAZ. In the dissimilar combination, hardness is little affected in the upper sheet and has a more significant drop in the lower sheet. This result was mostly credited to the dissolution and coarsening of GP Zone precipitates in SZ and HAZ.

(3) Metallographic analysis from OFAT results enabled the measurement of the hook for both combinations of alloys. In the similar combination, hook height was apparently closely related to LSS performance, confirming previous work from literature. The size and pointing direction of the hook tip also showed to be related to weld tearing mode. According to computational simulations, the hook can change the magnitude of stress fields that inhibits or accelerate the propagation of cracks around the SZ. For the dissimilar combination, microscopy observations revealed the occurrence of rupture of the oxide layer, enabling some material from the upper sheet (AA5754) to mix with the lower sheet

(AA6061). Also, the mixture revealed some interesting features caused by the engulfment of one material into the other. Another important result observed was the change of microstructure in the HAZ from elongated grains to equiaxed grains. This change was attributed to recovery and partial recrystallization, even though the process temperature and time were not theoretically enough for triggering SRX. By analyzing TMAZ, serrated grains were observed and GDRX and CDRX mechanisms were pointed out as most likely mechanisms undergoing during RFSSW.

(4) The occurrence of mixture between the alloys motivated the investigation on material flow during the process by means of stop-action method. Stop action gave insight on the movement of materials during the process and explained the occurrence of the engulfment feature. Stop-action also showed that the lower sheet material deflects to some extend inside the weld cavity without breaking its oxide layer. It showed that the oxide layer change it shape depending on the distance from the shearing sleeve. The deflection of the oxide layer enables it to become closer to the tool, forming a staircase comprised of alternating layers of AA5754 and AA6051.

(5) Further investigation on the microstructural change in HAZ was carried out. The clamping force was varied in a logarithmic scale of 2, which revealed that the recrystallized zone under the clamping ring increases with the clamping force. Therefore, this recrystallization phenomenon is dependent on the amount of static pressure applied.

7. SUGGESTIONS FOR FUTURE WORK

The recommendations for future work are summarized below:

(1) As mentioned in Section 4.4, an investigation on the difference between the work of Suhuddin et al [54], appointing PD as a non-significant factor on LSS and RS and DT as the most significant factors. An experiment varying sheet thickness, dwell time as feeding rate could elucidate the sources of those differences.

(2) A study on the Zener-Hollomon parameter, strain rate, grain size and temperature measurements. EBSD could be used to accurately measure grain size and grain misorientation. Temperature measurements would be useful to determine the exact temperature on a given grain size. From Equations 4 and 5, it would be possible to calculate the empirically derived constants for alloys welded by RFSSW Those derived parameters would be of great value for computer models on the process.

(3) A study on the corrosion resistance of AA5754/AA6061 RFSSW joints since those alloys are particularly used in structures exposed to environmental corrosion.

8. REFERENCES

[1] I. K. Pokhodnya, “Welding materials: Current state and development tendencies,” *Weld. Int.*, vol. 17, no. 11, pp. 905–917, 2003.

[2] P. Kah and J. Martikainen, “Current trends in welding processes and materials,” *Rev.Adv.Mater. Sci.*, vol. 30, no. September 2011, pp. 189–200, 2012.

[3] A. M. Da Silva *et al.*, “Friction spot and friction stir spot welding processes–a literature review,” *Bull. Natl. R&D Inst. Weld. Mater. Testing, ISSN*, pp. 392–1453, 2007.

[4] S. T. Amancio-Filho, A. P. C. Camillo, L. Bergmann, J. F. dos Santos, S. E. Kury, and N. G. A. Machado, “Preliminary Investigation of the Microstructure and Mechanical Behaviour of 2024 Aluminium Alloy Friction Spot Welds,” *Mater. Trans.*, vol. 52, no. 5, pp. 985–991, 2011.

[5] P. Lacki and A. Derlatka, “Strength evaluation of beam made of the aluminum 6061-T6 and titanium grade 5 alloys sheets joined by RFSSW and RSW,” *Compos. Struct.*, vol. 159, pp. 491–497, 2017.

[6] L. C. Campanelli, U. F. H. Suhuddin, J. F. Dos Santos, and N. G. Alcantara, “Preliminary investigation on friction spot welding of AZ31 magnesium alloy,” in *Materials Science Forum*, 2012, vol. 706, pp. 3016–3021.

[7] P. Vigneshwaran, M. P. Prabakaran, T. Selvaraj, and G. R. Kannan, “Weld Strength Optimization by using Box-Behnken Design,” in *International Journal of Engineering Research and Technology*, vol. 3, no. 4, pp. 1879–1882, 2014.

[8] A. H. Plaine, A. R. Gonzalez, U. F. H. Suhuddin, J. F. Dos Santos, and N. G. Alcântara, “The optimization of friction spot welding process parameters in AA6181-T4 and Ti6Al4V dissimilar joints,” *Mater. Des.*, vol. 83, pp. 36–41, 2015.

[9] J. G. Kaufman, *Introduction to aluminum alloys and tempers*. ASM international, 2000.

[10] A. Association, “Secretariat, ANSI H35. 1 Alloy and Temper Designation Systems for Aluminum.” Aluminum Association, Washington, DC, 1997.

[11] W. H. Cubberly, *Tool and Manufacturing Engineers Handbook Desk Edition*, vol. 5. Society of Manufacturing Engineers, 1989.

[12] Ø. Ryen, B. Holmedal, O. Nijs, E. Nes, E. Sjölander, and H.-E. Ekström, “Strengthening mechanisms in solid solution aluminum alloys,” *Metall. Mater. Trans. A*, vol. 37, no. 6, pp. 1999–2006, 2006.

[13] G. Casalino, S. L. Campanelli, N. Contuzzi, A. Angelastro, and A. D. Ludovico, “Laser-assisted friction stir welding of aluminum alloy lap joints: microstructural and microhardness characterizations,” in *High-Power Laser Materials Processing: Lasers, Beam Delivery, Diagnostics, and Applications III*, 2014, vol. 8963, p. 896316.

[14] D. Guest, “Built-In Lightweight Performance,” 2017. [Online]. Available: http://blog.rapidreadytech.com/article/built-in-lightweight-performance/. [Accessed: 30-Apr-2019].

[15] D. Guest, “Built-In Lightweight Performance,” 2017. .

[16] N. G. de Alcântara and J. F. dos Santos, “FSpW Valuation in the Automotive Industry,” 2015.

[17] W. S. Miller *et al.*, “Recent development in aluminium alloys for the automotive industry,” *Mater. Sci. Eng. A*, vol. 280, no. 1, pp. 37–49, 2000.

[18] Z. Qin and P. K. MAllick, “A Study on the bending springback of aluminum alloy 5754,” SAE Technical Paper, 2003.

[19] N. . MAHWAH, “The New Jaguar Xe - Featuring Aluminum-Intensive Construction,” 2014. [Online]. Available: https://media.jaguar.com/en-us/news/2014/07/new-jaguar-xe-featuring-aluminum-intensive-construction. [Accessed: 30-Apr-2019].

[20] M. Kato, T. Fujii, and S. Onaka, “Elastic strain energies of sphere, plate and needle inclusions,” *Mater. Sci. Eng. A*, vol. 211, no. 1–2, pp. 95–103, 1996.

[21] A. K. Gupta and D. J. Lloyd, “Precipitation hardening in Al–Mg–Si alloys with and without excess Si,” *Mater. Sci. Eng. A*, vol. 316, no. 1–2, pp. 11–17, 2001.

[22] Z. Y. Ma, “Friction stir processing technology: a review,” *Metall. Mater. Trans. A*, vol. 39, no. 3, pp. 642–658, 2008.

[23] R. E. Reed-Hill, R. Abbaschian, and R. Abbaschian, *Physical metallurgy principles*, vol. 17. Van Nostrand New York, 1973.

[24] F. A. Mirza, A. Macwan, S. D. Bhole, and D. L. Chen, “Microstructure and fatigue properties of ultrasonic spot welded joints of aluminum 5754 alloy,” *JOM*, vol. 68, no. 5, pp. 1465–1475, 2016.

[25] S. Ogata, J. Li, and S. Yip, “Ideal pure shear strength of aluminum and copper,” *Science.*, vol. 298, no. 5594, pp. 807–811, 2002.

[26] D. A. Hughes, “Microstructural evolution in a non-cell forming metal: Al - Mg,” *Acta Metall. Mater.*, vol. 41, no. 5, pp. 1421–1430, 1993.

[27] F. J. Humphreys, “A unified theory of recovery, recrystallization and grain growth, based on the stability and growth of cellular microstructures—I. The basic model,” *Acta Mater.*, vol. 45, no. 10, pp. 4231–4240, 1997.

[28] F. J. Humphreys, “Inhomogeneous deformation of some aluminium alloys at elevated temperature,” in *Strength of Metals and Alloys (ICSMA 6)*, Elsevier, 1982, pp. 625–630.

[29] F. J. Humphreys and M. Hatherly, "Recrystallization and related annealing phenomena". Elsevier, 2012.

[30] R. D. Doherty *et al.*, “Current issues in recrystallization: a review,” *Mater. Sci. Eng. A*, vol. 238, no. 2, pp. 219–274, 1997.

[31] M. E. Kassner and M. E. McMahon, “The dislocation microstructure of aluminum,” *Metall. Mater. Trans. A*, vol. 18, no. 5, pp. 835–846, 1987.

[32] H. Loitz, J. Wulfsberg, J. von der Wense, A. Von Strombeck, C. Schilling, and J. Dos Santos, “Apparatus for connection of workpieces using the friction stir welding method.” U.S. Patent Application No. 11/160,249.

[33] Coldwater Machine Company, “No Title.” [Online]. Available: https://www.coldwatermachine.com/spot-friction-welding/.

[34] Y. Song, X. Yang, L. Cui, X. Hou, Z. Shen, and Y. Xu, “Defect features and mechanical properties of friction stir lap welded dissimilar AA2024–AA7075 aluminum alloy sheets,” *Mater. Des.*, vol. 55, pp. 9–18, 2014.

[35] Y. Q. Zhao, H. J. Liu, S. X. Chen, Z. Lin, and J. C. Hou, “Effects of sleeve plunge depth on microstructures and mechanical properties of friction spot welded alclad 7B04-T74 aluminum alloy,” *Mater. Des.*, vol. 62, pp.

40–46, 2014.

[36] L. C. Campanelli, U. F. H. Suhuddin, J. F. dos Santos, and N. G. de Alcântara, “Parameters optimization for friction spot welding of AZ31 magnesium alloy by Taguchi method,” *Soldag. Inspeção*, vol. 17, no. 1, pp. 26–31, 2012.

[37] L. C. Campanelli, U. F. H. Suhuddin, A. Í. S. Antonialli, J. F. Dos Santos, N. G. De Alcantara, and C. Bolfarini, “Metallurgy and mechanical performance of AZ31 magnesium alloy friction spot welds,” *J. Mater. Process. Technol.*, vol. 213, no. 4, pp. 515–521, 2013.

[38] J. V Esteves, S. M. Goushegir, J. F. Dos Santos, L. B. Canto, E. Hage Jr, and S. T. Amancio-Filho, “Friction spot joining of aluminum AA6181-T4 and carbon fiber-reinforced poly (phenylene sulfide): Effects of process parameters on the microstructure and mechanical strength,” *Mater. Des.*, vol. 66, pp. 437–445, 2015.

[39] M. D. Tier *et al.*, “The influence of refill FSSW parameters on the microstructure and shear strength of 5042 aluminium welds,” *J. Mater. Process. Technol.*, vol. 213, no. 6, pp. 997–1005, 2013.

[40] S. Bozzi, A. L. Helbert-Etter, T. Baudin, V. Klosek, J. G. Kerbiguet, and B. Criqui, “Influence of FSSW parameters on fracture mechanisms of 5182 aluminium welds,” *J. Mater. Process. Technol.*, vol. 210, no. 11, pp. 1429–1435, 2010.

[41] W. Yuan *et al.*, “Effect of tool design and process parameters on properties of Al alloy 6016 friction stir spot welds,” *J. Mater. Process. Technol.*, vol. 211, no. 6, pp. 972–977, 2011.

[42] J. Y. Cao, M. Wang, L. Kong, H. X. Zhao, and P. Chai, “Microstructure, texture and mechanical properties during refill friction stir spot welding of 6061-T6 alloy,” *Mater. Charact.*, vol. 128, pp. 54–62, 2017.

[43] Y. Zhao, H. Liu, T. Yang, Z. Lin, and Y. Hu, “Study of temperature and material flow during friction spot welding of 7B04-T74 aluminum alloy,” *Int. J. Adv. Manuf. Technol.*, vol. 83, no. 9–12, pp. 1467–1475, 2016.

[44] H. Badarinarayan, Y. Shi, X. Li, and K. Okamoto, “Effect of tool geometry on hook formation and static strength of friction stir spot welded aluminum

5754-O sheets," *Int. J. Mach. Tools Manuf.*, vol. 49, no. 11, pp. 814–823, 2009.

[45] B. Parra, V. T. Saccon, N. G. de Alcântara, T. Rosendo, and J. F. dos Santos, "An investigation on friction spot welding in AA6181-T4 alloy," *Tecnol. em Metal. Mater. e Mineração*, vol. 8, no. 3, p. 184, 2011.

[46] Y. S. Sato, T. W. Nelson, C. J. Sterling, R. J. Steel, and C.-O. Pettersson, "Microstructure and mechanical properties of friction stir welded SAF 2507 super duplex stainless steel," *Mater. Sci. Eng. A*, vol. 397, no. 1–2, pp. 376–384, 2005.

[47] Z. Xu, Z. Li, S. Ji, and L. Zhang, "Refill friction stir spot welding of 5083-O aluminum alloy," *J. Mater. Sci. Technol.*, 2017.

[48] S. L. C. Ferreira *et al.*, "Box-Behnken design: An alternative for the optimization of analytical methods," *Anal. Chim. Acta*, vol. 597, no. 2, pp. 179–186, 2007.

[49] B. Vierneusel, T. Schneider, S. Tremmel, S. Wartzack, and T. Gradt, "Humidity resistant MoS2 coatings deposited by unbalanced magnetron sputtering," *Surf. Coatings Technol.*, vol. 235, pp. 97–107, 2013.

[50] "No Title." [Online]. Available: https://www.makeitfrom.com/material-properties/5754-AlMg3-3.3535-A95754-Aluminum/. [Accessed: 14-May-2019].

[51] Y.-P. Yang, F. Orth, W. Peterson, and J. Gould, "Accurate Spot Weld Testing," *Adv. Mater. Process.*, p. 19, 2014.

[52] G. E. P. Box and D. W. Behnken, "Some New Three Level Designs for the Study of Quantitative Variables," *Technometrics*, vol. 2, no. 4. pp. 455–475, 1960.

[53] E. DIN, "14273. Specimen dimensions and procedure for tensile-shear testing resistance spot, seam and embossed projection welds," *DIN, Ger. Inst. Stand.*, 2014.

[54] U. F. H. Suhuddin, D. Piccolo, V. Fischer, and J. F. dos Santos, "Friction Spot Welding of Similar AA5754 to AA5754 Aluminum Alloys and Dissimilar AA5754 Aluminum to AZ31 Magnesium Alloys," in *Advanced Materials Research*, 2015, vol. 1112, pp. 485–488.

[55] T. Rosendo *et al.*, “Mechanical and microstructural investigation of friction spot welded AA6181-T4 aluminium alloy,” *Mater. Des.*, vol. 32, no. 3, pp. 1094–1100, 2011.

[56] A. Kubit, M. Bucior, D. Wydrzyński, T. Trzepieciński, and M. Pytel, “Failure mechanisms of refill friction stir spot welded 7075-T6 aluminium alloy single-lap joints,” *Int. J. Adv. Manuf. Technol.*, vol. 94, no. 9–12, pp. 4479–4491, 2018.

[57] L. C. Campanelli, P. O. R. Ponto, and D. E. M. Modelagem, “Lap Shear Test of a Magnesium Friction Spot Joint : Numeric Modeling,” T*ecnologia em Metalurgia, Materiais e Mineração* pp. 97–102, 2013.

[58] S. G. Arul, S. F. Miller, G. H. Kruger, T.-Y. Pan, P. K. Mallick, and A. J. Shih, “Experimental study of joint performance in spot friction welding of 6111-T4 aluminium alloy,” *Sci. Technol. Weld. Join.*, vol. 13, no. 7, pp. 629–637, 2008.

[59] C. Albuquerque, “WMP Final Presentation,” 2015.

[60] A. Gerlich, M. Yamamoto, and T. H. North, “Strain rates and grain growth in Al 5754 and Al 6061 friction stir spot welds,” *Metall. Mater. Trans. A*, vol. 38, no. 6, pp. 1291–1302, 2007.

[61] A. Arora, Z. Zhang, A. De, and T. DebRoy, “Strains and strain rates during friction stir welding,” *Scr. Mater.*, vol. 61, no. 9, pp. 863–866, 2009.

[62] S. Mukherjee and A. K. Ghosh, “Flow visualization and estimation of strain and strain-rate during friction stir process,” *Mater. Sci. Eng. A*, vol. 527, no. 20, pp. 5130–5135, 2010.

[63] A. Gerlich, G. Avramovic-Cingara, and T. H. North, “Stir zone microstructure and strain rate during Al 7075-T6 friction stir spot welding,” *Metall. Mater. Trans. A*, vol. 37, no. 9, pp. 2773–2786, 2006.

[64] W. H. Van Geertruyden, W. Z. Misiolek, and P. T. Wang, “Grain structure evolution in a 6061 aluminum alloy during hot torsion,” *Mater. Sci. Eng. A*, vol. 419, no. 1–2, pp. 105–114, 2006.

[65] C. Zener and J. H. Hollomon, “Effect of strain rate upon plastic flow of steel,” *J. Appl. Phys.*, vol. 15, no. 1, pp. 22–32, 1944.

[66] G. Avramovic-Cingara, D. D. Perovic, and H. J. McQueen, “Hot

deformation mechanisms of a solution-treated Al-Li-Cu-Mg-Zr alloy," *Metall. Mater. Trans. A*, vol. 27, no. 11, pp. 3478–3490, 1996.

[67] E. Cerri, E. Evangelista, A. Forcellese, and H. J. McQueen, "Comparative hot workability of 7012 and 7075 alloys after different pretreatments," *Mater. Sci. Eng. A*, vol. 197, no. 2, pp. 181–198, 1995.

[68] A. L. Etter, T. Baudin, N. Fredj, and R. Penelle, "Recrystallization mechanisms in 5251 H14 and 5251 O aluminum friction stir welds," *Mater. Sci. Eng. A*, vol. 445, pp. 94–99, 2007.

[69] R. W. Cahn, "Recrystallization of single crystals after plastic bending," *J. Inst. Met.*, vol. 76, no. 2, p. 121, 1949.

[70] H. J. Aval, S. Serajzadeh, N. A. Sakharova, A. H. Kokabi, and A. Loureiro, "A study on microstructures and residual stress distributions in dissimilar friction-stir welding of AA5086–AA6061," *J. Mater. Sci.*, vol. 47, no. 14, pp. 5428–5437, 2012.

[71] A. P. Zhilyaev and T. G. Langdon, "Using high-pressure torsion for metal processing: Fundamentals and applications," *Prog. Mater. Sci.*, vol. 53, no. 6, pp. 893–979, 2008.

[72] L. E. Tanner and S. V Radcliffe, "Effect of hydrostatic pressure on the kinetics of recrystallization in high-purity copper," *Acta Metall.*, vol. 10, no. 12, pp. 1161–1169, 1962.

[73] M. Winning and C. Schäfer, "Influencing recrystallization behaviour by mechanical loads," *Mater. Sci. Eng. A*, vol. 419, no. 1–2, pp. 18–24, 2006.

ANNEXES

ANNEXE A: AA5754-AA5754 Similar Results

Welding parameters (Sample No: 1)

Rotational speed:1800 rpm

Feeding rate: 3.5 mm/s

Plunge depth: 1.5 mm

Macrograph

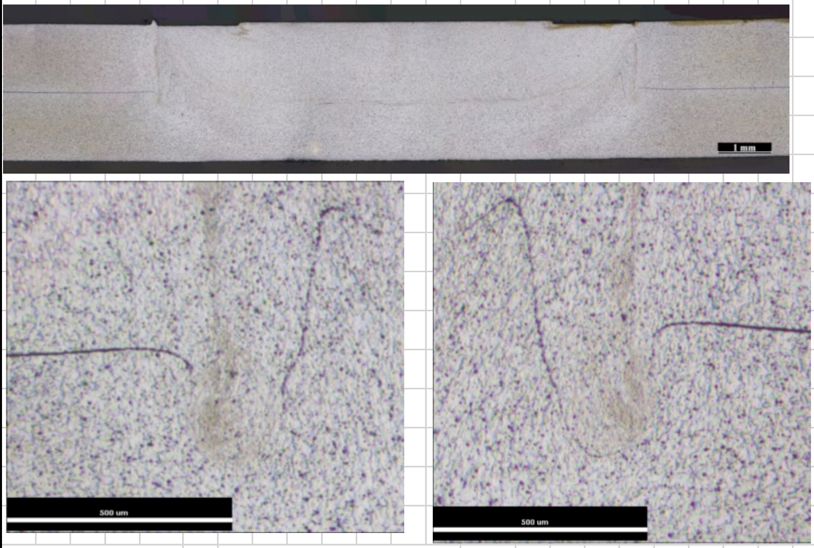

h/t ratio (%): 1,9

Bounded width: 8.971 mm

Lap Shear Strength

Average: 5197 N

Amplitude: 75 N

Fracture Surface:

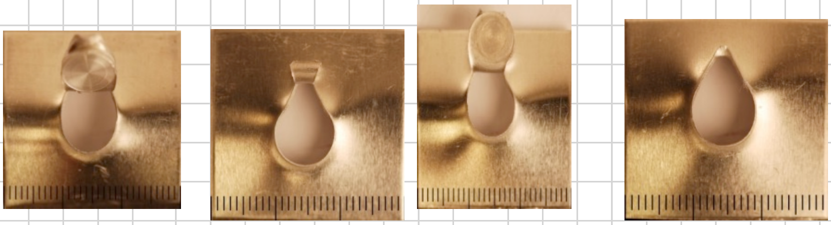

Welding parameters (Sample No: 2)

Rotational speed: 1200 rpm

Feeding rate: 3.5 mm/s

Plunge depth: 1.5 mm

Macrograph

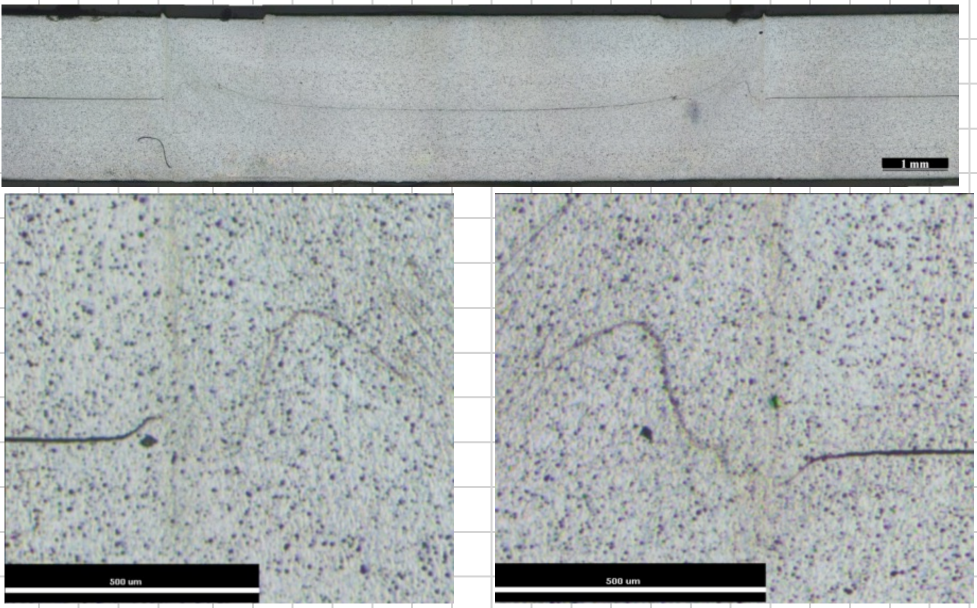

h/t ratio (%): 5.9 Bounded width: 8.982 mm

Lap Shear Strength

Average: 4902 N

Amplitude: 54 N

Fracture Surface:

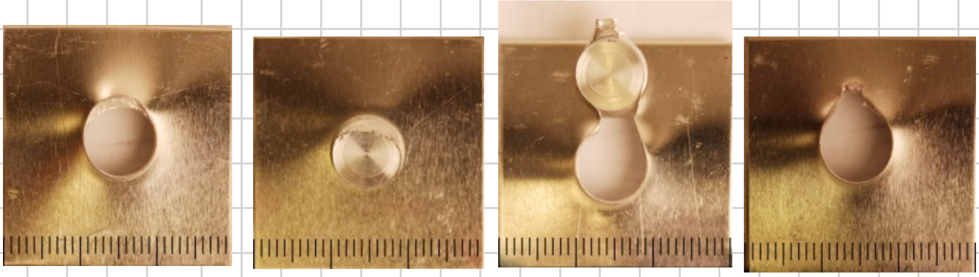

Welding parameters (Sample No: 3)

Rotational speed: 2400 rpm

Feeding rate: 3.5 mm/s

Plunge depth: 1.5 mm

Macrograph

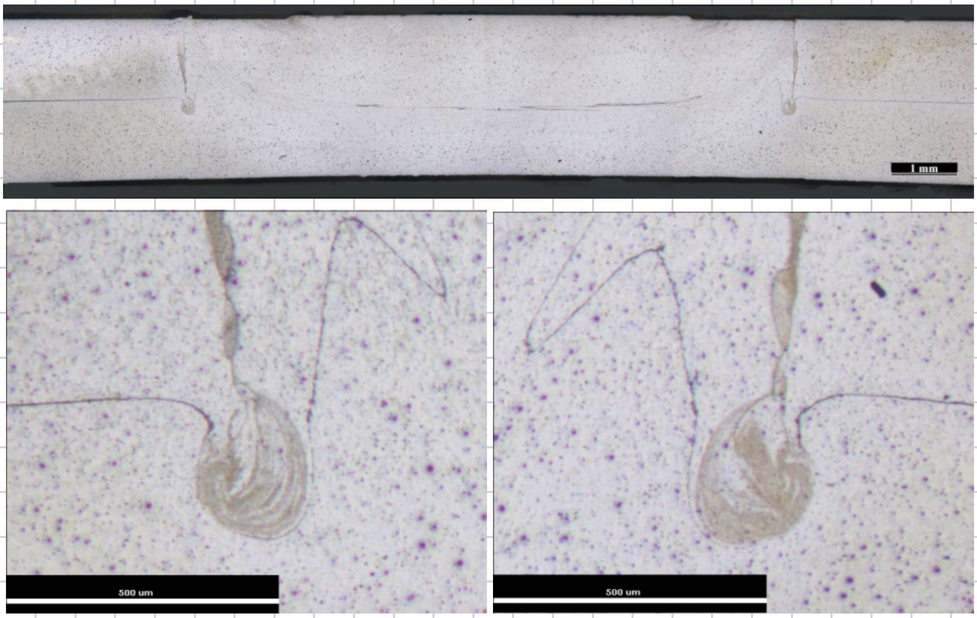

h/t ratio (%): 2.7 Bounded width: 8.993 mm

Lap Shear Strength

Average: 5163 N

Amplitude: 41 N

Fracture Surface:

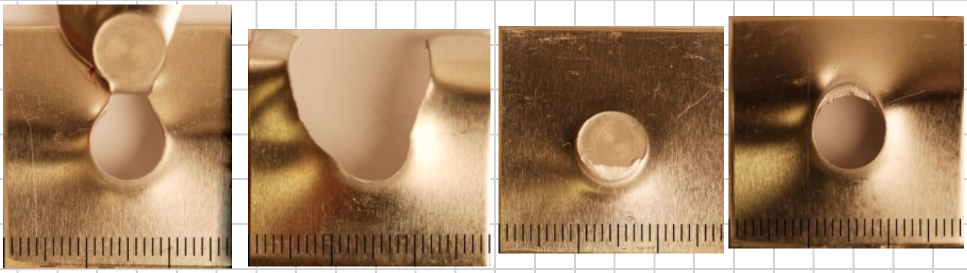

Welding parameters (Sample No: 4)

Rotational speed:1800 rpm

Feeding rate: 3.5 mm/s

Plunge depth: 1.3 mm

Macrograph

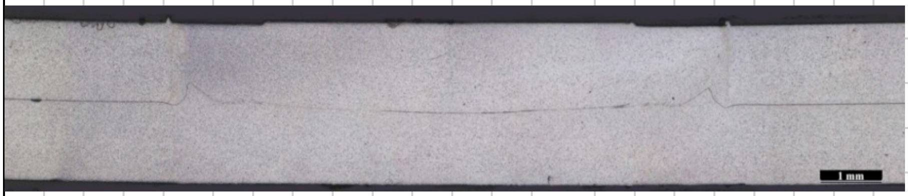

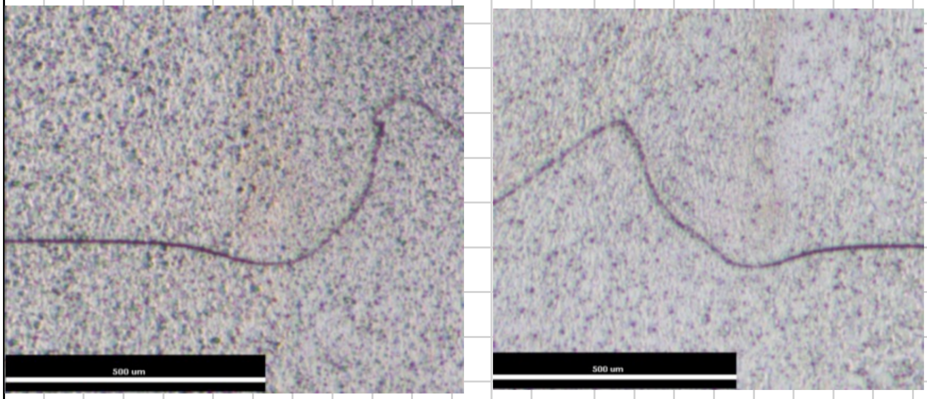

h/t ratio (%): 21.3 Bounded width: 8.351 mm

Lap Shear Strength

Average: 5062 N

Amplitude: 71 N

Fracture Surface:

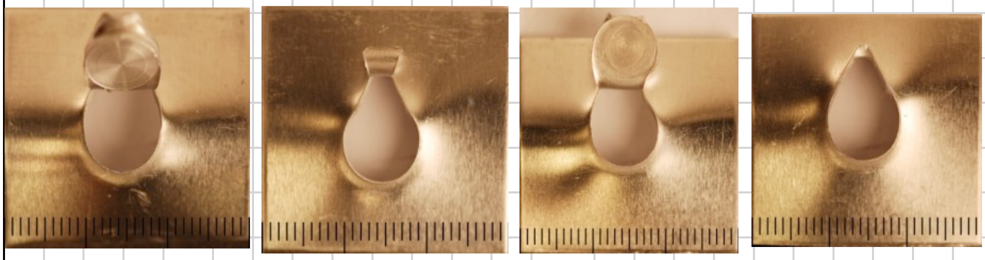

Welding parameters (Sample No: 5)

Rotational speed:1800 rpm

Feeding rate: 3.5 mm/s

Plunge depth: 1.7 mm

Macrograph

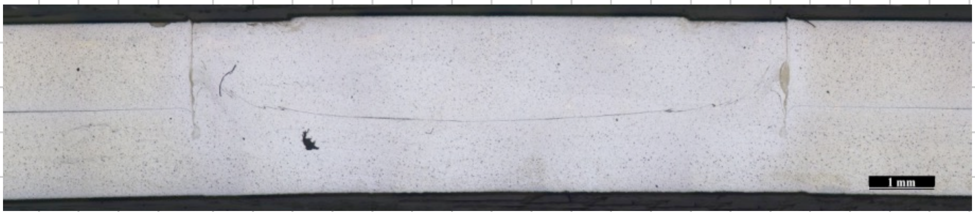

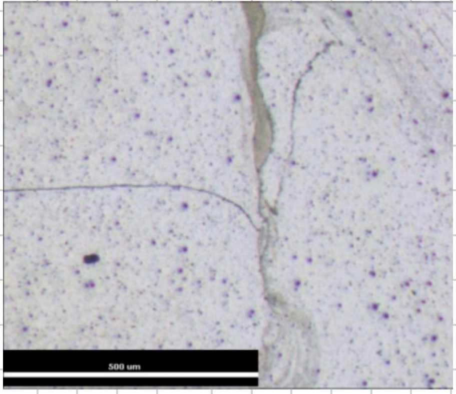

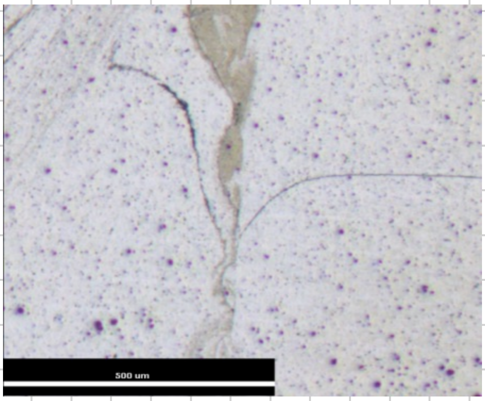

h/t ratio (%): 9.1

Bounded width: 8.987 mm

Lap Shear Strength

Average: 4753 N

Amplitude: 91 N

Fracture Surface:

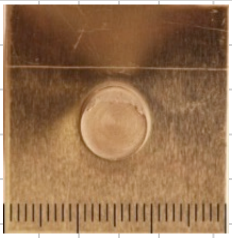

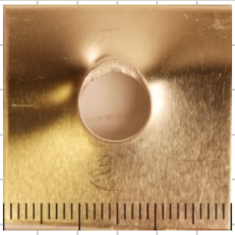

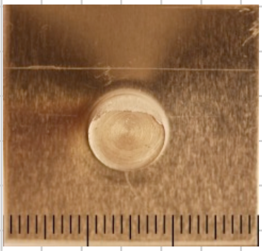

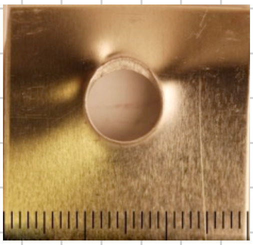

Welding parameters (Sample No: 6)

Rotational speed:1800 rpm

Feeding rate: 3 mm/s

Plunge depth: 1.5 mm

Macrograph

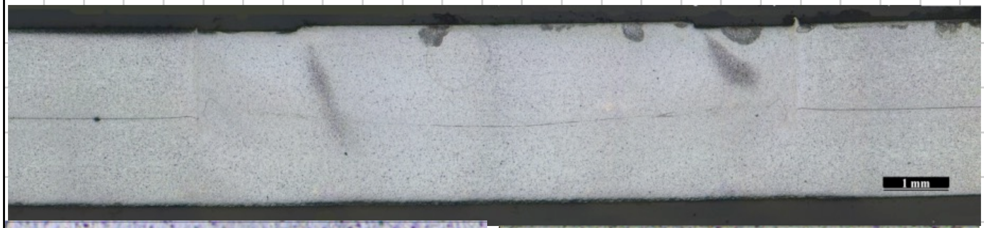

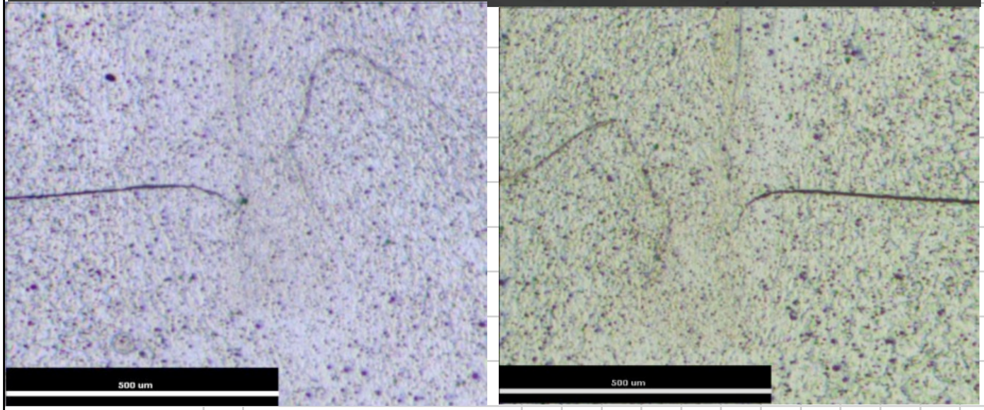

h/t ratio (%): 7,8

Bounded width: 8.901 mm

Lap Shear Strength

Average: 5143 N

Amplitude: 27 N

Fracture Surface:

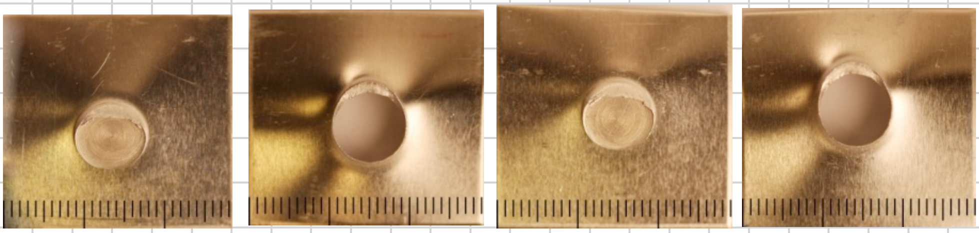

Welding parameters (Sample No: 7)

Rotational speed:1800 rpm

Feeding rate: 4 mm/s

Plunge depth: 1.5 mm

Macrograph

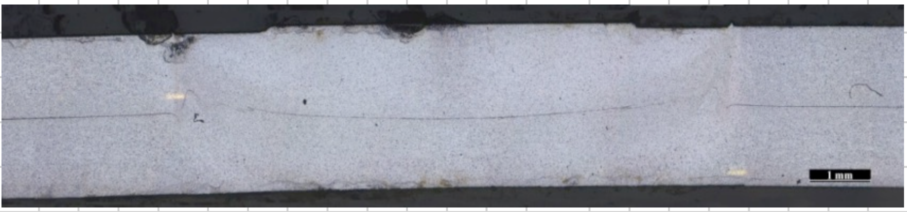

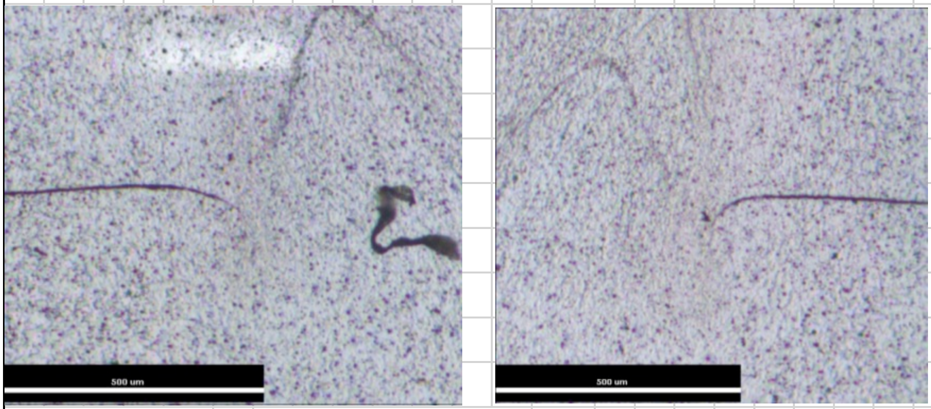

h/t ratio (%): 2.7

Bounded width: 8.965 mm

Lap Shear Strength

Average: 5072 N

Amplitude: 105 N

Fracture Surface:

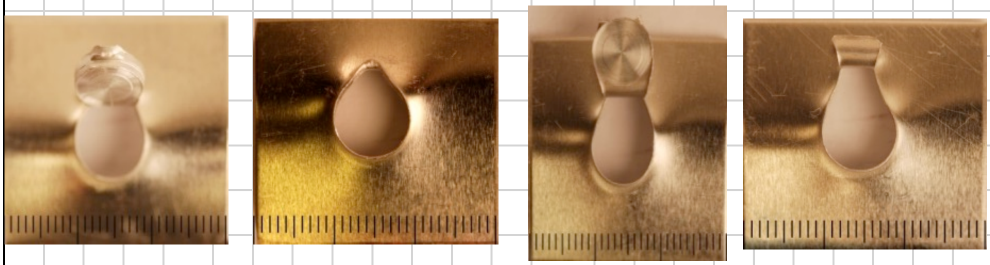

ANNEXE B: AA5754-AA6061 Dissimilar Results

Welding parameters (Sample No: 1)

Rotational speed:1150 rpm

Feeding rate: 3 mm/s

Plunge depth: 1.6 mm

Macrograph

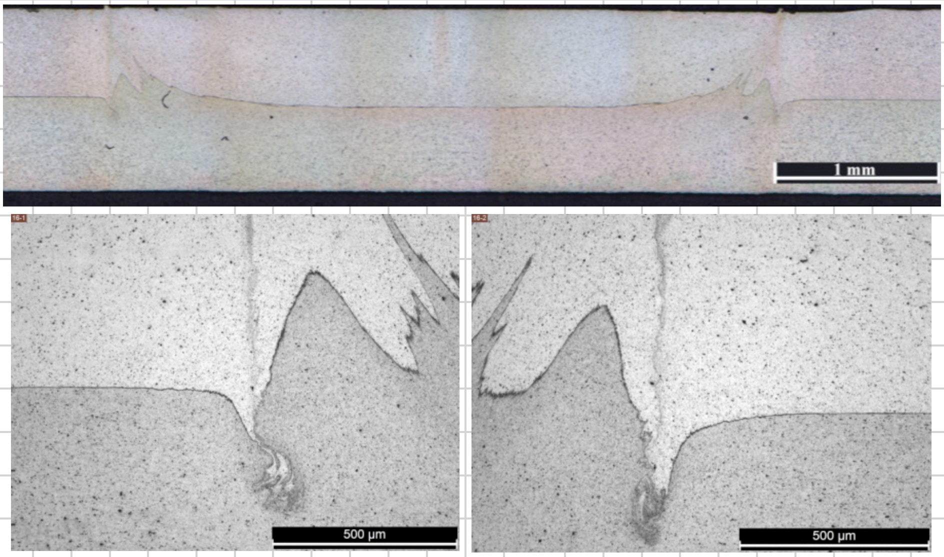

h/t ratio (%): 12,893

Lap Shear Strength

Average: 5703,750 N

STD DEV: 71,633

Fracture Surface:

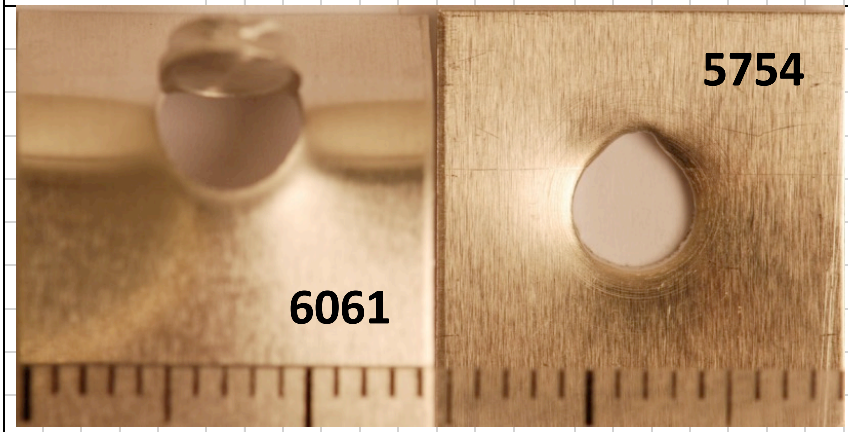

Welding parameters (Sample No: 2)

Rotational speed: 1000 rpm

Feeding rate: 3 mm/s

Plunge depth: 1.6 mm

Macrograph

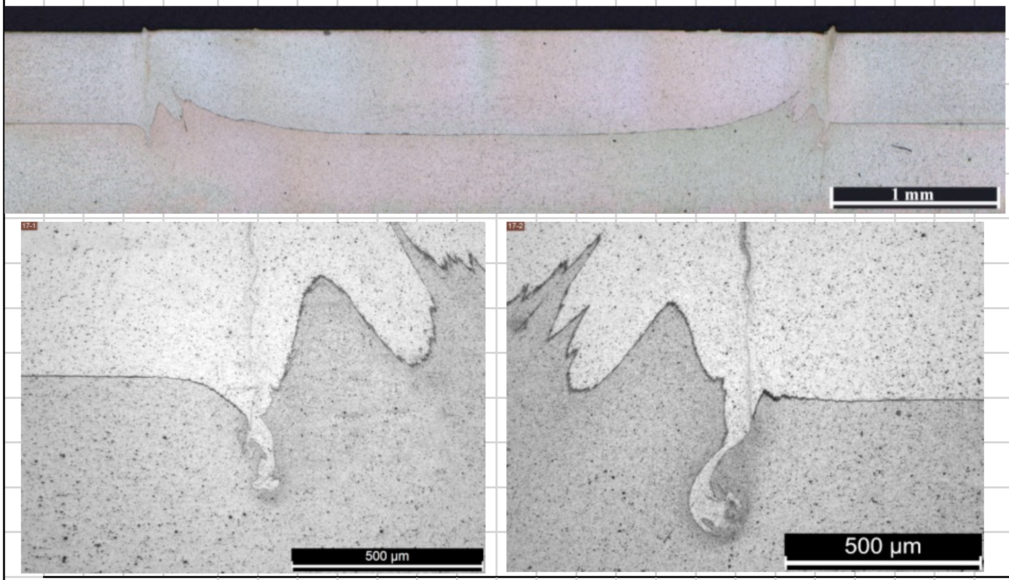
1 mm
17-1
500 µm
17-2
500 µm

h/t ratio (%): 8,276

Lap Shear Strength

Average: 5654,757 N

STD DEV: 135,4686

Fracture Surface:

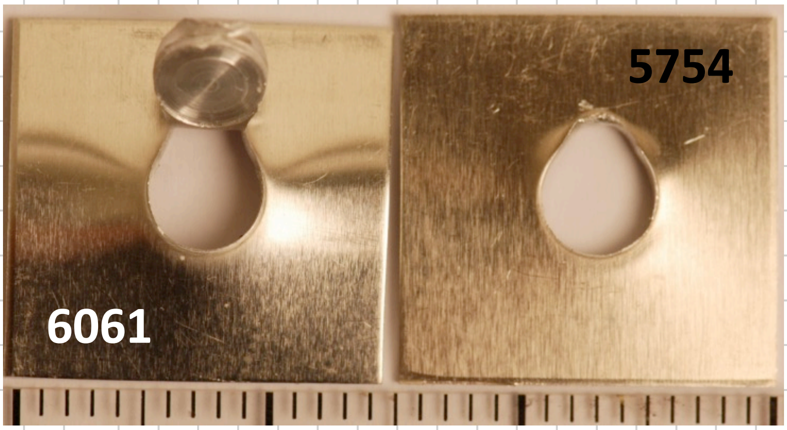

Welding parameters (Sample No: 3)

Rotational speed: 800 rpm

Feeding rate: 3 mm/s

Plunge depth: 1.6 mm

Macrograph

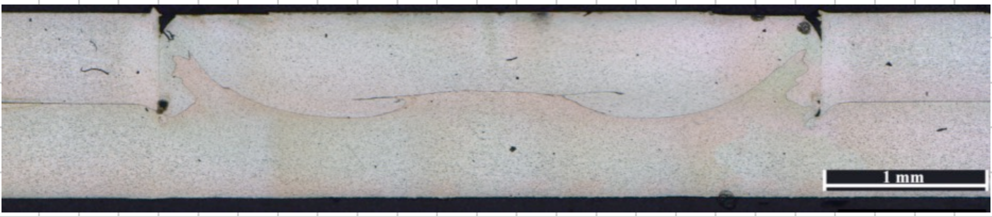

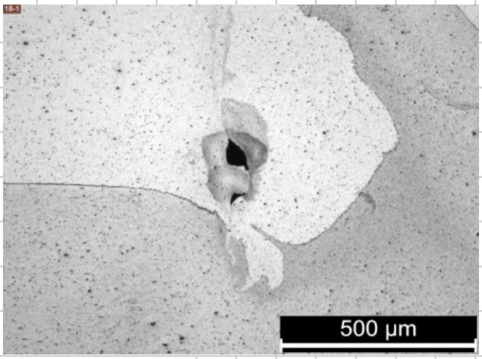

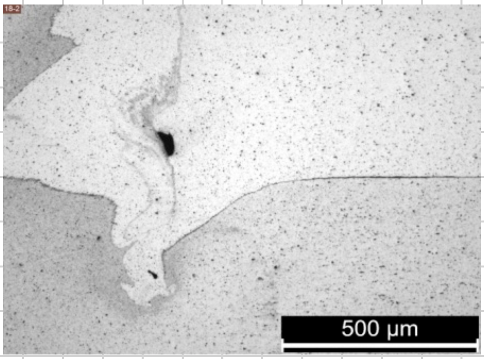

h/t ratio (%): 14,88

Lap Shear Strength

Average: 4372,587 N

STD DEV: 242,728

Fracture Surface:

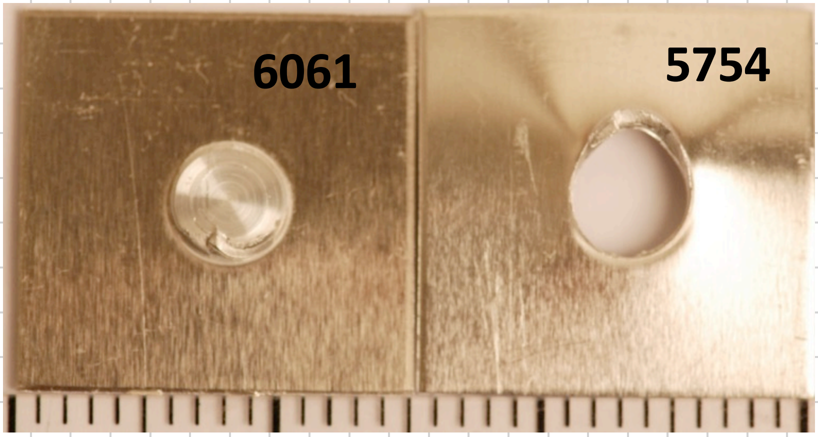

Welding parameters (Sample No: 4)

Rotational speed:1500 rpm

Feeding rate: 3 mm/s

Plunge depth: 1.6 mm

Macrograph

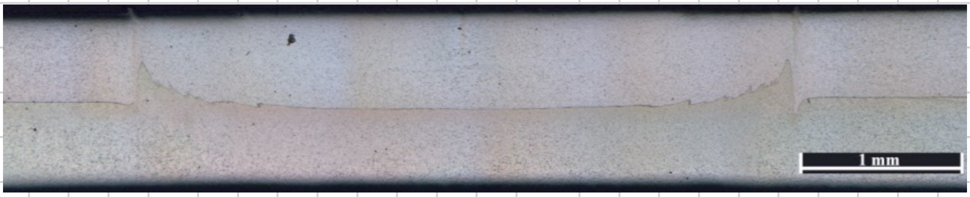

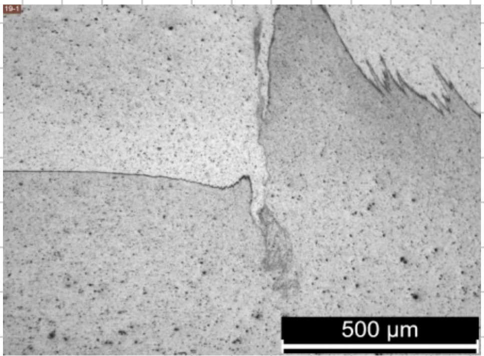

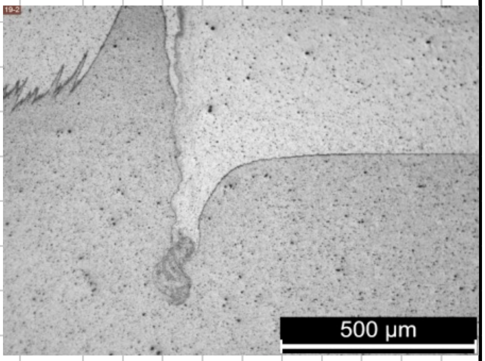

h/t ratio (%): 9,504

Lap Shear Strength

Average: 5720,773 N

STD DEV: 19,89919

Fracture Surface:

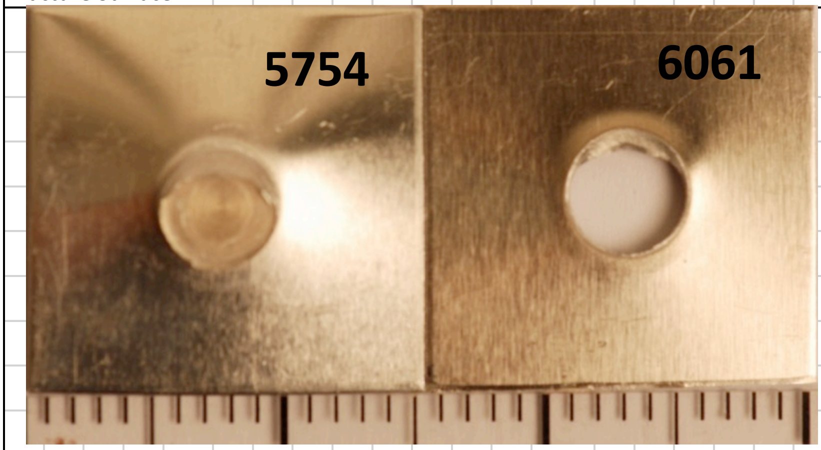

Welding parameters (Sample No: 5)

Rotational speed:1150 rpm

Feeding rate: 3 mm/s

Plunge depth: 1.8 mm

Macrograph

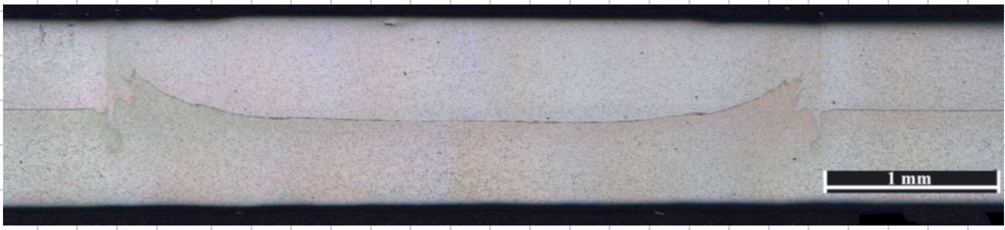

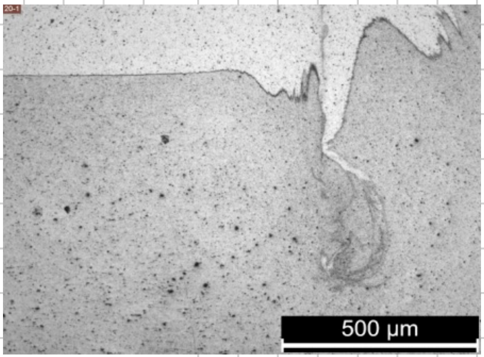

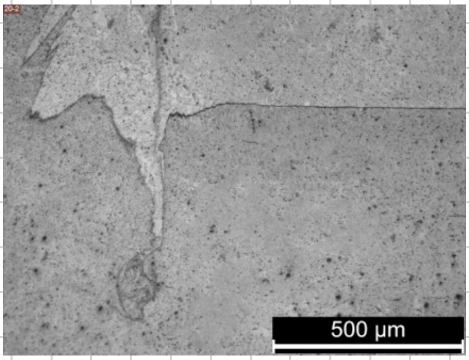

h/t ratio (%): 8,939

Lap Shear Strength

Average: 5789,763 N

Amplitude: 7,996701 N

Fracture Surface:

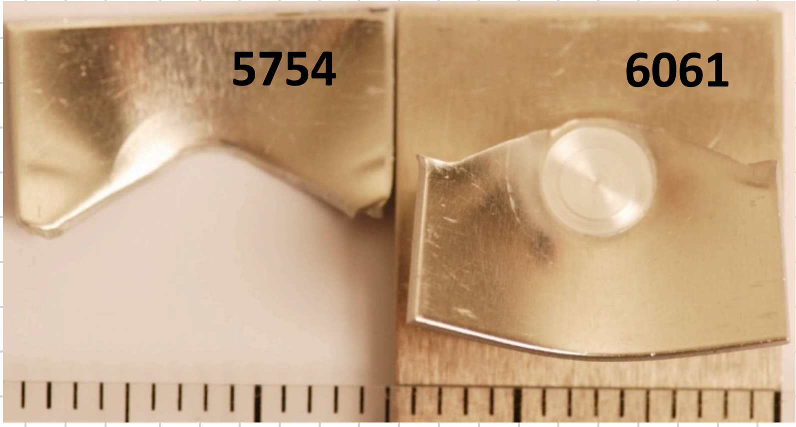

Welding parameters (Sample No: 6)

Rotational speed:1150 rpm

Feeding rate: 3 mm/s

Plunge depth: 1.4 mm

Macrograph

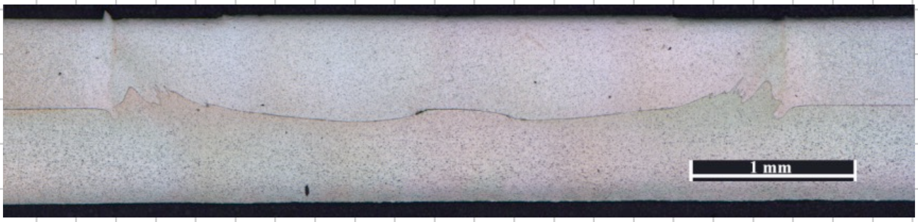

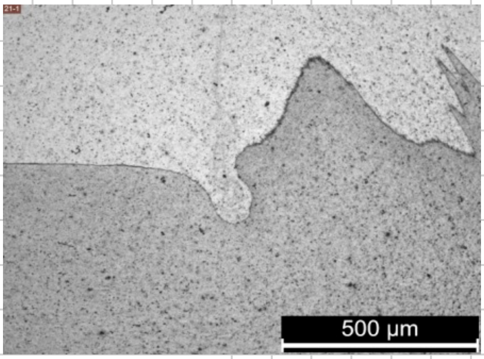

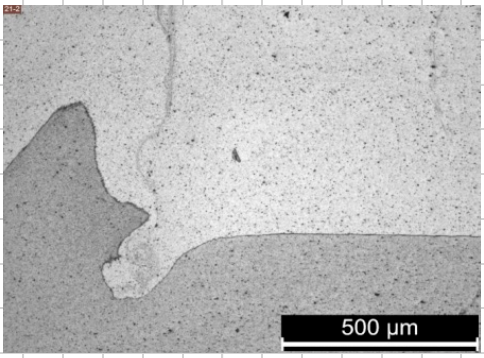

h/t ratio (%): 11,321

Lap Shear Strength

Average: 5643,393 N

STD DEV: 70,00737

Fracture Surface:

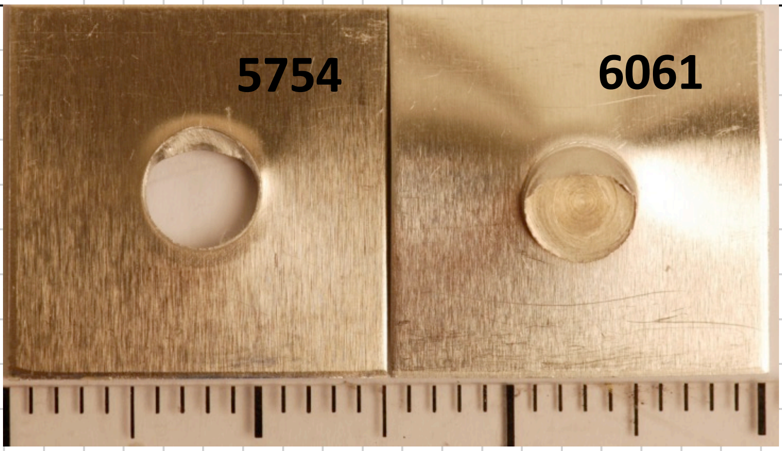

Welding parameters (Sample No: 7)

Rotational speed:1150 rpm

Feeding rate: 2,5 mm/s

Plunge depth: 1.6 mm

Macrograph

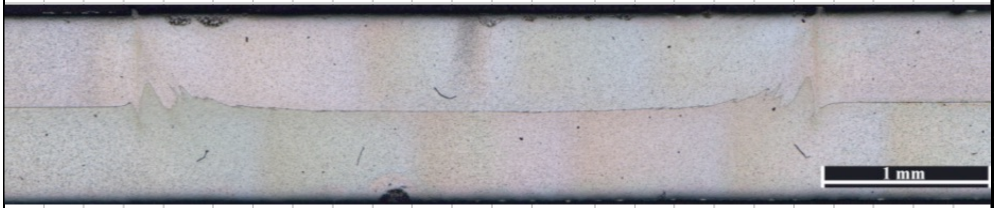

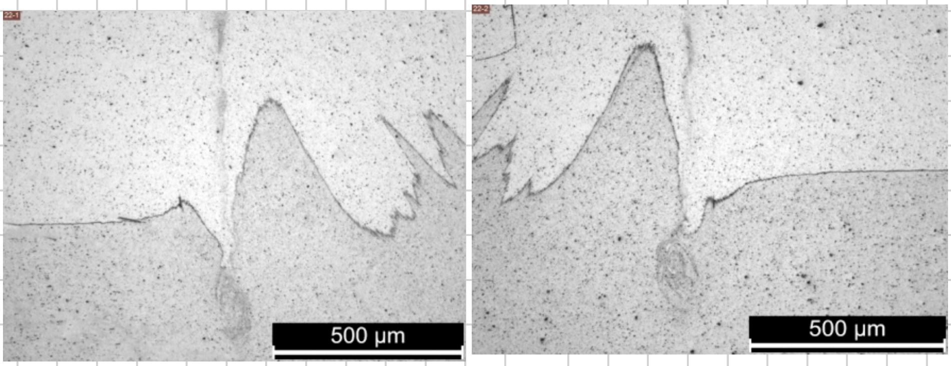
22-1
500 µm
22-2
500 µm

h/t ratio (%): 6,238

Lap Shear Strength

Average: 5802,723 N

STD DEV: 36,30576

Fracture Surface:

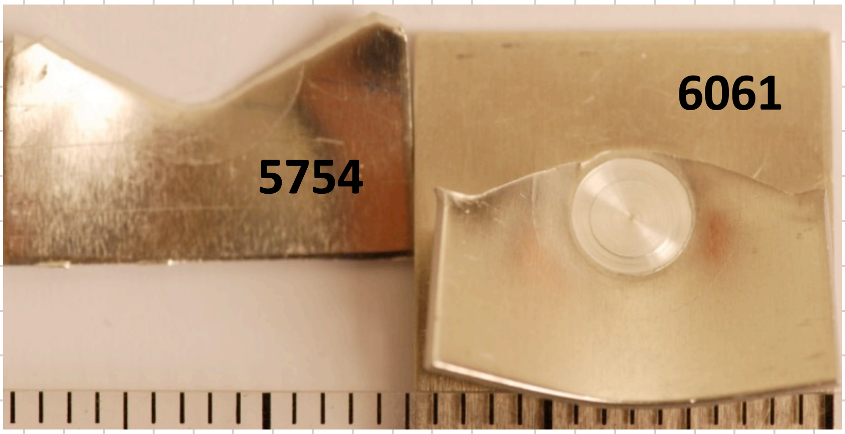

Welding parameters (Sample No: 8)

Rotational speed:1150 rpm

Feeding rate: 3,5 mm/s

Plunge depth: 1.6 mm

Macrograph

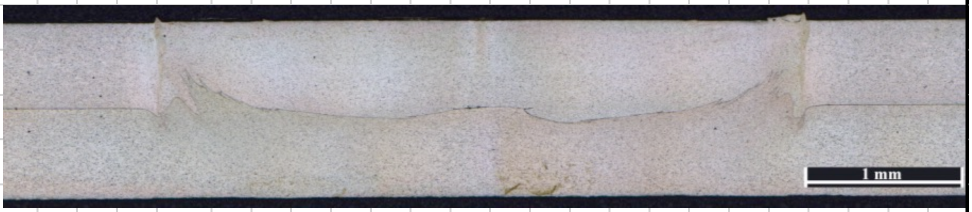

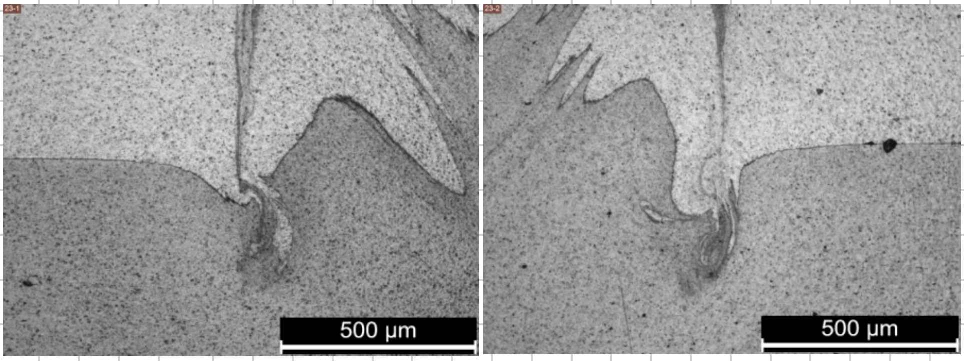
500 µm
500 µm

h/t ratio (%): 8,571

Lap Shear Strength

Average: 5838,953 N

STD DEV: 52,80849

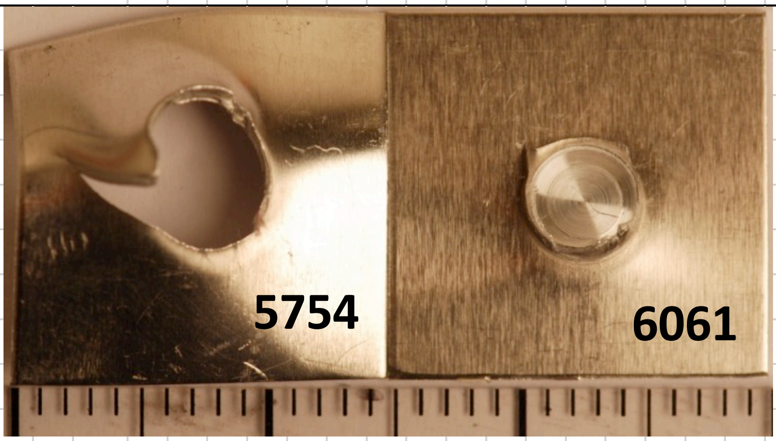Fracture Surface: